Measurement of nutrient and contaminant flux dynamics at the water-sediment interface in aquatic environments.

Guilherme Calabro Souza

▶ **To cite this version:**

Guilherme Calabro Souza. Measurement of nutrient and contaminant flux dynamics at the water-sediment interface in aquatic environments.. Earth Sciences. École des Ponts ParisTech, 2022. English. NNT : 2022ENPC0016 . tel-04199685

HAL Id: tel-04199685
https://pastel.hal.science/tel-04199685

Submitted on 8 Sep 2023

HAL is a multi-disciplinary open access archive for the deposit and dissemination of scientific research documents, whether they are published or not. The documents may come from teaching and research institutions in France or abroad, or from public or private research centers.

L'archive ouverte pluridisciplinaire **HAL**, est destinée au dépôt et à la diffusion de documents scientifiques de niveau recherche, publiés ou non, émanant des établissements d'enseignement et de recherche français ou étrangers, des laboratoires publics ou privés.

École des Ponts ParisTech

THÈSE DE DOCTORAT
de l'École des Ponts ParisTech

Measurement of nutrient and contaminant flux dynamics at the water-sediment interface in aquatic environments

École doctorale Science, Ingénierie et Environnement

Spécialité du doctorat : Sciences et Techniques de l'Environnement

Thèse préparée au sein du Laboratoire Eau Environnement et Systèmes Urbains et du Laboratoire d'Hydraulique Saint-Venant de l'Ecole des Ponts ParisTech

Thèse soutenue le 7 juin 2022, par
Guilherme CALABRO SOUZA

Composition du jury :

Sophie GUILLON Assistante de recherche, Mines ParisTech	*Rapporteure*
Yves BRUNET Directeur de recherche, UMR ISPA - INRAe	*Rapporteur*
Christophe RABOUILLE Directeur de Recherche, UMR LSCE – CNRS	*Examinateur*
Thierry LABASQUE Ingénieur de Recherche, Géosciences Rennes	*Examinateur*
Régis MOILLERON Professeur, LEESU - UPEC	*Directeur de thèse*
Bruno LEMAIRE IPEF, HYCAR - AgroParisTech	*Co-Encadrant de thèse*
Magali JODEAU Ingénieure-Chercheur, LHSV – EDF R&D	*Co-Encadrante de thèse*
Brigitte VINÇON-LEITE Directrice de Recherche, LEESU – ENPC	*Co-Encadrante de thèse*

ABSTRACT

Freshwater quality in natural environments is of major concern for the agricultural, industrial, and domestic sectors. Despite decades of efforts to reduce the pollutant inputs, water quality recovery can be slow, due to the pollutant stock in the sediment of aquatic ecosystems. For example, the so-called internal load presents a notable contribution to the dynamics of eutrophication. Such benthic fluxes (i.e. at the interface between the sediment and the water column) result from microbiological and chemical activity in the sediment. They have different drivers including hydrodynamics. Turbulence affects the benthic boundary layer, more specifically fluxes through the thickness of the diffusive sublayer (DBL). Different techniques are widely used to quantify benthic fluxes (e.g., benthic chambers, dialysis chambers or concentration profilers). Only aquatic eddy covariance (EC) makes it possible to measure turbulent benthic fluxes over a large sediment area without perturbing the flow, but for a limited range of fluxes (heat, dissolved oxygen, nitrates, particles and alkalinity). The adaptation to the aquatic environment of relaxed eddy accumulation (REA), a micrometeorology technique, was shown to be theoretically feasible. REA consists of a sampling conditioned by the direction of the turbulent fluctuation of the vertical velocity: different samples are accumulated for updrafts and downdrafts and the benthic flux is proportional to the concentration difference between sample pairs. The objective of this work was to develop a prototype, to validate the technique with a reference method, and to acquire first time series at an hourly time step of turbulent benthic fluxes of nutrients.

During the development of a prototype, the principles of REA were transferred to aquatic environments through various tests, experiments and simulations. These were carried out in collaboration with the Institute for Environmental Studies of the University of Koblenz-Landau, Germany.

A technical validation of the aquatic REA was carried out by comparing oxygen fluxes measured simultaneously by REA and by eddy covariance. Campaigns were conducted in 2020 at four different sites with different hydrodynamic and ecological conditions, ranging from a laboratory flume to a highly eutrophic shallow lake. REA was validated and the measurements gave insights on its operating conditions.

Benthic fluxes measured by four different techniques were compared in collaboration with the Soil and Water Research Infrastructure (SoWa) of the University of South Bohemia, Czech Republic. The first Fick's law was applied both (i) to diffusive fluxes in ex-situ sediment cores by measuring concentration microprofiles with diffusive thin films and (ii) to turbulent fluxes by measuring in situ the concentration gap between the diffusive and the turbulent sublayers of the benthic boundary layer and computing a mass transfer coefficient proportional to the friction velocity (MTC, another innovative technique); the prototype equipped for (iii) eddy covariance and (iv) REA was also deployed. Fluxes of dissolved oxygen and of phosphate, ammonium, sulphate, iron and manganese ions were measured in a eutrophic,

small and shallow lake, the Lake Champs-sur-Marne in June 2021. The turbulent fluxes of nutrients and metallic ions measured by REA and by MTC were comparable, increasing the confidence in both new techniques. In addition, the measurements showed a strong oxygen dynamic over the day and that the oxygen influx towards the sediment did not cover the sediment demand, helping in hypoxia.

The development, validation and application of the aquatic REA are described and discussed in this work. The measurement requirements and the range of use are also illustrated. Even if REA still requires further development, fluxes of nutrients and metallic ions were measured by the new technique and exhibited fast dynamics. All these elements allow us to present REA as a reliable technique for monitoring the fast dynamics of benthic fluxes, and thus their contribution to the biogeochemical processes of aquatic ecosystems.

Key words: Hydrodynamics; Water-sediment interface; Benthic fluxes; Relaxed eddy accumulation.

RESUME

La qualité des eaux douces dans les milieux naturels est une préoccupation majeure pour les secteurs agricole, industriel et domestique. Malgré des décennies d'efforts pour réduire les apports de polluants, la récupération de la qualité de l'eau peut être lente, en raison du stock de polluants dans les sédiments des écosystèmes aquatiques. Par exemple, la charge dite interne présente une contribution notable à la dynamique de l'eutrophisation. Ces flux benthiques (c'est-à-dire à l'interface entre les sédiments et la colonne d'eau) résultent de l'activité microbiologique et chimique dans les sédiments. Ils ont différents facteurs, dont l'hydrodynamique. La turbulence affecte la couche limite benthique, plus précisément l'épaisseur de sa sous-couche diffusive qui souvent limitante pour les flux. Différentes techniques sont largement utilisées pour quantifier les flux benthiques (par exemple, les chambres benthiques, les chambres à dialyse ou les profileurs de concentration). Seule la covariance turbulente permet de mesurer les flux benthiques turbulents sur une grande surface de sédiments sans perturber l'écoulement, mais pour une gamme limitée de flux (chaleur, oxygène dissous, nitrates, particules et alcalinité). L'adaptation au milieu aquatique de la relaxed eddy accumulation (REA), une technique de micrométéorologie, s'est avérée théoriquement faisable. La REA consiste en un échantillonnage asservi à la direction de la fluctuation turbulente de la vitesse verticale : on collecte des échantillons séparés pour les courants ascendants et descendants ; le flux benthique est proportionnel à la différence de concentration entre les deux échantillons résultants. L'objectif de ce travail était de développer un prototype, de valider la technique avec une méthode de référence, et d'acquérir les premières séries temporelles à un pas de temps horaire des flux benthiques turbulents de nutriments et d'ions métalliques.

Au cours du développement d'un prototype, différents tests, expériences et simulations ont permis de transférer les principes de la REA à l'environnement aquatique. Ceux-ci ont été réalisés en collaboration avec l'Institut d'études environnementales de l'Université de Coblence-Landau, en Allemagne.

La validation technique de la REA aquatique a consisté à comparer les flux d'oxygène mesurés simultanément par REA et par covariance turbulente. Des campagnes ont été menées en 2020 sur quatre sites différents présentant des conditions hydrodynamiques et écologiques différentes, allant d'un canal de laboratoire à un lac peu profond très eutrophe. La REA a été validée et les mesures ont permis de mieux comprendre ses conditions d'utilisation.

Les flux benthiques mesurés par quatre techniques différentes ont été comparés en collaboration avec l'Infrastructure de recherche sur le sol et l'eau (SoWa) de l'Université de Bohème du Sud, en République tchèque. La première loi de Fick a été appliquée à la fois (i) aux flux diffusifs dans des carottes de sédiments ex-situ en mesurant les microprofils de concentration avec des chambres à dialyse et un microprofileur d'oxygène et (ii) aux flux turbulents en mesurant in situ l'écart de concentration entre les sous-couches diffusives et turbulentes de la couche limite benthique et en calculant un coefficient de

transfert de masse proportionnel à la vitesse de friction (MTC pour *mean transfer coefficient*, une autre technique innovante). Le prototype a mis en œuvre (iii) la covariance turbulente et (iv) la REA. Les flux d'oxygène dissous, de phosphate, d'ammonium, de sulfate, de fer et de manganèse ont été mesurés en juin 2021dans un petit lac eutrophe peu profond, le lac de Champs-sur-Marne. Les flux turbulents de nutriments et d'ions métalliques mesurés par REA et par MTC se sont avérés comparables, ce qui donne confiance dans les deux nouvelles techniques. De plus, les mesures ont montré une forte dynamique de l'oxygène au cours de la journée et que le flux d'oxygène vers le sédiment ne couvrait pas sa demande en oxygène, favorisant l'hypoxie au fond du lac.

Cette thèse décrit le développement, la validation et l'application de la REA aquatique dans ce travail. Il donne le cahier des charges et les spécifications du prototype, ainsi que sa gamme d'utilisation. Même si le développement de la REA n'est pas achevé, des flux de nutriments et d'ions métalliques ont été mesurés avec cette nouvelle technique et ont montré une dynamique rapide. Tous ces éléments nous permettent de présenter la REA comme une technique fiable pour suivre la dynamique rapide des flux benthiques, et donc leur contribution aux processus biogéochimiques des écosystèmes aquatiques.

Mot clés : Hydrodynamique ; Interface eau-sédiment ; Flux benthiques ; Relaxed eddy accumulation.

ACKNOWLEDGMENTS

All the work developed during my PhD would not have been possible without the scholarship granted by Ecole des Ponts ParisTech and the working conditions provided. But also, the funding of equipment granted by AgroParisTech and OSU-EFLUVE. I sincerely thank all these institutions.

My doctorate was not achieved by one person, but by a cooperation of people and institutions who gave their time, advice and knowledge. For this, I would like to thank the technical cell of Leesu and LHSV. The synergy of these two laboratories allowed the work done during my thesis to progress. I would like to thank Annick Piazza, Catherine Charleaux, Mohamed Saad, Emilie Caupos, Lila Boudahmane, Franck Lebert and all the technical staff of the LHSV, but also of the LNHE and EDF R&D in Chatou. Philippe Dubois, one of the brains of my PhD, deserves special thanks for all the energy, design skills and humor he deployed during these almost four years.

The external members of the jury of my thesis allowed me to put forward the importance of my work and helped me in the scientific reflection. For that, I thank Sophie Guillon, Yves Brunet, Christophe Rabouille and Thierry Labasque.

I would like to thank my four thesis directors. Each director has contributed to this work. Régis Moilleron, thank you for helping me to find an administrative and scientific path when I was in need. Magali Jodeau, thank you for all the support during the campaigns and I really appreciated the way you synthesize the meetings. It always impressed me. Brigitte Vinçon-Leite, thank you very much for the many hours spent with me discussing biogeochemistry, lake hydrodynamics, organizing and planning my field campaigns, and finally analyzing the results. Finally, Bruno Lemaire (not the minister), thank you very much for making all this work possible, for the many hours of discussion on just about everything (from mathematics to children's education). Thanks also to the Lemaire family whose indirect support has been overwhelming. I would also like to extend my special gratitude to my unofficial thesis supervisors Andreas Lorke, Christian Noss, Bruno Tassin, Rachid Dris and Damien Tedoldi. I really appreciate the advice of all kinds that you have given me.

As mentioned before, different institutions helped me during this journey. A big thank you to the Base de Loisirs de Champs-sur-Marne, in particular to Laurance Godard. Thanks to Alexis Millot and Gérard Lacroix and all the team of Planaqua, Gwendal Communel and Hocine Delmi from the Navier laboratory, Vivian Russel from the Maker Space of the ENPC. A big thank you to Eric Viollier, Bruno Bombled, Christophe Rabouille of the LSCE Oceanis team. Many thanks to Julien Tournebize and Arnaud Blanchouin from HYCAR - INRAe.

The great synergy and scientific dynamism of Felipe Panorasin Breton and Jakub Borovec, both from the University of South Bohemia, were a major turning point in my work. The interns Celia Ramos Sanches and Clement Molinier have also been fundamental to my work.

I would like to thank all the researchers, in particular Martin Seidl and Bernard de Gouvelo (the beer lovers), the PhD students and post-docs of Leesu who helped me directly or indirectly during these years. You were an important encouragement for me to cross the Marne on the RER A every morning.

Finally, my family and friends have allowed me to stay connected to another reality than the academic world during all these years. A big thank you to Morgane and Noah who supported and encouraged me in all the moments I needed it.

Guilherme Calabro

TABLE OF CONTENTS

TABLE OF FIGURES

LIST OF TABLES

1 GENERAL INTRODUCTION

Freshwater quality is a major concern for territories where anthropic activities have been intensive (Tang et al., 2012; Mateo-Sagasta et al., 2017; Camara et al., 2019). Excessive nutrient and metal ion loading contributes to eutrophication and to a loss of biodiversity, especially during warm seasons (Rast and Thornton, 2007). Many waterbodies worldwide have been experiencing enhanced systematic algae blooms over the years (Jia et al., 2019). The excessive and rapid growth of algae, mostly caused by the high availability of nitrogen and phosphorus, promotes the imbalance of the biogeochemical cycle. It directly and indirectly affects the costs of freshwater use and consumption (Kouakou and Poder, 2019). Several policies have addressed the issue of reducing pollutants in freshwaters, and it has been partially successful (e.g., the Nitrate Directive 1991 and the Water Framework Directive 2000). However, some water bodies resist improving their quality, thus reinforcing the role of sediments in the biogeochemical cycles of inland water bodies through the so-called internal load. (Welch and Cooke, 1995; Søndergaard, 2007).

Through benthic fluxes, the contribution of the sediment to water quality can be significant. The mineralisation of organic matter in the sediment results in nutrient fluxes. These are often considered as constant at the daily to weekly scales and mostly driven by diffusive transport (Berner, 1971; Robson, 2014). However, the drivers of these fluxes are multiple: the organic matter supply, microbial activity function of temperature and redox conditions, fauna (bioturbation and bio-irrigation), the near-bed current speed (Woodruff et al., 1999; Wuest and Lorke, 2003; Norling and Kautsky, 2007; Lorke and Macintyre, 2009). The spatial-temporal characteristics of these drivers can be very heterogeneous depending on the time of year and the type of water body. In shallow and small waterbodies, the dynamics is fast and the resulting short-term fluxes remain unknown. These types of water bodies are frequent on a global scale and their contribution to global biogeochemical cycles is very significant therefore it is of great concern to access such fluxes (Downing et al., 2006; Mendonça et al., 2017).

Though the resulting fast spatio-temporal dynamics of the benthic flux is still a challenge to be measured, several techniques are employed to measure benthic fluxes (Viollier et al., 2003). All of them have some kind of limitation so that they cannot cover all the drivers simultaneously. The benthic chambers and the passive samplers (e.g., diffusive gradients in thin films (DGT) and diffusive equilibration in thin films (DET) (Huang et al., 2019)) have limited spatial representation. Both techniques quantify fluxes for a few square centimetres of the sediment surface. For instance, a sediment in which the organic matter is not homogeneously distributed lead to biased flux measured by those techniques. Or even, these techniques cannot measure a sediment covered by gravel. Additionally, the temporal resolution of the fluxes is also limited. These techniques require at least 6 hours of measurement to measure and average the flux. As mentioned earlier, algal blooms can have a time scale

of very few days. Therefore, better temporal resolution can improve knowledge of the triggers and processes of such an event.

Another issue concerns the hydrodynamics contribution to the fluxes. Turbulence is a strong driver of the short-term dynamics of, for example, oxygen fluxes (McGinnis et al., 2008; Murniati et al., 2015). Turbulence determines the thickness of the benthic boundary layer was first theoretically demonstrated (Boudreau and Jørgensen, 2001) and then empirically measured (Lorke and Peeters, 2006). The thickness of the diffusive boundary sub-layer (bottom sub-layer of the benthic boundary layer) decreases when the friction velocity due to near-bed currents increases, and, thus increase oxygen supply to the sediment. The aquatic eddy covariance (EC) is the only technique capable of assessing such fast turbulence-driven dynamics (Berg et al., 2022). The spatial representation of the flux is better than for the previously quoted techniques due to a larger footprint, i.e., the sediment surface that contributes to the flux (Berg et al., 2007; Rheuban and Berg, 2013). However, the lack of fast sensors for most compounds limits the technique to the measurements of oxygen, heat, particles, nitrate and alkalinity fluxes.

Micrometeorologists have overcome this barrier by developing the relaxed eddy accumulation (REA) technique (Desjardins, 1977; Hicks and McMillen, 1984; Baldocchi, 2014). REA consists of a sampling conditioned by the direction of the turbulent fluctuation of the vertical velocity (Bowling et al., 1998). During accumulation periods sample pairs are accumulated separately for updrafts and downdrafts. The benthic flux is thus proportional to the concentration difference between simultaneous samples and increases with turbulence. The theoretical feasibility of adapting REA to aquatic environments has been proven (Lemaire et al., 2017).

Measured oxygen fluxes presents a very dynamic short temporal variation. The nutrient and metallic ion fluxes are very likely to follow similar fast dynamic, also driven by the turbulence. The application of REA can be suitable to track the turbulence contribution to these fluxes. The main question of this work is based on the influence of turbulence on the spatio-temporal dynamics of benthic fluxes, other than those measured by EC, using REA.

This thesis is divided into four chapters followed by conclusions and perspectives. The chapters are: a literature review opening on the research objectives, the development of a REA prototype, the technical validation of the REA technique and its use to characterise the dynamics of benthic fluxes of nutrients and metallic ions of REA to explore in a natural aquatic environment, a shallow lake.

The literature review presents the biogeochemical cycles in the natural aquatic environment that we aim to assess by REA, the drivers of benthic flux and the main techniques for quantifying benthic fluxes and ends with the research objectives.

REA is presented as a promising technique in aquatic environment to overcome the limitations of other techniques. The steps in the development of a prototype based on REA principles are presented in the second chapter. Various technical challenges were addressed through tests and simulations in order to develop a robust and reliable prototype capable of meeting the specifications set by the basic principles of the technique. An automation system was developed to process the velocity data and drive the conditional sampling of REA.

The third chapter deals with the technical validation of the REA with a reference method, namely the eddy covariance (EC) and with the range of hydrodynamic conditions for a proper use of the technique.

In the fourth chapter, the potential of two innovative techniques to measure turbulent benthic fluxes, including REA, is assessed and compared to two well-established ones, eddy covariance and diffusive gradients in thin films in sediment cores.

The main conclusions and perspectives of this work are presented by the end of this document.

2 LITERATURE REVIEW

In this section the literature review is presented. The objective is to understand the role of the sediments on the biogeochemical cycles of aquatic systems and the drivers of the benthic fluxes. But also, to find and present limitations of the techniques used to measure these fluxes concerning spatio-temporal scales. This chapter is separated on three parts: the oxidative state of the main biogeochemical cycles and main paths and kinetics; the spatio-temporal drivers of fluxes in rivers and lakes; and finally, the main techniques and approaches on resolving the benthic fluxes.

2.1 BIOGEOCHEMICAL CYCLES IN INLAND AQUATIC SYSTEMS AND THE ROLE OF SEDIMENTS

Worldwide, the dynamics of **freshwater quality deterioration** is driven by industrialization, urbanization, agriculture and aquiculture in different territories (Mateo-Sagasta et al., 2017). The examples of the effects of the anthropisation are numerous. The watershed of the Lake Boste in China has undergone intense dynamics of land use change and industrialisation over the past 50 years. During that period the lake changed status from freshwater to oligosalt (Tang et al., 2012; Zhang et al., 2019). Camara et al., (2019) present feedbacks of the fast economic development of Malaysia on physical (silting), chemical (P and N high input) and biological (biodiversity loss) parameters of freshwater (Figure 1) . Problems with poor water quality lead to concerns related to human health, costs on water treatment, water availability, etc. (Dearmont et al., 1998; Ebenstein, 2012; Price and Heberling, 2018).

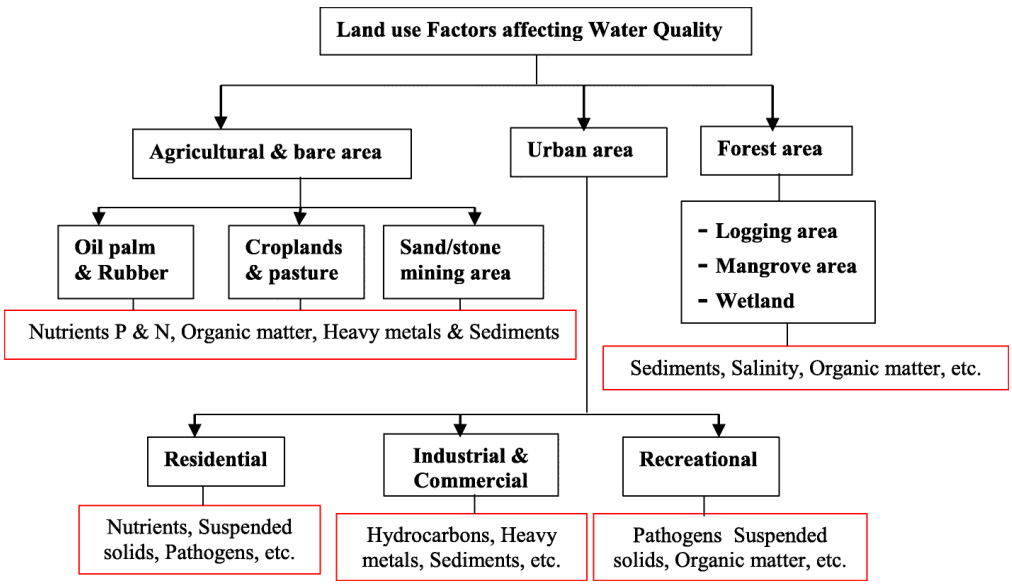

Figure 1 - Main resulting issues concerning the effects of land use on freshwater quality in Malaysia (Camara et al., 2019).

In Europe, late 1970's environmental policies advocate on good practices to **reduce pollutants input into freshwaters**. In the lower Seine River in France, for instance, rates of ammonium and phosphate significantly improved since the creation of specific European and French regulations (Romero et al., 2016). However, after a reduction of nutrients input some waterbodies presented **slow reduction of**

nutrient concentration in the water (Sas, 1990; Welch and Cooke, 1995; Søndergaard, 2007). Years of bad water quality intensify the biogeochemical cycles through the high loading of particulate organic matter and nutrients into the sediments of rivers, lakes and estuaries (Ruiz-Fernández et al., 2002; Ni et al., 2015; Wang et al., 2021). The organic matter (OM) present in the sediment when mineralized by the benthic community release nutrients in the reduced state to the sediment pore water. These nutrients are potentially released to the water column via benthic fluxes.

2.1.1 Organic matter dynamics and its early dynamics

The quantity and type of OM in the sediment is heterogeneous and resulting fluxes tends to be spatially diverse. The OM source and sedimentation are important drivers on this context. The OM entry in an aquatic ecosystem follow **autochthonous and/or allochthonous paths**. Autochthonous is an internal recirculation of OM, nutrient or metallic ions. Generally, they are less resistant to oxidation. Allochthonous concerns external input of OM, nutrients or metallic ions to a waterbody (Wetzel, 2001). Natural autochthonous input of OM covers mostly algae, zooplanktons, while natural allochthonous input of OM covers rest of plants.

In lakes, **sedimentation rates**, for allochthonous and autochthonous paths can vary according to the trophic state of the water body and the quality of inflow waters (Meyers and Teranes, 2001). For instance, the sedimentation rate of particulate organic matter (POM) in the late 90's in the eutrophic Lake Võrtsjärv (Estonia), was in average 1.7 g m^{-2} day^{-1} (Nõges et al., 1999). Another example is the Lake Superior (USA), the largest and deeper oligotrophic lake in the world. The settling rate of POM there in the 2000's was around 0.2 g m^{-2} day^{-1} (McManus et al., 2003). The two fates of the OM deposited in the sediment is **mineralization or burial**. Brady et al., (2013) presents on their biogeochemical model for benthic fluxes an idea of the POM variety on the sediment. They classified the POM into three groups according to mineralization decay: Labile, with a decay rate 1/20 day^{-1}; Semi-labile, medium reactive with a decay rate 1/365 day^{-1}; refractory. For example, biodegradation of lignified materials is a two-stage process: early for fungal species and late for bacteria. The first stage is responsible for the degradation of the less refractory components and the second stage for the more refractory ones. On the other hand, non-vascular plants (e.g., phytoplankton) on the sediment are more easily degradable by bacteria than vascularized plants (Bauerfeind, 1985; Meyers and Teranes, 2001).

The OM labile and semi-labile fractions on the sediment passes through a series of physical, biological and chemical processes, so called early diagenesis (Henrichs, 1992). It occurs in function of the benthic community present on the sediment, in which do not necessarily vary with seasonality, the bacteria growth rate and the salinity and temperature of the water (Peleg, 1996; Pepper et al., 2011; Tšertova et al., 2011; Li et al., 2022). The OM mineralization is largely executed by the microbiological community inhabiting the sediment to gain energy using electron acceptors (Jørgensen and Kasten, 2006). The **cascade of electron acceptors** used relies on its availability but also energy production per quantity of

OM oxidized. The preference follows: dissolved oxygen, nitrate, ferric oxyhydroxide, manganese dioxide, sulphate and CO_2 (Froelich et al., 1979; Thomsen et al., 2004) (Figure 3B).

2.1.2 Oxygen dynamics in different waterbodies

The most demanded electron acceptor in the sediment is the **oxygen**. Its **input into inland water bodies** comes strictly from two sources: the air-water interface and the internal photosynthetic activity. Dissolution has a series of mechanisms depending on, water temperature, pH and salinity, which trigger oxygen solubility, as well as chemical and biological processes and finally the effect of turbulence in water surface and subsurface, related to the diffusion of the gases (Holley, 1977; Berg and Pace, 2017). Photosynthesis rate is seasonal depending on conditions for photosynthetic organisms to develop like: water temperature, concentration of nutrients, turbidity, competition for resources and depth (Dar et al., 2014). Macrophytes, for instance, tends to be denser in shallow lakes or shallow areas of deep lakes (Lewerentz et al., 2021). Oxygen enrichment of the water column through photosynthesis can reach important levels in some waterbody types. For instance, Andersen et al. (2017) measured 200% of O_2 saturation in the top and middle of the water column during the summer of 2016 on four shallow lakes (0.24 – 0.4 m depth) at Öland in Sweden.

The oxygen supply by the water column and the oxygen demand by the sediment often has not similar time-scales. The supply is often limited during high benthic activity. Limiting oxygen supply produces a gradient between the sediment sub-surface (anoxic) and water column (oxic).

In fact, the oxygen penetration into the sediment relies on different parameters related to waterbody trophic state (Figure 2), OM concentration in the sediment, sediment grain size and shape and bed currents (Nøhr Glud et al., 1994; Brune et al., 2000; Jørgensen and Kasten, 2006; Lorke and Peeters, 2006; Ahmerkamp et al., 2020). A sandy soil, for instance, is less demanding of oxygen than a sediment rich in organic matter, leading to different expected scales of oxygen demand (Thomann and Mueller, 1987).

A positive correlation is found between oxygen availability in the water column and its uptake by sediments in relation to the **seasonality** of temperature over the year, when the thermal stratification (presented on subsection 5.2.1) in lakes is not permanent (Gallagher and Daiber, 1974; Hargrave, 1969; Zhang et al., 2013; Rajwa-Kuligiewicz et al., 2015). Oxygen availability varies rapidly in the daily scale in well homogenized environments like rivers and streams (Berg et al., 2013).

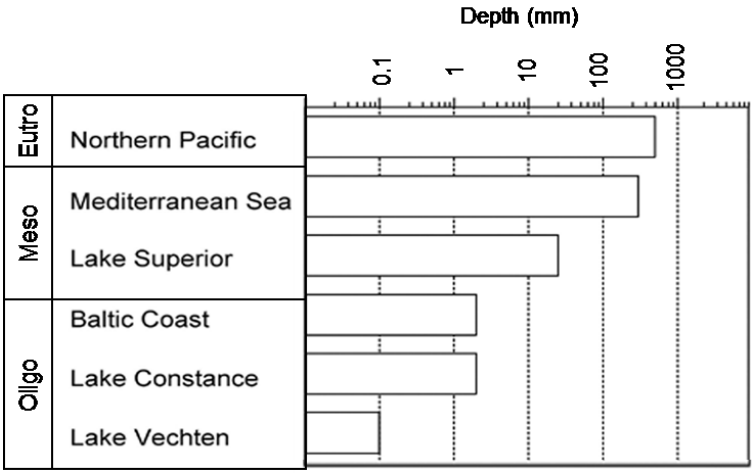

Figure 2 - Oxygen penetration on different trophic states of the waterbodies. Lake Vechten, Mediterranean Sean and Lake Superior are oligotrophic. Baltic Coast and Lake Constance are mesotrophic. Northern Pacific is eutrophic. (Brune et al., 2000).

The seasonal or perennial aquatic fauna and flora present in the pelagic and in the benthic zone in natural waterbodies influences the oxygen dynamics. For instance, the roots of aquatic macrophytes increase oxygen penetration in the sediment and the irrigation and bioturbation in the sediment sub-surface create oxic pools (Wang, 1981; Brune et al., 2000; Bloesch, 2009).

The importance of the oxygen availability impacts the oxidative state of the sediment as well as the OM mineralization rates. Therefore, its importance on the main oxidative states of the biogeochemical cycles is direct.

2.1.3 Main oxidative and reducing paths of biogeochemical cycles

On this section some biogeochemical cycles are presented as well as some reaction kinetics on different oxic states. The compounds were selected according to the importance and scope of the work developed here.

2.1.3.1 Nitrogen

The POM deposition on the sediment feeds main biogeochemical cycles in aquatic environments. In the nitrogen cycle **heterotrophic bacteria decompose nitrogenous compounds** (e.g., proteins, aminoacids, etc.) in the sediment sub-surface (Wetzel, 2001). In the upper parts of the sediment (suboxic zone) the oxygen availability and concentration governs **ammonification** ($N_{org} \rightarrow NH_4^+$) whereas in the lower parts it is the sulphate availability. The oxi-reduction kinetics of the reactions gives the rates and time scales of the reactions. Wong-Chong and Loehr, (1975) present in their article the **kinetics** of ammonification under laboratory conditions which, O is the convertible fraction of the organic nitrogen and k_1 the average kinetics (0.1 h^{-1}) at pH ranging from 6.5 to 8. Higher pH (>7) lead to smaller k_1 (0.08 h^{-1}).

$$\frac{dO}{dt} = -k_1 O \qquad \text{(Eq. 1)}$$

A biogeochemical model approach from Vanderborght et al., (1977) presented ammonification rate in the oxic/hypoxic zone of 6 $mmol.m^{-2}.day^{-1}$ and in the anoxic zone of 0.7 $mmol.m^{-2}.day^{-1}$ containing 100% dissolved oxygen at the sediment-water interface. In both examples temperature, pH and oxygen content plays an important role in the ammonium accumulation in the pore water.

Pauer and Auer, (2000) find that most of the **nitrification** occured in the upper parts of the sediment. Low nitrifying bacteria is found in the water column in contrast to observations on sediment. Under oxic environment, *Nitrosomonas* and *Nitrobacter* oxidize ammonium into nitrite and then nitrate. Briefly, two moles of oxygen are required to oxidize the ammonium into nitrate.

$$NH_4^+ + 2O_2 \rightarrow 2H^+ + NO_3^- + H_2O \qquad \text{(Eq. 2)}$$

In laboratory experiments, ammonium genesis is relatively faster than nitrification, with the maximum concentration reached by nitrate in twice the time of ammonification (Wong-Chong and Loehr, 1975).

Nitrate in the water column is either consumed by microorganisms or macro-organisms present in the waterbody or to be **denitrified**. The latter aerobically or anaerobically reduction of nitrate in suboxic environment ($\leq$ 0.2 mg O_2 L^{-1}) by enzyme nitrogen reductase leads to N_2O and to N_2 (Wetzel, 2001). Denitrification requires organic carbon, and thus the C:N ratio is a key parameter in the reaction. The kinetics in the sediments is uncertain given the lack of knowledge in some steps to the N_2 production (Seitzinger et al., 2006).

$$C_6H_{12}O_6 + 12NO_3^- \leftrightharpoons 12NO_2^- + 6CO_2 + 6H_2O$$
$$C_6H_{12}O_6 + 8NO_2^- \leftrightharpoons 4N_2 + 2CO_2 + 4CO_3^{2-} + 6H_2O \qquad \text{(Eq. 3,4)}$$

The main product of denitrification depends on the water temperature: N_2 dominates at high temperatures and N_2O dominates at low temperatures. The latter is an important greenhouse gas on which, can be released from the sediment to the atmosphere (Dawson and Murphy, 1972).

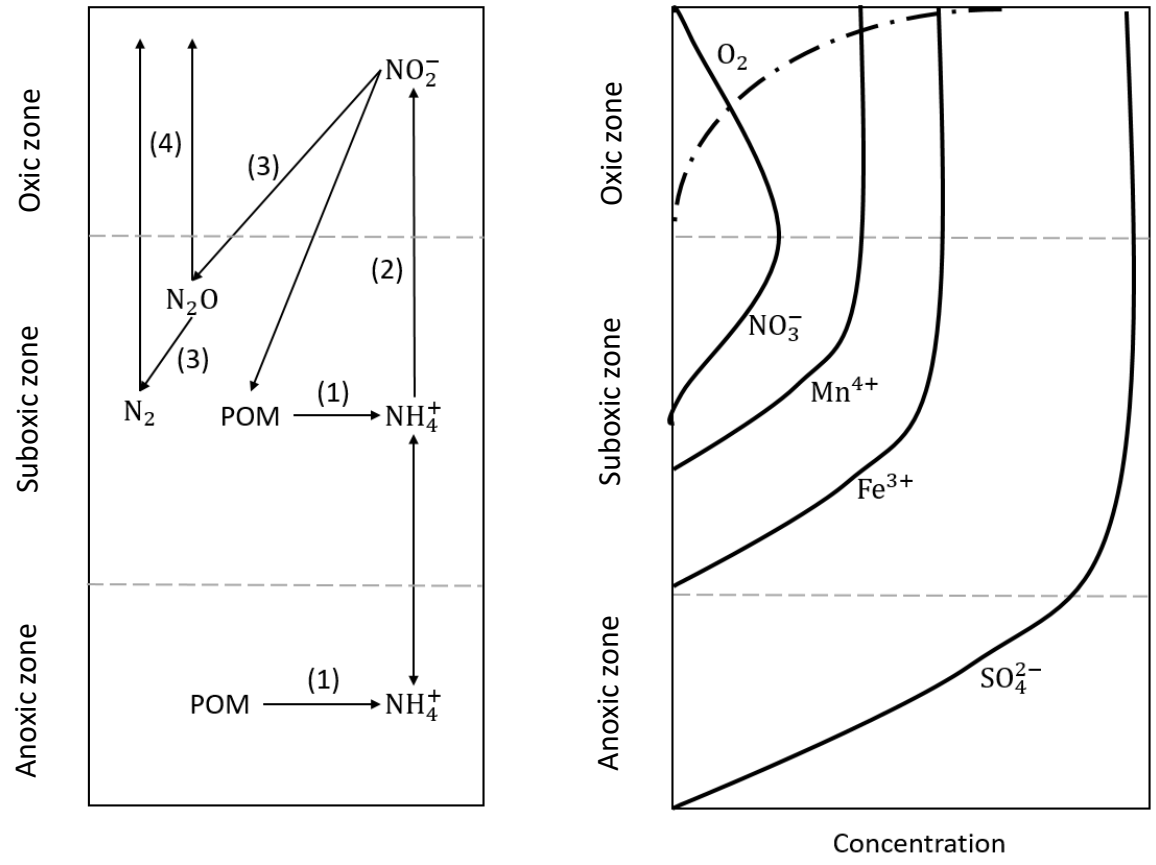

Figure 3 - On the left-hand side the different N-cycle paths in different oxidative states: (1) Ammonification; (2) Nitrification; (3) Denitrification; (4) Nitrogen loss. On the right-hand side the idealized representation of electron acceptors on every oxidative state of the sediment (after Kristensen, 2000).

2.1.3.2 Phosphorus

Phosphorus cycle is more complex than nitrogen. In the pelagic and benthic zones, the main oxidative state of phosphorus is soluble reactive phosphorus (SRP). Depending on the pH, Phosphate (PO_4^{3-}) at neutral or orthophosphoric acid (HPO_4^{3-}) at acid are observed. The input of organic and inorganic phosphorus in the sediment has multiple paths as well as multiple forms (Syers et al., 1973; Søndergaard, 2007a; Reitzel et al., 2012). The slow decomposition of inorganic and organic compounds is very likely to promote phosphate release, within other forms, in pore water (Gomez et al., 1998). Some P forms directly settle to the sediment or after OM mineralization are refractory, and can resist degradation resulting in permanent burial in the sediment (Reitzel et al., 2012). The bacterial activity is a great engine in the phosphorus cycle by increasing availability of dissolved phosphorus in pore water or accumulating it as polyphosphate (Wetzel, 2001). The adsorption by POM and consumption by benthic microorganisms are two mechanisms preventing soluble phosphate diffusion within the pore water towards the water column (Gächter and Meyer, 1993).

In hard water lake the sorption and adsorption of phosphate on $CaCO_3$ is often observed limiting P release of the sediment or even triggering particulate phosphorus sedimentation (Jacobsen, 1978).

In the sediment iron interacts with phosphorus and regulates P fluxes. High redox potential leads to binding of ferric iron with phosphate, while low redox potential favours ferrous iron and prevents P-binding. Therefore, net P release into the water column is low when Fe:P ratio is high (Jensen et al., 1992).

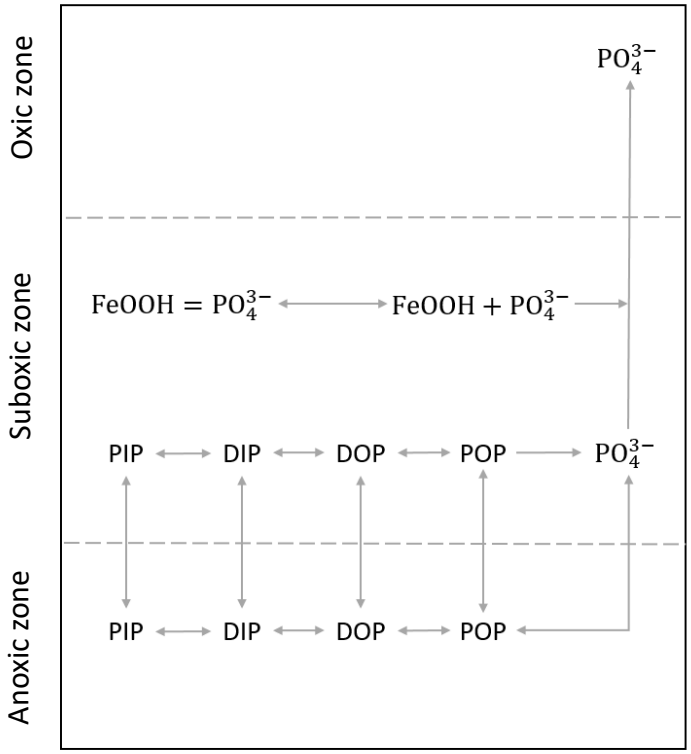

Figure 4 - P-cycle paths in different oxidative states mainly driven by bacterial activity (Adapted from Gächter & Meyer, 1993)

In shallow lakes, phosphorus concentrations in the sediment are more than 100 times higher than in the water column therefore it can lead to high fluxes. When turbidity is low several mechanisms are involved in phosphorus retention including the reduced sedimentation of organic matter, which reduces oxygen consumption and prevents low redox conditions (Søndergaard et al., 2003).

2.1.3.3 Iron

A very important driver of the iron oxidative state is the redox potential and the pH of the water body. In reduced environments prevails ferrous iron (Fe(II)) and in oxidative environment the ferric iron is favoured (Fe(III)) (Figure 5) (Berry, 1950; Stumm and Lee, 1960). The redox potential (Eh) is not very influenced by temperature but by the concentration of dissolved oxygen. The more oxidative form of Iron is the ferrihydrite ($Fe(OH)_2$), which is largely found in the water column (Canfield et al., 2005a). At neutral pH, when iron oxides present in clay reaches suboxic/anoxic zones of the sediment, they are oxidized by bacteria used as electron acceptor. Resulting ferrous irons is accumulated in the sediment of natural environments (Kostka et al., 1995; König et al., 1997; Thamdrup, 2000).

$$4Fe^{2+} + O_2 + 4H^+ \rightarrow 4Fe^{3+} + 2H_2O \quad \text{(Eq. 5)}$$

When the oxygen concentration is low in the water-sediment interface great concentrations of ferrous ions is found on the sediment. In deep layers of the sediment, where the potential redox is low and the environment is anaerobic, bacterial activity reduces sulphate to sulphide which in excess decreases Fe(II) concentration, forming pyrite (FeS_2) (Schieber, 2011).

The water hardness also plays on the availability of the Iron. In hard water Fe(II) availability is controlled by the solubility of siderite ($FeCO_3$). Greater concentrations of Fe(II) is expected in soft waters (low concentrations of $CaCO_3$) (Nealson and Saffarini, 1994).

Davison, (1993) presents a kinetic (k) of 6.3 10^{-17} M^{-3} min^{-1} for

$$\frac{d[\text{Fe(II)}]}{dt} = k[\text{Fe(II)}]pO_2(OH^-)^2 \quad \text{(Eq. 6)}$$

leading to half-life of Fe(II) on different hardness, temperature and pH of water. On neutral pH and in soft water, the half-life is shorter than for hard water, respectively, 1.8 and 3.8 min at 10°C and 0.27 and 0.55 min at 20°C.

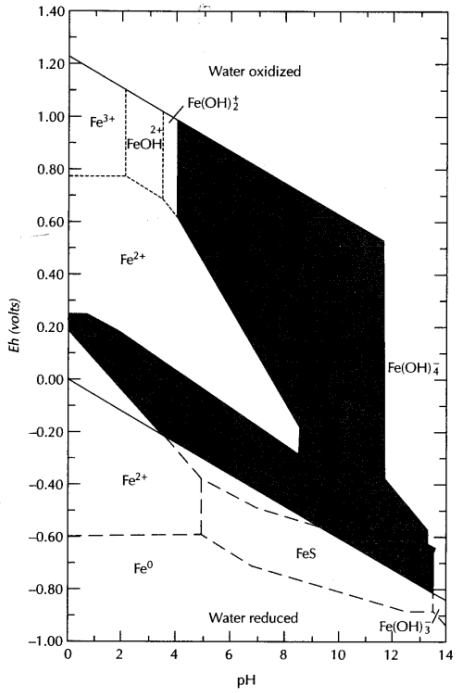

Figure 5 - Different forms of Iron in function of the redox-potential and pH (Fetter, 2018).

2.1.3.4 *Manganese*

The input of iron in an aquatic system is linked to the erosion of iron-rich clay particles or to the nature of waterbody bedrock. Manganese has the same input sources. There are two forms of Mn and Fe reaching the sediment: free oxide and silicates (Canfield et al., 2005a).

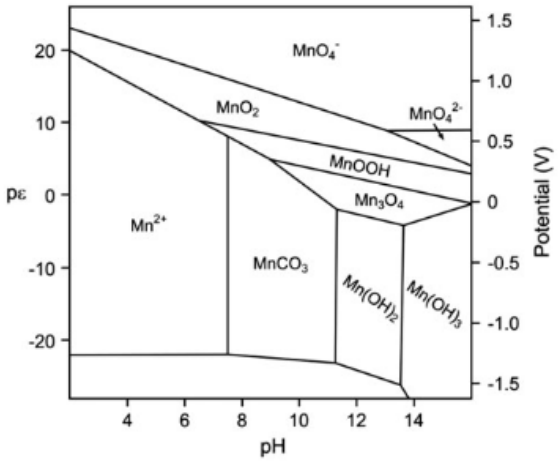

Figure 6 - Different forms of Manganese according to electron activity (pε), pH and redox-potential (Bruins et al., 2014).

Different oxidative states of the manganese are described in aquatic environments (e.g., Mn(II), Mn(IV) and vernadite (δ-$Mn0_2$)) (Vitre and Davison, 1993; Straub et al., 1996). The Mn(II) is largely present on very reduced environments whereas in oxidative environments Mn(IV) is more present (Figure 6). The manganese oxidation (Mn(II)→Mn(IV)) due to microbial activity is much slower than manganese reduction (Mn(IV)→Mn(II)) (Bruins et al., 2014). Mn(II) oxidation is also a much slower reaction than Fe(II) oxidation at neutral pH and its half-life reaches some months (Stumm and Morgan, 1981). Davison, (1993) presents the oxidation equation of manganese and the kinetics (k) is 10^{18} $M^{-4}.day^{-1}$.

$$\frac{-d\mathrm{Mn(II)}}{dt} = k[\mathrm{Mn(II)}][\mathrm{O_2}](\mathrm{OH^-})^2(\mathrm{MnO_2})\mathrm{s}$$
$$\frac{-d\mathrm{Mn(II)}}{dt} = k[\mathrm{Mn(II)}][\mathrm{O_2}](\mathrm{OH^-})^2(\gamma\mathrm{FeOOH})\mathrm{s} \quad \text{(Eq. 7, 8)}$$

2.1.3.5 *Sulphate*

The sulphate cycle is studied since the late XIX century trough the discovery of the Sulphate Reducing Bacteria (SRB) (Drews, 2000). The vertical distribution of SRB in the sediment finds peak in the hypoxic and anoxic zones of the sediment. In those zones the SRB uses sulphate as electron acceptor to mineralize the OM (Holmer and Storkholm, 2001). The complete reduction of sulphate by SRB leads to hydrogen sulphide (H_2S) in anoxic environments. Several oxidation steps take place in suboxic and anoxic zones with sulphur intermediates, sulphur (S^0), thiosulfate ($S_2O_3^{2-}$), tetrathionate ($S_4O_6^{2-}$) and sulfite (SO_3^{2-}) until the sulfate release to the oxic zone (Jørgensen et al., 2019).

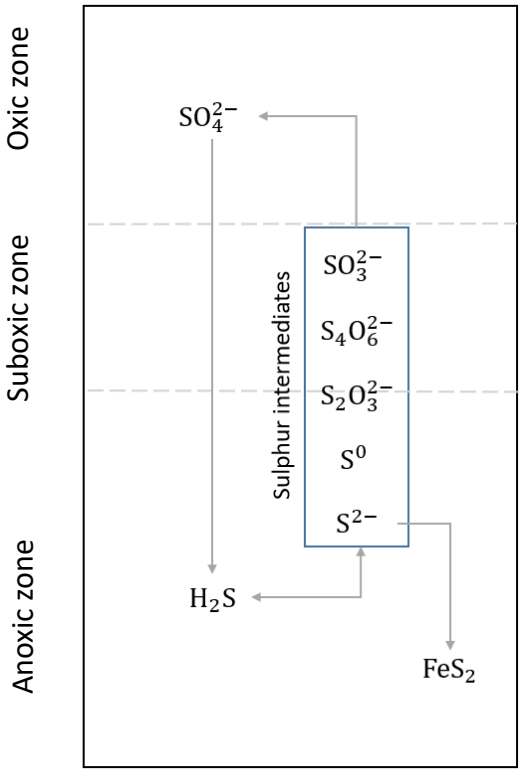

Figure 7 - Sulphur cycle over the different reducing and oxidizing environments. (Modified from Holmer and Storkholm, (2001) and Jørgensen et. al, (2019)).

The main reactions and kinetics are still surrounded by uncertainties, especially in relation to the presence of oxygen and buried Fe(III) (Jørgensen, 1982). In anoxic zone, the main burial of sulphur can occur when sulphide reacts with buried Fe(II) forming iron sulphide (FeS) and pyrite (FeS_2) (Canfield et al., 2005b).

$$FeS + H_2S \rightarrow FeS_2 + H_2$$
$$FeS + S_x^{2-} \rightarrow FeS_2 + S_{x-1}^{2-} \quad \text{(Eq. 9, 10)}$$

Sulphate is used as electron acceptor by the benthic community in anoxic zones. Thus, the flux is normally from the water column towards the sediment.

The presented elements spotted uncertainties and kinetics of the paths of the main biogeochemical cycles. A few conclusions can be taken concerning the benthic fluxes. The oxygen, when towards the sediment, will not necessarily reply to a direct positive or negative feedback from nutrients or metallic ions flux. The ammonium and phosphate fluxes, for instance, are linked to the OM mineralization. The aerobic degradation of the OM accelerates ammonification and phosphate concentration in the pore water. They are transported by diffusion until the sediment surface. Specifically, the phosphate flux can find transport obstacles (consumption by microorganisms and binding with iron). Ammonium flux in the very surface of the sediment can pass through nitrification. Iron (II) and manganese (II) are released from the sediment in sub-oxic environments and their oxidation can be inevitable. Sulphate largely present in the water column feeds the deep layers of the sediment and participated in the OM mineralization in anoxic environments.

Several are the parameters governing the cycles and some of them were already resolved. For instance, the fluxes of oxygen are not directly related to fluxes of the other compounds. So, can oxygen fluxes create an indirect feedback on the fluxes of other compounds? What is their temporal variation?

2.2 SPATIAL AND TEMPORAL DRIVERS INFLUENCING THE BENTHIC FLUXES DYNAMICS

The previous sub-chapter enlightened some of the main paths and drivers of the biogeochemical cycles in freshwater aquatic systems. Special attention was given to the redox potential of the environment.

An important concept for this sub-chapter is the benthic fluxes. The aquatic ecosystems are divided in pelagic and benthic zones. Roughly, the benthic zone corresponds to the waters overlying the sediment (King, 2011) and the rest is considered as the pelagic zone. Benthic fluxes are the results of the interaction of the sediment and water column. Here the spatio-temporal drivers of the benthic fluxes are investigated on different waterbodies types. It allows us to understand if there is a potential spatio-temporal variation of the fluxes.

2.2.1 Oxic-anoxic boundary dynamics and drivers on aquatic environments

OM mineralization relies on the electron acceptor presence in the SWI and in the first layers of the sediment sub-surface. Oxygen is the most effective electron acceptor and its use relies on its supply from sediment overlying water. Hourly oxygen consumption used to OM mineralization will lead, for instance, to reduced forms of nutrients (e.g., Ammonium). These nutrient are often driven from the pore water towards the water column. They will not necessarily be directly related to the oxygen fluxes. A temporal variation of the nutrient and metallic ion fluxes will rely on the concentrations on the pore water.

A deeper look in the various temporal variations of the oxygen concentration and availability allows to understand the nutrient dynamics in the sediment. The first important concept is the oxic-anoxic boundary or interface. It is the oxygen gradient slope between the oxic and the hypoxic/anoxic zones

(Wetzel, 2001). The distance and position of this interface, regarding the sediment surface, is not constant and its dynamics varies with regarding some parameter.

I**n streams,** rivers **and lakes**, the spatial variation of oxygen uptake by the sediments can be high. Particles (e.g., POM or minerals) are not accumulated evenly on the bed. Different grain size, morphology and source has different impacts of sedimentation dynamics and also in the waterbody biogeochemistry (Thoms, 1987; Stone and Droppo, 1994; Stutter et al., 2021). Debris accumulation in running waters mainly relies on the river and stream line complexity, macrophytes presence, slope, secondary currents and sediment grain size (Richards, 2004; Sukhodolov et al., 2009; Sukhodolov and Sukhodolova, 2010).

A common mistake is to assume sedimentation hotspots are only related to slow currents (Wood and Armitage, 1997) for instance, the Hjulström-Sundborg diagram. The diagram uses as parameters the flow speed and particle size to determine particles fate: erosion, transportation or deposition. In fact, the sedimentation dynamics can be relied to when traction force is smaller than gravity force (Richards, 2004). For the resuspension and the sediment transport, Shields, (1936) proposes the influence of bed-shear to the sedimentary dynamics. The proposed Shields curve, a threshold of grain movement, takes into account the Boundary Reynolds Number (Re_*) and the Dimensionless shear stress ($\tau *_c$) (Graf and Mortimer, 1979):

$$Re_* = \frac{u_{*c} D}{\nu}$$
$$\tau *_c = \frac{\tau_c}{(\gamma_s - \gamma) D} \qquad \text{(Eq. 11, 12)}$$

where u_{*c} is the critical shear velocity, D the particle diameter, ν the kinematic viscosity, γ_s is the sediment specific weight (density of the sediment particle), γ water specific weight and τ_c the critical shear stress. Roughly speaking, the flow velocity plays on the friction velocity and on the traction force. The bed current is not constant within complex architecture of the bed of the waterbody. It leads to different spatial residence time (Sukhodolov et al., 2009). Thus, different settling and resuspension of particles promoting spatial variability of sediment presence and, as well as, on the sediment thickness.

In streams and rivers, the residence time promotes different oxygen behaviour by sediment uptake or photosynthetic activity (Baker et al., 2000). In addition, oxic pools can be find in different depths on sediment profile in function of the grain size profile (Figure 8). In function of the texture profile, running water can pass through large pores in the sediment promoting the oxic pools. However, porosity in river sediment is temporally variable as fine sediment can settle within large sediment pores and clog it.

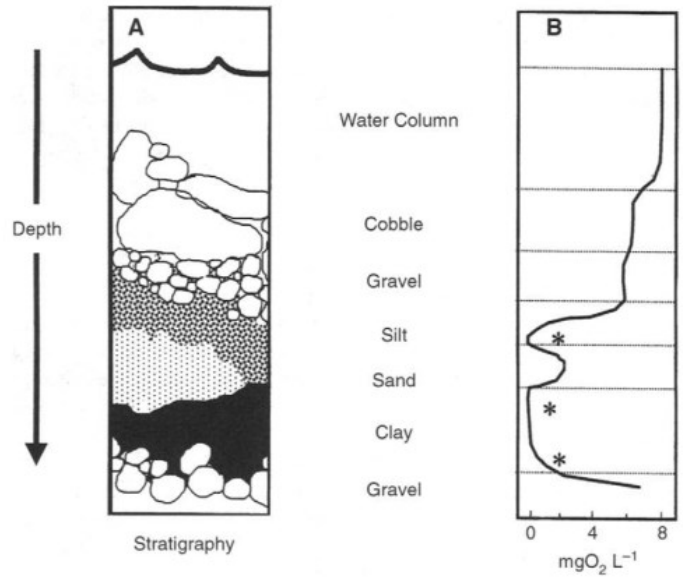

Figure 8 - Texture profile of an ideal sediment profile (left-hand side) and resulting oxic-anoxic interfaces (* in the right-hand side) (Baker et al., 2000).

In lakes the oxic-anoxic boundary dynamics relies on different parameters. The water temperature is one of them. Energy input comes specifically from solar radiation and air temperature. The wind friction on the water surface homogenizes temperature in the epilimnion (the upper part of the lake water column) (Figure 9). The thermal stratification of lakes is widely described in the literature (Reviewed at Boehrer and Schultze, 2008). The phenomenon occurs in shallow and deep lakes. During the warm seasons of the year, the heat input is not homogeneous in the vertical axis of the water bodies. Layers of different density and viscosity are formed within the water column. Upper layers are warmer and less dense than lower ones.

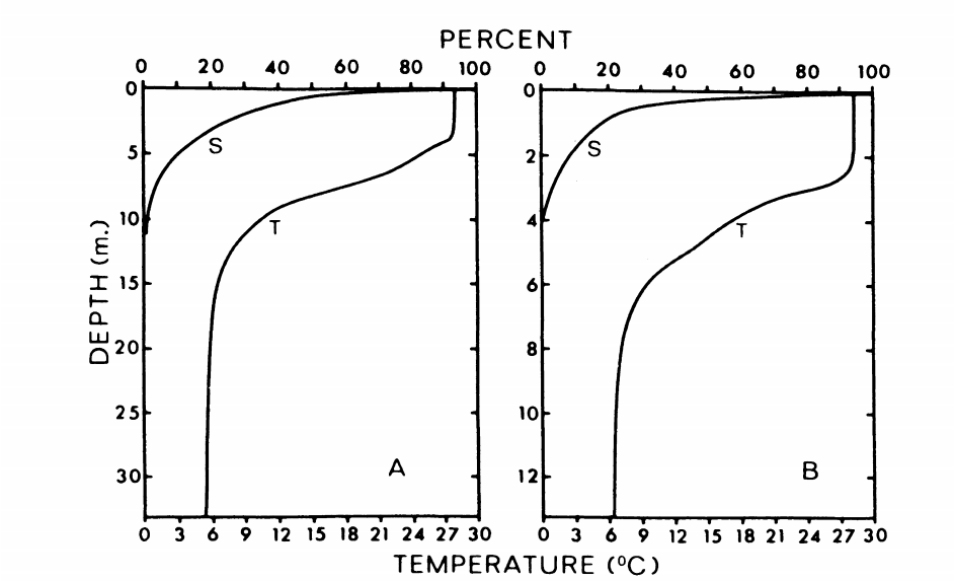

Figure 9 - Temperature (T) and solar radiation (S) profiles in Crooked Lake (A) and Little Crooked Lake (USA) during July 1964. Respective, surface areas are 79 ha and 5.3 ha. (Wetzel, 2001, using Wetzel, unpublished data)

The stability if the thermal stratification of a lake is in function of the temperature gradient. Idso, (1973) presents adapted Schmidt stability to quantify required energy to break the thermal stability of a lake. It takes into account the lake depth, volume and area, the gravity and the water density. The thermal stratification dynamics is different from each lake type depending on the local climate, depth and trophic state. For this work we will focus on eutrophic lakes in temperate and sub-temperate zones.

For deep lakes, the stratification dynamics can follow the seasons of the year being permanent during warm seasons (dimictic lakes) or during the whole year (meromictic lakes). Both presents a thermocline. This layer in the water column is where the temperature gradient is sharp. Oxygen cannot diffuse sufficiently through the thermocline. This leads to oxygen depletion in the hypolimnion (bottom waters of the lakes) drive by oxygen uptake by the sediment and respiration of the benthic community. The anoxia stablished in the bottom of the deep lakes is seasonal or permanent in function of the depth. Studies and recordings about this events in deep lakes are not recent (e.g., Smith and Bella, 1973; Golterman, 1975), as well as, the resulting biogeochemical and mixing effects (Vinçon-Leite and Tassin, 1990; Bonhomme et al., 2016; Jézéquel et al., 2016).

For shallow lakes the understanding and studies are more recent. The interest in such waterbody type comes from the large presence in various territories of the northern hemisphere (Verpoorter et al., 2014). In shallow lakes time-scales of the stratification is daily to weekly. For instance, Martinsen et al., (2019) studied nine shallow lakes in Sjælland (Denmark) from October 2015 to October 2016. Average depths of the lakes varied from 0.5 to 2 meters. All nine lakes showed daily thermal stratification during warm season. The deepest lakes of the survey maintained thermal stability for a few days longer compared to shallower lakes. Zdorovennova et al., (2016), studied also the thermal stratification in Lake Vendyurskoe (Russia – average depth 11m). This lake presents less dynamical mixing than the example presented before. On their measurements we can see the effect of the stratification on the oxygen availability (Figure 10). In detail, we can see that during the whole month of July 2013 in that lake the depth of the oxic-anoxic boundary was not constant. When the thermal stratification disrupts the hypolimnion become oxic.

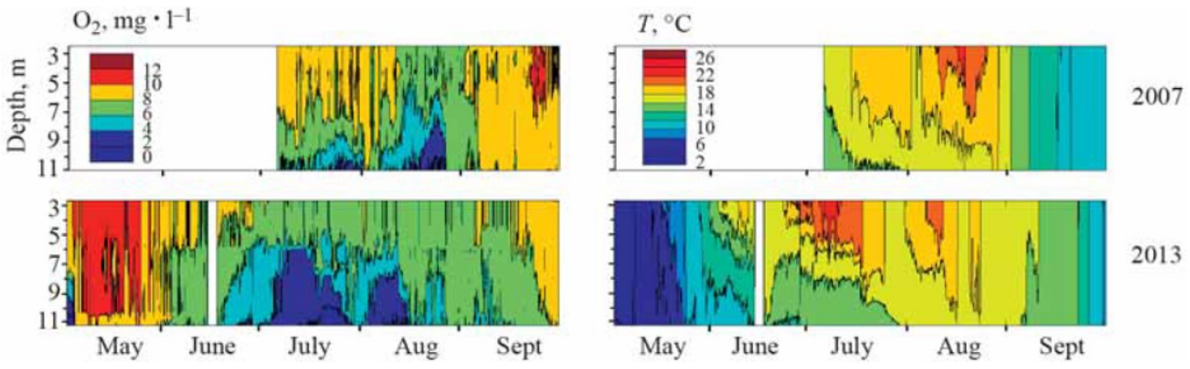

Figure 10 - Seasonal temperature and oxygen profiles in Lake Vendyurskoe (Russia) (Zdorovennova et al., 2016).

D'Autilia et al., (2004) presents measurements in the shallow lagoon Fogliano (Italy) during July 1999 and July 2001 (Average depth 2m). They captured a strong oxygen dynamic varying in 3-8h cycles from minimum of 2 mg l^{-1} to a maximum of 11.5 mg l^{-1}. The oxic-anoxic boundary movement perpendicular to the sediment surface is on the daily scale. This strong day-night variation found is linked to the strong presence of photosynthetic organisms in the waterbody. During day-time the oxygen budget is positive. During night-time the budget is negative. Without sub light the oxygen production stops and the oxygen is depleted by the sediment consumption and respiration.

As highlighted in the previous sub-chapters, the oxygen availability will enhance or prevent certain paths of the biogeochemical cycles in the sediment. The oxic-anoxic boundary dynamics is different on different waterbodies. In streams and rivers, the spatial distribution is major. The oxygen consumption by the sediment relies on the residence time of the overlying water, sediment deposition and erosion. For lakes, the oxic-anoxic boundary can be very stable (meromitic) or very unsteady (shallow lakes). In shallow or very shallow lakes the water temperature changes rapidly (hourly to daily), as well as the oxygen availability. The impacts in the resulting fluxes still uncertain. Changes of the oxygen availability (oxic-anoxic-oxic) presents to disturb the biogeochemical cycles in estuarine sediments (Faganeli and Ogrinc, 2009). So the oxygen temporal dynamics in natural environments can be fast and its consequences on biogeochemical cycles is not empirically known.

2.2.2 Flux drivers of sediment-water interface: highlighting the hydrodynamics

The sediment-water interface, namely, benthic boundary layer (BBL) is formed by three sublayers: diffusive (DBL – closer to the sediment surface), viscous (VBL – on the top of the DBL) and turbulent (TBL – on the top of the VBL). For the first two sublayers the velocity distribution is linear on rigid or smooth surface denoting laminar flow (Lorke and Macintyre, 2009). In the TBL the regime is turbulent. In any spatial scale the sediment-water interface will be submitted to the same characteristics.

Molecular diffusion is often assumed to be dominant transport between sediment and water column, through the BBL. The application of the Fick's First Law (Berner, 1971) is often used to estimate diffusive transport contribution to the fluxes (*F*):

$$F = -\phi D \frac{\partial C}{\partial z} \qquad \text{(Eq. 13)}$$

where, *D* is the diffusion coefficient, ϕ is the sediment porosity and $\partial C/\partial z$ is the concentration gradient (e.g., (Lyons et al., 1982; Hensen et al., 1998)) within the pore water and the VBL. However, Ullman and Aller, (1982), among others, propose that porosity itself can be disturbed in function of geometrical tortuosity (θ) (Figure 11). The tortuosity is the shortest path in a determined length of the sediment (Guo, 2012).

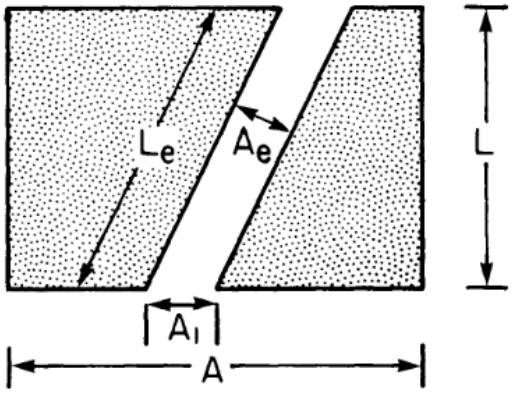

Figure 11 - Model representation of the porosity ($\phi = A_l L/AL$) and tortuosity ($\theta = L_e/L$). The areas of the cross-section are A, A_l, and A_e and the lengths are L and L_e. (Ullman and Aller, 1982)

Thus the application of tortuosity to the Fick's first law gives:

$$F = -\frac{\phi D}{\theta^2}\frac{\partial C}{\partial z} \qquad \text{(Eq. 14)}$$

Tortuosity was already related to the formation factor (f) empirically obtained from electric resistivity and the porosity. However, Boudreau, (1996) presents new insights in a direct approach of tortuosity to porosity.

$$\theta^2 = 1 - \ln(\phi^2) \qquad \text{(Eq. 15)}$$

Another parameter to take into account is the turbulence contribution to the fluxes (Boudreau and Jørgensen, 2001; Wetzel, 2001). The DBL is often the bottleneck in the interactions between sediment and water column. Thicker is the DBL lower is the flux. The thickness (δ_D) of the DBL is related to the bed shear. For this Lorke and Peeters, (2006) presented the application of turbulence effect on the Fick's law through a transfer coefficient (k), and its application to the Fick's law leads to:

$$F = k(C_\infty - C_0)$$
$$k = \frac{D}{\delta_D} \approx \frac{1}{9} Sc^{-1/2} u_* \qquad \text{(Eq. 16, 17)}$$

where Sc is the Schmidt's number, u_* the friction velocity, C_∞ is the compound concentration on the top of the DBL and C_0 is the compound concentration on the bottom of the DBL (Figure 12).

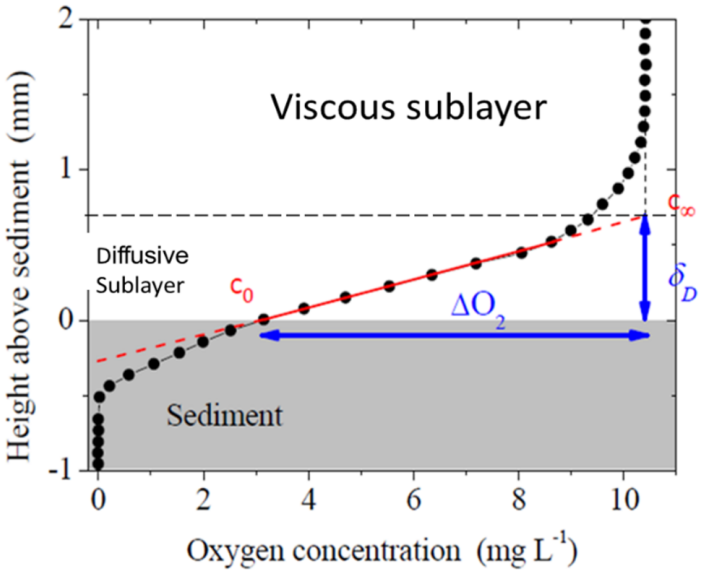

Figure 12 - The oxygen concentration profile at Lake Alpnach (Switzerland) and representation of the sublayers of the BBL. (Adapted from Lorke et al., (2002) and Lorke and Macintyre, (2009))

This new approach gives some new insights in the spatial distribution of the benthic fluxes as bed currents and turbulence are not homogenously distributed in the bed of some waterbodies and neither constant.

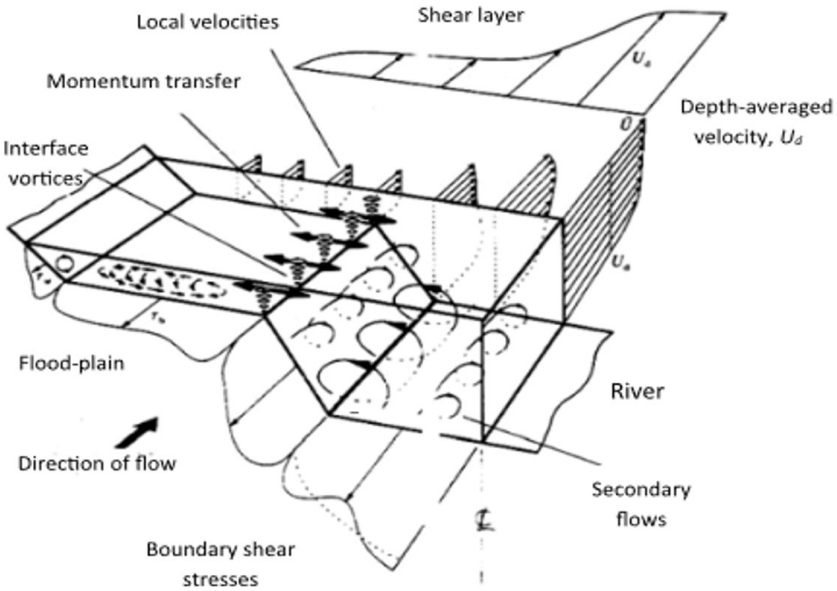

Figure 13 - Different hydrodynamics in the water column of a river cross section. The flow speed variation is considerably low in temporal scale, but in the spatial scale it is notably high (Shiono and Knight, 1991).

In rivers and streams the temporal variation of bed current and turbulence is low, however the spatial heterogeneity is high (Figure 13). In lakes, depth and thermal stratification are factors varying the spatio-temporal intensity of bed currents. The focus here is on shallow lakes, since bed currents in deep lakes are generally weak and producing low-energy turbulence (e.g., Cannon and Troy, (2018)). In shallow

lakes, the stratification disrupts by water surface wind and water and air temperature. When the required work (Schmidt stability index) is not supplied by the surface wind, this one promotes mixing of the hypolimnion inducing currents. Wuest and Lorke, (2003) present extensive considerations regarding energy input into surface layer of lakes resulting on direct turbulence on the BBL (Figure 14). The wind stress, the roughness of water surface, the lake fetch and the surface waves lead to the Stokes drift, the resulting displacement of a fluid parcel. It is an important source of Turbulence Kinetic Energy, as well as wave break and buoyancy flux to the surface layer. When the lake is stratified part of this energy is applied on internal motions and diapycnal mixing (vertical mixing driven by turbulence). These forces induce currents in the bed, in which the sediment imply the energy loss of the eddies. The sediment architecture and lake bathymetry impacts differently the spatial and temporal energy loss of turbulence. The turbulence occurrence in the lake bed is not constant, and nor it is spatially equal. Therefore, the turbulence occurrence is variable in space and time on the benthic zone. As mentioned before, the turbulence affects the thickness of the DBL on different spatio-temporal scale. This affects the oxygen fluxes. They present temporal variation and in correlation with the friction velocity in lakes (McGinnis et al., 2008a; Murniati et al., 2015).

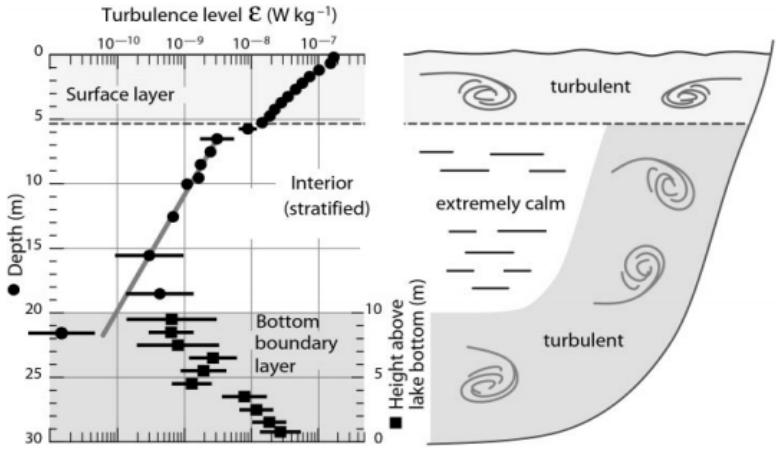

Figure 14 - On the left-hand side the turbulence level (ε – Dissipation of the turbulent kinetic energy) measured through the water column of a medium-size lake. On the right-hand side, the representation of energy transfer from surface layer to bottom boundary layer and both as turbulent zones. (Wuest and Lorke, 2003)

2.2.3 Biological aspects influencing benthic fluxes

Macro and microfauna have important role in the benthic dynamics and consequently to the fluxes. Previously on this work, the importance of bacterial activity in biogeochemical cycles was explained and the role of **macrofauna** was spotlighted. It is responsible for the bioturbation (e.g., fish scraping the sediment) and bioirrigation (e.g., animals buried in tunnels). This terms are widely used in the literature, and, the latest understanding, refers to the resulting effects of the animal community activities in the sediment (Kristensen et al., 2012). Intense bioturbation can lead to changes in the sediment architecture and in the oxygen penetration (Rhoads, 1974). The macrofauna activity promotes an increase of sediment surface area, especially in the first centimetres of sediment. Such activity can alter the oxygen

supply and penetration of oxygen deeper below the sediment surface. This oxygen regime transformation alters the biogeochemistry paths (e.g., Mayer et al., 1995; Aller and Aller, 1998) and the amount of macrofauna biomass is not the only factor contributing to it, but the specificity of the present species (e.g., Norling and Kautsky, 2007; Quintana et al., 2007) and their influence on microorganisms' community (Chen et al., 2017). Bioturbation is not homogenously present in the sediment since it depends on high oxygen availability.

Another structure influencing the fluxes spatial distribution is the **biofilm**. It is a conglomerate or matrix of bacterial and/or unicell algae capable to cover the sediment surface. The heterogeneous species in bacterial biofilms are specialized species and produce adhesive polymers to stick on sediment surface (Stoodley et al., 2002). For algae biofilms diatoms are the mainly present type. Their development in-vitro is fast (11h to double population) if environmental conditions are optimal (Cooksey et al., 1984). The development conditions of this biofilms rely on the light presence and nutrient availability in the water column (Prieto et al., 2016). The impact of the biofilm on biochemical cycles on controlled environments is presented at Woodruff et al., (1999). The study presented: the biofilm impacting the oxic-anoxic interface; Biofilm impacting solutes exchange between sediment and water column (Figure 15).

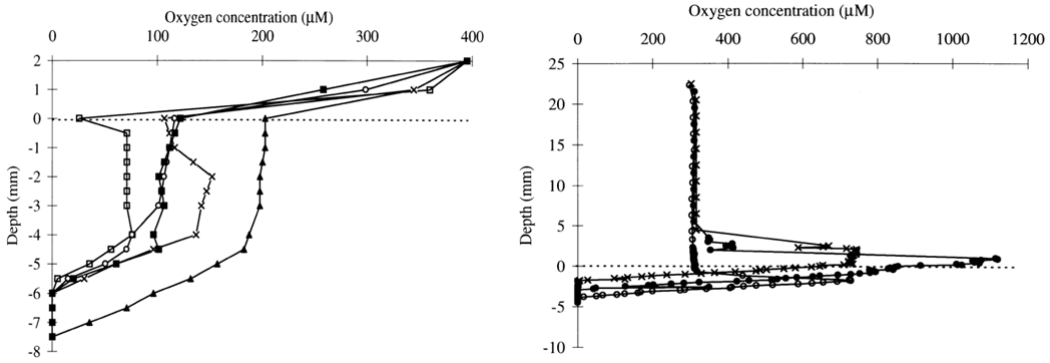

Figure 15 - Oxygen profile executed on different locations of the sediment on surrounding areas of the sediment surface. On the left-hand side the flume was covered and no light was reaching the biofilm. On the right-hand side the flume was exposed to light. (Woodruff et al., 1999)

Macrophytes also impact the fluxes. As mentioned before, their roots promote higher permeability to oxygen penetration. Also, their nutrient uptake occurs directly from pore water removing nutrients from that environment. In addition, dense macrophyte zone changes the hydrodynamics and thus the attenuation of turbulence to the fluxes. Serra et al., (2018) present modelled turbulence and current speed above and below rigid and flexible plants. Rigid plant can decrease in 25% de average velocity (From 4 to 3 cm s^{-1}) and enhanced turbulent kinetic energy in 50 % (from around 0.5 to around 0.8 cm^2 s^{-2}). Flexible plants did not affect the mean velocity but reduced turbulent kinetic energy on at least 20% (from around 0.5 to around 0.4 cm^2 s^{-2}). As mentioned before in another sub-chapter, the density of

macrophytes, especially in lakes, relies on the depth and the season of the year. Therefore, the direct and indirect influence of macrophytes on fluxes is not spatially homogenous on certain periods of the year.

The focus in this sub-chapter was to present the different processes that contribute to the exchanges between sediment and the water column. These mechanisms can have a fast temporal dynamics and a heterogeneous spatial distribution. So, what is the variability of the fluxes resulting from this spatio-temporal characteristic?

2.3 TECHNIQUES TO QUANTIFY BENTHIC FLUXES

A variety of techniques are used to quantify the interactions between sediment and water column (Viollier et al., 2003). Different ways to reach the unit of benthic fluxes (mmol m^{-2} day^{-1}) present the variety of techniques. These fluxes are estimated trough three main ways: The temporal (seconds) variation of mass (mmol) of a sediment surface (m^2); Spatial concentration gradient (mmol m^{-3}) over a temporal duration (h) on a 1D vertical plan (m); The concentration (mmol m^{-3}) related to a velocity (m s^{-1}).

2.3.1 Benthic chambers

One the techniques is the benthic chambers (first variant described by Odum, 1957). The main principle is to enclose sediment overlying water inside the chamber and at a constant time-steps collect samples from the inside for a period of time. The samples are analysed in laboratory to quantify the concentration of the compound of interest. The main principle is to follow the dynamics of a compound concentration, in mass (ΔM), inside the chamber for a certain period of time (Δt) of a surface (A) (Berner, 1980).

$$F = \frac{\Delta M}{\Delta t\, A} \qquad \text{(Eq. 18)}$$

The resulting slope of the mass in the temporal series gives the benthic flux. The chambers can be covered to avoid any photosynthetic activity. To calculate the net flux (Ft) the daily (24h) proportion of the flux measured in transparent chamber is added to the proportion of the flux in dark chamber (24-Δt) (Thorbergsdóttir et al., 2004).

The chambers can be deployed from water surface or using divers. After installing the chambers, the incubation period can vary for 1 to 2 h and minimal deployment duration required is 6h. Maximum deployment found was 270 h at Viana et al., (2018).

A great diversity of chambers setup exists in chamber shape and material (Buchholtz-ten Brink et al., 1989; Tengberg et al., 2004; Roth et al., 2019). Some chambers are coupled with a water-mixing mechanism on the chamber top to mimic hydrodynamics (Broström and Nilsson, 1999). However, the location of the foil and probes inside the chamber can bias the calculated flux (Tengberg et al., 2005).

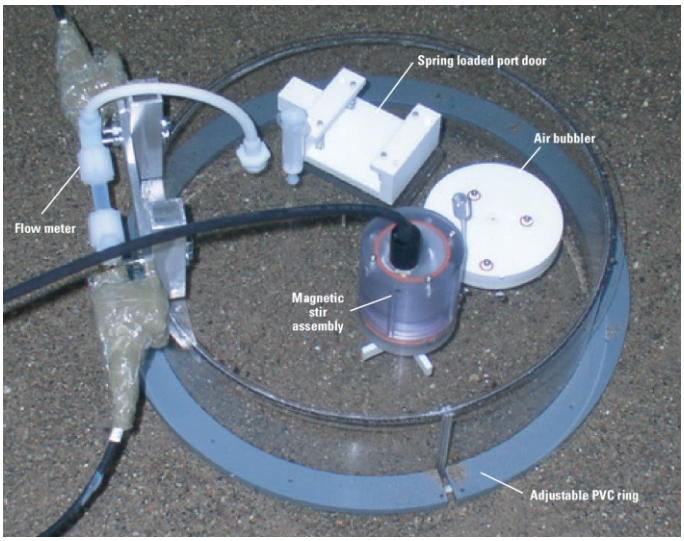

Figure 16 - Benthic chamber presented by Menheer, (2004). Its components for water sampling and mixing are presented.

This technique is very powerful in benthic zones when current speed is negligible or constant, but in turbulent environments it can underestimate the flux measurements (Berg et al., 2013). Also, the light penetration in the transparent chambers can be an issue to measure photosynthetic activity (Tengberg et al., 2004). Another limitation concerns sediment grain size. The chambers cannot be installed on rocky or gravel beds or on steep bathymetry. If so, the sediment is not completely enclosed by the chamber.

The flux representation of an ecosystem by the measurements obtained using the technique is limited. Sediment heterogeneity is often observed in a great part of waterbodies.

2.3.2 Ex-situ sediment core

The technique relies on the reproduction of the benthic zone through an ex-situ microcosm. The sediment cores are extracted from the waterbody bed using some corer device, often the gravity corer. The incubation period is required to a resetting of the sedimentary conditions after a possible disturbance produced during sampling. The average duration is of 24 to 72h under environmental conditions (e.g., light and temperature) depending on the natural environment and the objective of the measurements. During sampling period, after incubation period, the sediment-overlying water is gently mixed avoiding sediment resuspension and to homogenize the samples water. The overlying water is systematically sampled during a period of time. The flux is calculated as for the benthic chambers (Seitaj et al., 2017).

The problematics around the techniques is still the spatial representation of the waterbody, lack of turbulence influence (even under stirring) and the low spatio-temporal resolution.

Figure 17 - A sediment core from the Baye pond (France) made by the author in 2021.

2.3.3 Equilibrium by diffusion film

The techniques involving equilibrium by diffusion was first presented by Hesslein, (1976). The technique is widely applied to quantify the benthic fluxes and many designs have been developed over the years. The basic principle of the technique is to diffuse solutes from the BBL and from the pore water to enclosed inert solution (degassed pure water or hydrogel) through a porous film. After deployment period enclosed solution is analysed in laboratory. Resulting concentrations within SWI and pore water gives vertical 1D gradients of target compounds concentration (ΔC). The flux is calculated through first Fick's law:

$$F = -D \frac{\Delta C}{\Delta x} \qquad \text{(Eq.19)}$$

Where Δx is the concentration gradient in the vertical axis and D is the diffusion coefficient. For non-stirred water, at DBL, the D is equal the molecular diffusion (D_0). For stirred water, at TBL, D is equal to the eddy diffusion coefficient. For the pore water D take into account the porosity and tortuosity to the molecular diffusion ($D = \phi/\theta^2 D_0$). Values of diffusion coefficient were reviewed by Westrin et al., (1994) and are also presented at Shaw and Hanratty, (1977). The duration (above 6h) of the deployment depends on the diffusion coefficient to achieve equilibrium between the enclosed solution and the environment in contact (Zhang and Davison, 1999).

Dialysis cells (also called peepers), proposed by Hesslein, (1976), encloses degassed pure water in cells on acrylic sheet enclosed by a dialysis membrane. After deployment the solution in the cells are recovered and analysed. The cells distance presented to be problematic on measurement spatial

resolution sometimes below DBL thickness. Problematic on this design was presented by Davison et al., (1991). They introduced the Diffusive Equilibration in Thin films (DET) and the Diffusive Gradient in Thin films (DGT). The new approach replace water by agarose hydrogel and presented the continuous profile without the cells. New insights at Jézéquel et al., (2007) allowed to access 2D flux measurements.

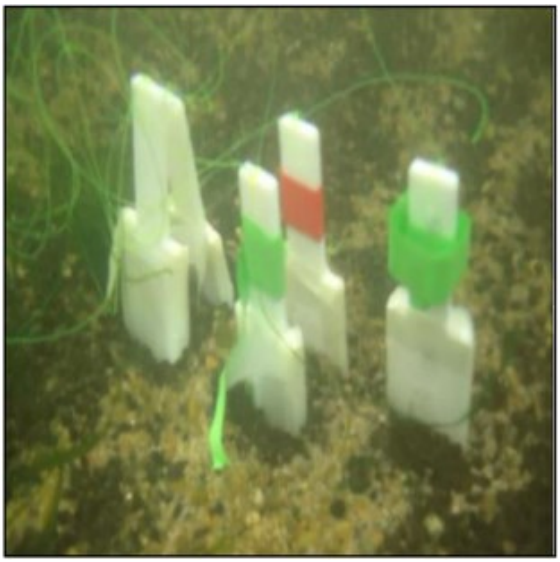

Figure 18 - Passive samplers deployed in the sediment by Bailon et al., (2019)

This technique presents similar problematics as the benthic chambers: The spatial representation of the sediment (few centimetres) and the sparse temporality. The turbulence contribution is captured by the probes but the diffusion coefficient in the TBL, obtained by experimental approach, is assumed to be constant during deployment.

2.3.4 Eddy Covariance

The aquatic eddy covariance (EC) presented by Berg et al. (2003) is one the most advanced techniques to quantify benthic fluxes. The AEC was adapted from homonymous technique applied on micrometeorology (Foken, 2008; Burba and Anderson, 2010; Baldocchi, 2014). The theoretical background for aquatic environment application comes from mass balance volume applied on a single-point measurement regarding flux averaging time and measurement height. It is well presented and explored at Lorke et al., (2013). The resulting equation is the covariance of the mean fluctuation of the vertical velocity (w) and of the concentration (c).

$$\bar{F} = cov(w, c) = \overline{w'c'} \qquad \text{(Eq. 20)}$$

The technique measures simultaneously at high frequency the vertical velocity and a concentration at certain height above the sediment surface in the TBL. For oxygen flux measurements on a single point measurement it is possible to observe the turbulence influencing the oxygen concentration. On figure 19 different characteristics of the technique can be observed:

- Turbulent transport: On the brief period we can observe an inverse dynamic between oxygen and vertical velocity. Before 15 s the oxygen concentration is above the average and vertical velocity is below the average. After 15 s the inverse is observed. Therefore, downwards currents have higher oxygen concentration than upwards currents.
- Eddy size: On the smoothed vertical velocity we can see the different eddy size and time-scales. A greater eddy can be seen on almost the whole data series passing through the measurement point. It starts at 0s and finishes at 25 s. Smaller eddy can be observed between 0 and 8s.

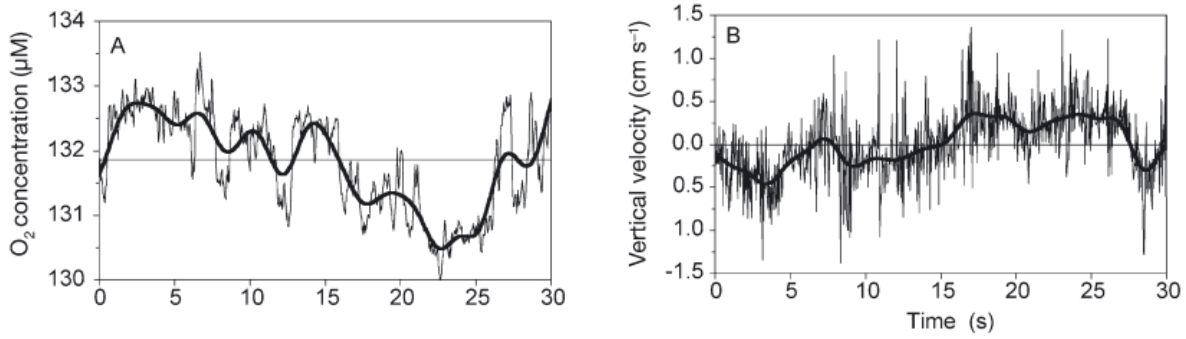

Figure 19 - Short time series measurement of oxygen concentration (left-hand side) and vertical velocity (right-hand side) for EC flux calculation. Black thick lines are the smoothed time series. Thin black line is the average of the period. (Berg et al., 2003)

The technique is limited to fluxes of oxygen, heat, particles, alkalinity (Long et al., 2015) and nitrates (Johnson et al., 2011), due to the lack of fast-response sensors for other substances. The flux averaging time is determined by eddy size in the measurement point. The flux average does not change when turbulence contribution becomes negligible (Berg et al., 2003; Lorke et al., 2013; Murniati et al., 2015; Berg et al., 2022). Typical duration is 30 minutes. Hourly variations in oxygen fluxes were measured, indicating current speed influence on fluxes (McGinnis et al., 2008a; Berg et al., 2013; Murniati et al., 2015).

EC measurements has a footprint, an oval-shaped surface area contributing to the measured flux (Foken, 2008 – Figure 20). Berg et al., (2007) presented the footprint adaptation for EC in aquatic environments. Main estimations are based on water column height (H) and measurement height (h). The footprint width (w):

$$w = 6.531h \quad \text{(Eq. 21)}$$

For $H > 27h$ the footprint length (l) is:

$$l = -2.783 - 158.7h + 159.2h^2 - 120.8h\log(z_0) \quad \text{(Eq. 22)}$$

where z_0 is the sediment surface roughness. For $6.7h < H < 27h$ the footprint length (l) is multiplied by $1 + 8.347\exp(-0.2453\, H/h)$. The conditions of use of these equations are isotropic turbulence, no thermal stratification, a sediment surface roughness between 7.04 10^{-6} (smooth surface) and 0.01 m (fine gravel), and no surface waves. For anisotropic turbulence l still stands. The measurement height is also important in the quality of the measurement on complex population in the footprint (Rheuban and Berg, 2013). It gives more resolution to the benthic community diversity in the footprint. The use of the EC's footprint allow to access greater sediment portion compared to the other techniques, but also the oxygen budget by photosynthetic organisms on complex and natural aquatic environments (Berg et al., 2019; Rodil et al., 2019).

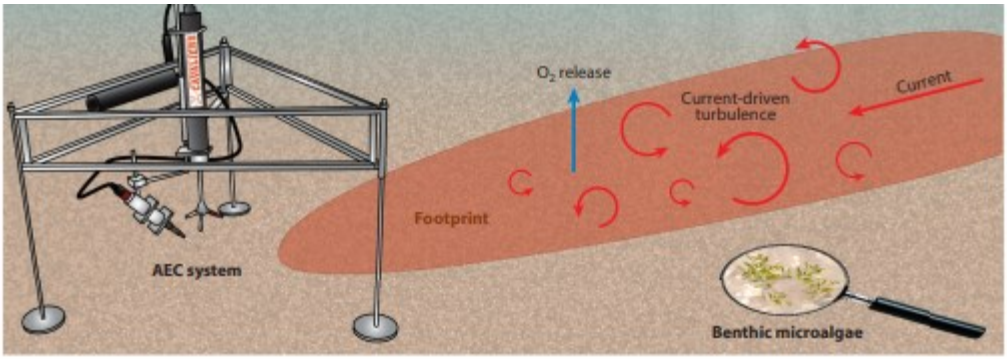

Figure 20 - Main aspects of the EC. The EC system on the seafloor and the footprint of the measurement. In the system the current meter and the oxygen probe are represented measuring at similar sampling volume. The benthic microalgae representing the heterogeneity of the benthic community and the oxygen production for O_2 release. (Adapted from Berg et al., 2022)

The main limitations of EC are the low range of fluxes which it can be used for and complicated data processing (see at Lorrai et al., 2010).

2.3.5 Compared techniques

Different studies present the comparison of fluxes measured by different techniques (Table 1). An overall observation of the results obtained by the compiled articles is that very often the techniques do not measure the exact same fluxes at same time and space. The differences for benthic chambers and dialysis chambers are attributed to lack of spatial representativeness. Between benthic chambers and sediment core, the compared fluxes are in the same range of values. Significant differences were found between eddy covariance and benthic chambers. Berg et al., (2003), Long et al., (2015) and Polsenaere et al., (2021) present different values for oxygen fluxes measured by the techniques, in which sometimes the differences are supported by statistical analysis. Flux differences were mainly attributed to the hydrodynamics contribution to the flux measured by EC. Donis et al., (2016) and Dale et al., (2021) measured similar fluxes under low-energetic environments and very homogeneous sediments.

Table 1 – Compiled articles found articles comparing techniques to measure benthic fluxes. BC – Benthic chambers; SC – Sediment cores; PP – Peepers; EC – Eddy covariance. The roman number after the technique abbreviation denotes two different sampling spots in the same water body. *Alkalinity

Reference Paper	Waterbody type	Depth (m)	Water temp (°C)	Technique	Fluxes (mmol.m^{-2}.day^{-1})						
					NO_3^-	NH_4^+	PO_4^{3-}	SRP	O_2	Mn	Alk*
Forja and Gómez-Parra, 1998	Bay of Cadiz (Spain)	8.5	18.4	Benthic chambers		20	6				
				Sediment core		3	0.5				
Hammond et al., 2004	California coast (USA)	897	5.2	Benthic chambers I	–1.24		0.1				
				Sediment core I	–0.95		0.1				
		1539	3.9	Benthic chambers II	-0.515		0.005				
				Sediment core II	–0.24		0				
Aller et al., 1998	Panama Basin	4000	2	Benthic chambers	0.19	0.04				0.02	
				Peepers	-0.008	0.02				0	
Grünebe rg et al., 2015	River Havel (Germany)	5.1	15	Benthic chambers		8.9		1.1			
				Peepers		1.6		0.2			
Grenz et al., 1991	Prévost lagoon (France)	0.8	22	Benthic chambers		12	3.6				
				Peepers		0.2	0.12				
Polsenaer e et al., 2021	Bay of Brest (France)	-	9.5	Eddy covariance I					35		
				Benthic chambers I					87.4		
		-		Eddy covariance II					-3.7		
				Benthic chambers II					-9.1		
Dale et al., 2021	North Sea (UK)	-	-	Eddy covariance					-6.7		
				Benthic chambers					-10		
Donis et al., 2016	Arctic sea	-	-	Eddy covariance					−0.9		
				Benthic chambers					−1.1		
Long et al., 2015	Waquoit Bay (USA)	1.2	26	Eddy covariance					180		-0.006
				Benthic chambers					60		-0.003
Berg et al., 2003	Aarhus Bay (Denmark)	12	-	Eddy covariance I					-39		
				Benthic chambers I					-28		
	Limfjorden Bay (Denmark)	8	-	Eddy covariance II					-46		
				Benthic chambers II					-41		

The techniques presented here are not perfectly capable to take into account all the parameters driving the benthic fluxes (Table 2). The objective of each study determines what kind of technique is more adapted. The study of fast events dynamics (e.g., algae blooms) cannot be assessed by the techniques. They all failed to follow with high temporal resolution and great range of compounds. Besides EC, all the others techniques failed to have a good spatial-representation of the sediment in which in dynamic waterbodies (e.g., Rivers, streams and shallow lakes) can bias measurements.

Table 2 - Different techniques used to quantify benthic fluxes and their characteristics.

Technique		Invasive?	Type of flux quantified	Flux compounds	Temporal resolution	Spatial representation
Benthic Chambers		Yes	Diffusive	All compounds	Min. 6h	Low, a few square meters
Equilibrium by diffusion	Ex-situ	Yes	Diffusive	All compounds, but some are very difficult to measure (e.g., dissolved gases)	Min. 6h	Low, a few square centimetres
	In-situ	No	Diffusive and/or Turbulent			
Sediment core		Yes	Diffusive	All compounds	Min. 6h	Low, a few square centimetres
Eddy covariance		No	Turbulent	Oxygen, temperature, nitrates, particles and alkalinity	Min. 30 min	High, several square meters (in function of Footprint parameters).

3 SCIENTIFIC OBJECTIVES AND GENERAL APPROACHES

Current techniques failed to follow at high spatio-temporal resolution the benthic fluxes for a broad range of compound. The theoretical feasibility study presented by Lemaire et al. (2017) showed that relaxed eddy accumulation (technique is presented in the section 4) presents a high potential to measure fluxes in aquatic environments. The overall objective of this work was to empirically quantify the fast dynamics of benthic fluxes using an innovating technique, REA. The main objective is divided into three objectives which correspond to three following chapters of this thesis:

- The development and tests of a prototype adapting REA to the aquatic environment;
- The technical validation of the prototype with a reference technique;
- Use of the prototype to explore nutrient and metallic ion fluxes in a natural environment to follow benthic fluxes with a small time step.

The general approaches are aligned with the established objectives. The development of the prototype addresses technical issues concerning the data processing performed by the prototype automation, the engine and the stability of the sampling, and the types of water bodies in which the prototype can be deployed. The validation and field of application of technique addresses the technical validation with the reference method, the type of fluxes the prototype can measure and the hydrodynamic conditions in which the technique can be used. Finally, the spatial and temporal variability of the fluxes helps on the understanding which environmental conditions determine the measured fluxes and the spatial

representation of the fluxes measured by REA (Figure 21). The last sub objective about the spatial variability was addressed in this work.

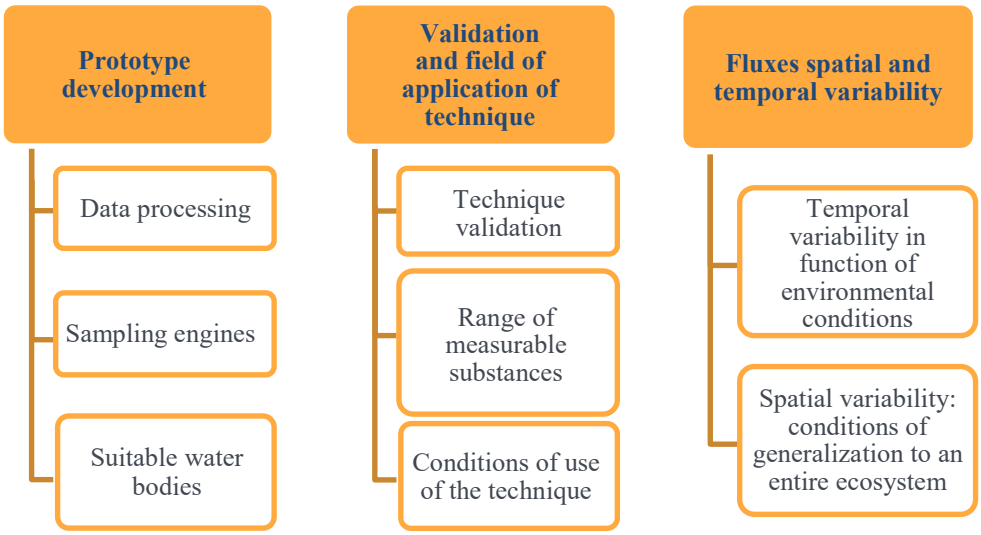

Figure 21 – The schematic presentation of the three general approaches of this PhD.

4 DEVELOPMENT OF A PROTOTYPE ADAPTING REA TO AQUATIC ENVIRONMENTS

4.1 INTRODUCTION

The drivers of the exchange of solutes between the sediment and the water column are multiple, among them the turbulence. The oxygen consumption by the sediment has a fast dynamic, at hourly scale and linked to turbulence (Berg et al., 2003; Chipman et al., 2016; Murniati et al., 2015). The question is whether solute fluxes resulting from the oxidation of organic matter can show similar time dynamics. Existing techniques (e.g., Benthic chambers and sediment cores – section 2.3) fail to capture benthic fluxes in such dynamics scale. The understanding of such dynamics would make it possible to access the contribution of benthic fluxes to fast events (e.g., algae blooms). Thus, a new technology is needed to meet the requirements of measuring solute fluxes between the sediment and the water column in aquatic environments. It should be non-invasive, avoid hydrodynamic disturbances, measure at high temporal frequency, in order to follow hourly flow dynamics, and cover a wide range of fluxes. The micrometeorologists have met this challenge by creating the **relaxed eddy accumulation** technique (Hicks and McMillen, 1984; Businger and Oncley, 1990; Baldocchi, 2014). REA was developed from eddy covariance (EC) by replacing fast probes by fast sampling. The main question of this chapter is: Can the REA technique be adapted to aquatic ecosystems and what are its conditions of use? After introducing the measurement principle and the main requirements for the system, this chapter presents the main tests and reflections about the design of a REA prototype adapted to the aquatic environments.

4.2 REA MEASUREMENT PRINCIPLE

REA is a sampling technique conditioned by current speed: samples are accumulated at constant flow rate when the instantaneous turbulent fluctuation of the vertical velocity is above a threshold ($|w'| \geq w_0$). During each accumulation period often called segment, two containers accumulates the samples, one when $w' \geq w_0$ (updraft samples) and the other when $w' \leq -w_0$ (downdraft samples) (Figure 22). The flux F by REA is the product of an empirical coefficient (b), the standard deviation of the vertical velocity (σ_w) and the concentration difference between updrafts $\overline{C_\uparrow}$ and downdrafts $\overline{C_\downarrow}$.

$$F = b\,\sigma_w\,(\overline{C_\uparrow} - \overline{C_\downarrow}) \qquad \text{(Eq. 23)}$$

The b coefficient depends on the threshold velocity for the segment, calculated before segment start (so-called pre-segment define on subsection 7.3.7.1) and σ_w measured during the segment.

$$b_{\text{fit}} = b_\infty + (b_0 - b_\infty)\exp\left(-a\frac{w_0}{\sigma_w}\right) \text{ for } 0 \leq \frac{w_0}{\sigma_w} \leq 2, \qquad \text{(Eq. 24)}$$

where b_0 corresponds to a dead band of w_0 = 0 m s^{-1}, b_∞ would be the asymptotic value for $w_0 >> \sigma_w$ and a is an attenuation coefficient.

The **threshold velocity** (w_0) is used to increase the concentration difference between accumulated samples ($\overline{C_\uparrow}$ and $\overline{C_\downarrow}$ in Eq. 23). The threshold velocity calculated as $w_0 = 0.75\,\sigma_w$ was shown empirically to minimise the discrepancies between EC and simulated REA fluxes (Ammann and Meixner, 2002; Lemaire et al. 2017).

A strong advantage of REA to resolve benthic fluxes with high spatial-temporal resolution is the **footprint** of the measurement (Foken, 2008, see subsection 2.3.4). The footprint is the surface area contributing to the measured flux. Berg et al., (2007) presented the approach for measurements using eddy covariance in aquatic environment. The footprint has an elliptic shape which increases according to lake depth, measurement height, friction velocity and sediment surface roughness. For instance, for a shallow lake of 3 m depth and a friction velocity of 0.0001 m s^{-1} at different sampling heights (typical values of measurements presented in the next chapters), and within the sediment roughness range indicated by Berg et al., (2007), (see Eq. 21 and 22) the footprint lengths changes by a factor 16 (Table 3).

Table 3 – Order of magnitude of width and length of the footprint of flux measurements for a shallow lake with low current speed and the range of sediment roughness indicated by Berg et al., (2007)

Sediment surface roughness (m)	Measurement height (m)	Footprint width (m)	Footprint length (m)
0.00000704	0.1	0.65	45.42
0.00000704	0.2	1.30	116.61
0.01	0.1	0.65	7.13
0.01	0.2	1.30	25.04

The large footprint of a REA measurement increases the representativeness of the measured fluxes, compared to techniques which investigate a small surface like benthic chambers or dialysis chambers.

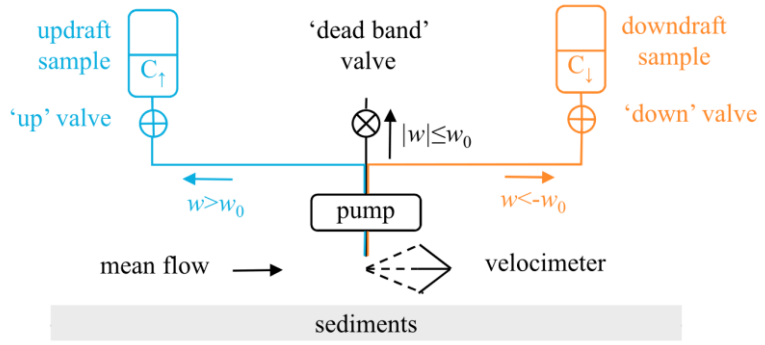

Figure 22 - Sketch of subaquatic REA measurement principle (Lemaire et al., 2017).

Measurements using REA, ideally, should be able to follow the hourly to daily dynamics of target fluxes, thus it is expected to execute measurements for at least 6 hours. The duration of an accumulation period (segment) is the same as for eddy covariance, from 15 to 30 min depending on the waterbody hydrodynamics (Lorrai et al., 2010). The duration depends on the characteristic time of turbulence dynamics. It should be shorter in rivers than in lakes where current direction and speed change. The quantity of segments per campaign relies also in the turbulence. Fewer segments should be needed in water bodies where turbulence is stable (e.g., rivers) because no hourly benthic dynamics is expected. On the other hand, in lentic environments turbulence is not constant, and therefore the number of segments per day shall be greater.

Some choices and requirements concerning the application and adaptation of the technique in aquatic environments were already established before the PhD start and are listed in the next subsection.

4.3 REQUIREMENTS FOR A REA PROTOTYPE

Some choices and requirements concerning the application and adaptation of the technique in aquatic environments were already established before the PhD start and are listed in this subsection.

4.3.1 Challenges presented by Lemaire et al. (2017) in their subaquatic REA feasibility article

- **Quantification limit** – REA requires a high analytical resolution to measure small concentration differences for fluxes determination. This plays an important role in the selection of the target compounds to be explored. For instance, metals in the sea, as presented by the article, present very small fluxes at very small average concentration, limiting REA application. However, the authors compared the expected limit of quantification of REA to diffusive fluxes collected with benthic chambers which underestimate the values of fluxes as shown by comparing benthic chambers and eddy covariance (Berg et al., 2013).
- **Axis alignment** – Axis alignment is required for REA to find the normal to the sediment surface and avoid any contribution to the measured fluxes of the advection of water by current, parallel to the sediment surface. The article presents the use of the 2-axis rotation method as a solution and the strategy is to sequence the segments of measurement and to transmit the alignment angles from one measurement segment to the next.
- **Turbulence fluctuation extraction** – The turbulent fluctuation extraction is executed through Reynolds decomposition ($w' = w - \overline{w}$). To filter low-frequency non-turbulent fluctuations, the subtraction of a 60s back-looking running mean of velocity data was proposed in the article. Is this suitable?
- **Hydraulic perturbation by sampling** – The authors present concern on the perturbation of the current speed measurement by the sampling action of the REA system.

4.3.2 Requirements concerning field of use and usability

- **Waterbody depth –** The omnipresence of shallow lakes (depth 2 to 5 m) and shallow rivers and streams (depth ≈ 1 m) in Europeans territories (e.g., Île-de-France, France) encourages the study of such waterbodies
- **Target fluxes –** In the development stage of the technique, stable or low reactivity compounds are favoured in order to avoid sample degradation during sampling, transfer and conservation before analysis. Initially targeted compounds are ammonium, nitrates, phosphate, sulphur, iron and manganese (section 2.1.3). Ammonium, nitrate and phosphate are important nutrients driving the algae bloom dynamics. Sulphate is an important electron acceptor used by the benthic community in anoxic environments. The metallic ions were selected by their relation to the other biogeochemical cycles and stability for conservation.
- **Sampled volume for chemical analysis –** Taking into account select target fluxes the estimated minimum required volume of sample for chemical analysis is around 200 mL: 120 mL for nutrient analysis using UV spectrophotometry to explore ammonium; 20 mL for ion-chromatography to explore nitrate, phosphate and sulphate; 50 mL for iron and manganese ions by inductively coupled plasma mass spectrometry.

4.3.3 Requirements concerning mechanical aspects

- **Prototype mechanical stability** – The prototype should be stiff enough so that its resonance frequency be higher than the sampling frequency.
- **Flow rate control** – Flow rate must be stable during a measurement segment, especially whatever the sampling duration towards a container over a single or several time steps (limited effect of transient flow after opening the valves), otherwise measured fluxes will be biased due to over or sub representation of samples.
- **Sampling based on turbulent fluctuation of vertical velocity** – Create an automation capable to sample at the desired frequency when the fluctuation of the vertical velocity is above a threshold velocity.
- **Sampling tube choice** – Different REA designs are used for atmospheric studies. Regarding specifically the sampling tubes, two main types of design are used: a common sampling tube for updraft and downdraft samples or a sampling line for each. The challenges are to separate correctly updrafts and downdrafts during each accumulation period, as well as samples of successive accumulation periods.

4.4 MATERIAL AND METHODS

In this section we present the technical choices and the tests that led to the final design and to the data processing of the subaquatic REA system.

4.4.1 Selected REA components

The components initially composing aquatic REA are:

- An Acoustic Doppler Velocimeter (ADV Vector – Nortek A.S) to measure current velocity in a single point (1 in figure 23);
- Tubes in PFA (Fluoropolymer) having outer diameter of 4 mm and inner diameter of 2.5 mm to collect the samples and drive them to the accumulation reservoirs (2 in figure 23);
- Two-way solenoid valves to trigger the sampling action when sampling decision is made (5 in figure 23);
- Peristaltic pumps to trigger the sampling action when sampling decision is made (4 in figure 23);
- An ON/OFF control module to control the energy supply of solenoid valves and/or peristaltic pumps.

4.4.2 Sampling mechanism choice for a fast response and a regular flow rate

The sampling trigger of REA relies on the constant comparison of the instantaneous fluctuation of the vertical velocity (w') to a fixed threshold velocity (w_0) during the whole segment. When $|w'| > w_0$, samples are accumulated in respective containers (up for upward samples and down for downward samples) while the condition is satisfied. The sampling mechanism of atmospheric REA is a pump. For subaquatic REA two sampling mechanisms were thought and tested: an **active** one and a **passive** one (Figure 23).

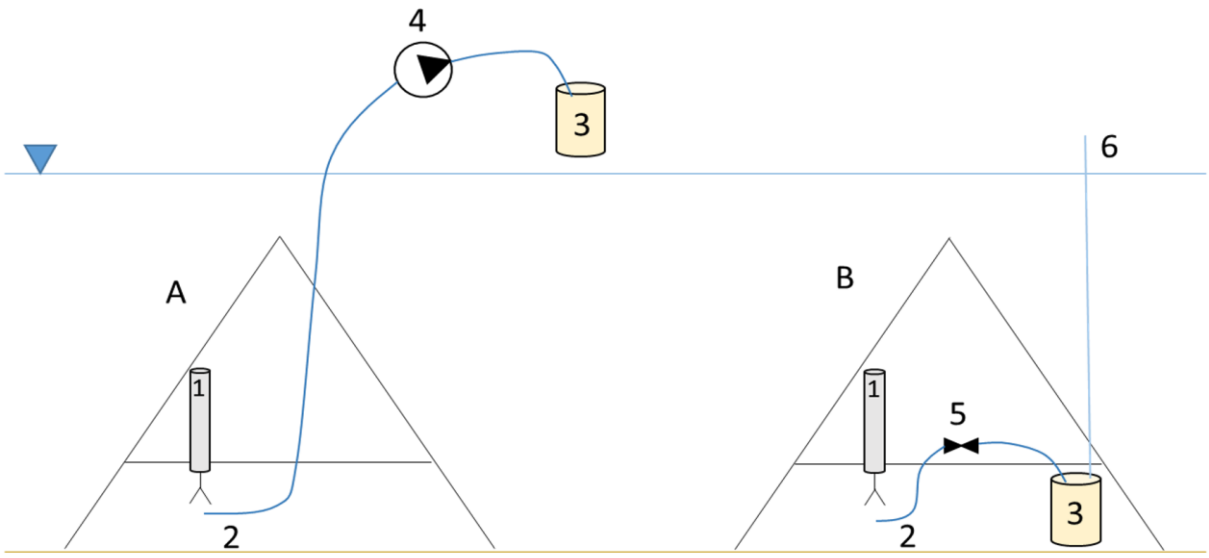

Figure 23 - The two sampling mechanisms implemented on the REA prototype. In the left-hand side (A) the active mechanism and in the right-hand side (B) the passive mechanism. The components include: i) for both mechanisms, the current meter (1), the sampling tube (2) and the accumulation reservoir (3); ii) specifically for the active mechanism, the peristaltic pump (4); iii) specifically for the passive mechanism the solenoid valve (5) and the venting tube (6). In the figure the prototype is mounted in a tripod.

The active mechanism uses a peristaltic pump (flow rate capacity of around 2 L h^{-1} for 3 m of water depth neglecting head loss in laminar flow) which is activated when the sampling condition is valid. The passive mechanism uses the pressure difference between the hydrostatic pressure at the tube inlet and the atmospheric pressure in the accumulation container permitted by the venting tube, and a solenoid valve which opens for sampling (Figure 23). The accumulation container of this system is a perfusion bag (300 mL) inside of a bottle (2 L). The sampled water is released by the outlet tube drop by drop in contact with the air. If the outlet were placed at the bottom of the perfusion bag, the weight of water accumulating above the outlet would decrease the pressure difference and the flow rate in the sampling tube during the accumulation period. The bottle is connected to the atmosphere through a tube (venting tube) thus pressure inside the bottle (p_{bottle}) is equal to atmospheric pressure (p_0). The pressure in the inlet of the sampling tubes is $p = \rho g h + p_0$, where h is the sampling depth in the water column (referring to the water surface), g is the acceleration of gravity, p_0 the atmospheric pressure and ρ the water density. So, the pressure difference between inlet and outlet is $\Delta P = \rho g h$.

Both mechanisms passed through two tests: one concerning the time response to follow turbulence fluctuations addressing the requirement of **sampling based on turbulent fluctuation of vertical velocity** and **hydraulic perturbation by sampling;** one concerning the flow rate stability during sampling addressing the requirement of **flow rate control**, **waterbody depth** and **sampled volume for chemical analysis**.

4.4.2.1 *Sampling time response*

The first test was executed in a flume located in the facilities of the Institute of environmental sciences in the University of Koblenz-Landau (Germany). The two mechanisms were deployed in a flume (36 cm wide, 3 m long) to execute REA and Particle Image Velocimetry (PIV) measurements simultaneously. PIV is widely used for hydrodynamic and turbulence studies. The main steps of its functioning are: 1) Transparent plastic beads (20 µm polyamide) are poured into the water; 2) A laser sheet is emitted through the water; 3) Orthogonally to the laser beam a camera takes pictures at high frequency (50 frames per second). The reflex of the laser in the beads is captured in photo, which is processed to calculate resulting velocity vectors. More explanations about the PIV setup can be found in Koca et al. (2017).

The two mechanisms were tested in the flume at average current speed of 0.01 m s^{-1} and in stagnant water. By using the PIV technique, we can assess which mechanism better actively and accurately samples turbulence fluctuations in fast time response.

4.4.2.2 *Stability of sampling flow rate*

For REA, as mentioned above, the sampling flow rate needs to be stable during a segment. A variation of the sampling volume over the sampled downdrafts and updrafts could lead to a biased accumulation of samples and, hence, to a biased flux. The objective is to measure the flow rate of the passive and the active mechanisms under different conditions to test the sampling reliability of the mechanisms.

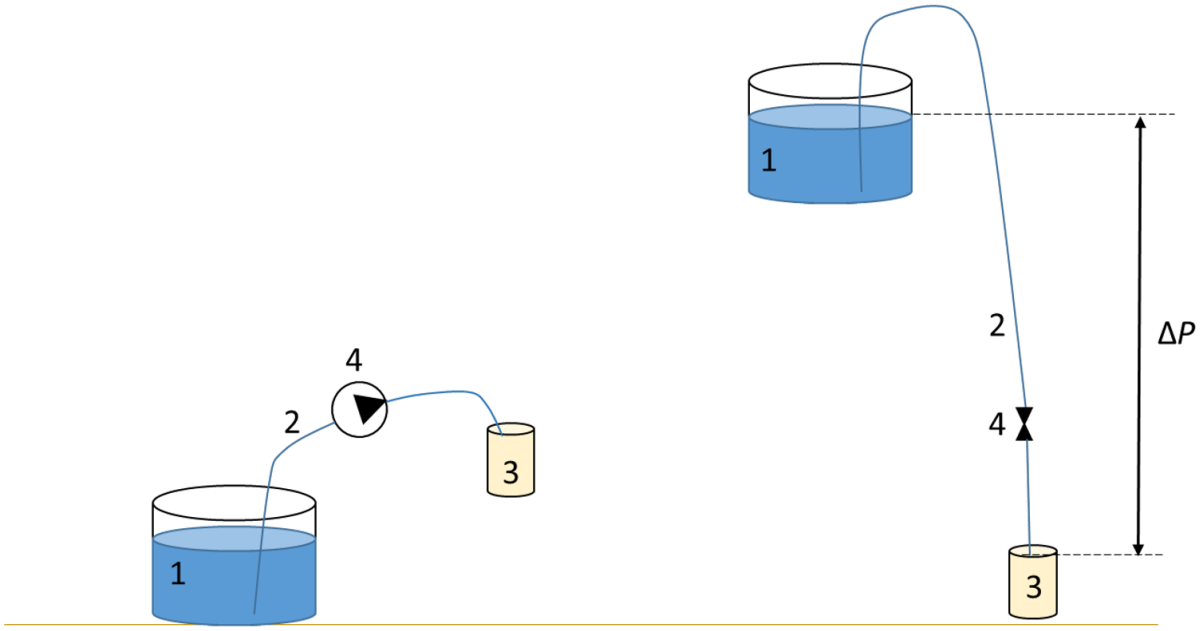

Figure 24 - Schematic setup for flow rate test. The mechanisms partially use the same components: The full of water (1), sampling tube (2) and accumulation bottles (3). On the left-hand side of the figure the active mechanism using a peristaltic pump (4) and on the right-hand side the passive system using a solenoid valve (4).

For the test of the passive mechanism a plastic jug full of water was placed at six different heights: 3.25, 2.75, 2.25, 1.75, 1.2 and 0.75 m (Figure 24). The tube inlet was placed inside the container and the whole sampling tube was filled with water. The valve was activated for the total duration of 60 s.

For the active mechanism no height difference between inlet and outlet was imposed. The tube inlet was placed inside a plastic jug full of water. The pump was activated and deactivated for the same total duration (60 s) for different individual pumping durations: 5, 2.4, 2, 1.5 and 1s (e.g., the pump is switched on for 5 s, then off for 5 s).

In each test, the sampled water was weighed and the average flow rate was computed.

4.4.3 Passive sampling assisted by vacuum

For the passive mechanism, the sampled volume was lower than required (200 mL) for accumulation periods of less than 30 min and pressure difference $\Delta P \leq 0.1$ bar (less than 1 m of water depth). This would limit the time resolution of REA fluxes in shallow rivers or streams. To improve the range of use of REA an adaptation of the prototype the pressure inside the bottles needed to be decreased in order to increase the pressure difference between the inlet and outlet of sampling tubes. The driver of depression is a vacuum pump connected to the bottles through the venting tubes (Figure 25). A manometer and a tap were included to the venting tube to monitor and control the depression created inside the bottles.

The test setup is the same as in section 4.4.2.2., but a minimum water height above the sampling tube inlet was used, 0.5 m corresponding to ΔP = 0.05 bar without depression. Two series of measurements were run for different depressions inside the bottles: $p_{bottles} - p_{atm}$ = -0,52 bar and $p_{bottles} - p_{atm}$ = -0.27 bar, increasing the pressure difference between inlet and outlet to $\Delta P' = \Delta P - (p_{bottles} - p_{atm}) = 0.57$ and 0.32 bar, equivalent to more than 3 and 5 m of water column respectively. The experiment was repeated six times by opening the valves for a period of 60 s. The water sampled during each run was collected in flasks and the average flow rate was assessed by weighing the flasks.

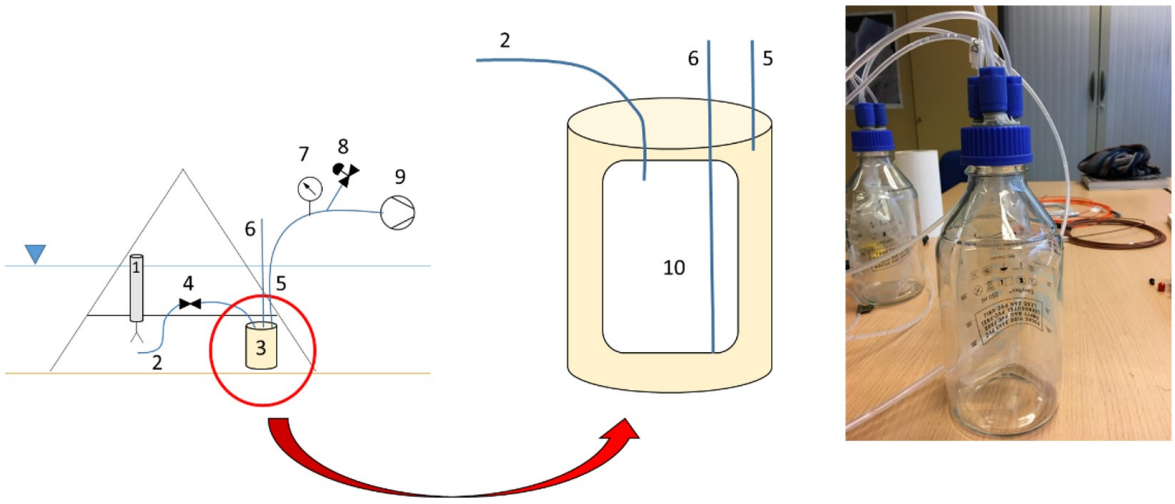

Figure 25 - On the left-hand side of the figure, the schematic presentation of the prototype containing the passive mechanism assisted by a vacuum pump (9) using also a pneumatic tap (8) and a manometer (7). The passive mechanism composed by the current meter (1), the sampling tube (2), the sample storage system (3), the sampling valve (4), the venting tube (5) and the sampling recovery tube (6). In the middle of the figure, a focus on the position of the tubes 2, 5 and 6 and of the perfusion bag (10) to store the samples. On the right-hand side a photograph of the sample storage.

4.4.4 Separated sampling tubes avoiding sampling mixing between segments

There is a question about the type of sampling tubes which should be used in a subaquatic REA device: a common sampling tube for updrafts and downdrafts or one tube for each. Firstly, to obtain 200 mL of sample, which is the minimum required volume for chemical analysis, the required flow rate was calculated. The conditional sampler based on a threshold velocity ($w_0 = 0.75\ \sigma_w$) will actively sample 45% of the total time. For segments of 20 and 10 min, the required flow rate (Q) is, respectively, 2.7 and 5.5 L h^{-1}. The sampling tube inner diameter (d) is 0.0025m. The mean velocity ($\bar{u}$) in the tube for each Q is calculated through,

$$\bar{u} = \frac{4\,Q}{\pi\,d^2} \qquad \text{(Eq. 25)}$$

resulting in 0.15 m s^{-1} for Q = 2.7 L h^{-1} and 0.31 m s^{-1} for Q = 5.5 L h^{-1}. For both average velocities the Reynolds number was calculated through,

$$Re = \frac{\bar{u}\,d\,\rho}{\eta} \qquad \text{(Eq. 26)}$$

Where ρ the viscosity and η the water dynamic viscosity. Resulting in Re = 778 and 381 for, respectively, flow rates of 2.7 and 5.5 L h^{-1}. For both Q, samples flow in the tubes in laminar regime (Re < 2100). The velocity profile was calculated through Poiseuille's law,

$$u(r) = u_{max}\left(1 - \frac{4r^2}{d^2}\right) \quad \text{(Eq. 27)}$$

where r is the radius from the centre of the tube for the velocity of interest.

The theoretical parabolic velocity profile of laminar flow by itself imposes the separation of updrafts and downdrafts sampling lines. Within a single tube, successive samples of updrafts and downdrafts would be stretched over time in laminar flow and soon impossible to distinguish by a valve: water would travel along the axis at maximum speed, and very slowly close to the walls. In the atmosphere, transport in the tubes is turbulent and the smearing of successive samples can be neglected. In a continuous flow analyser, successive liquid samples traveling in laminar are separated by bubbles, but this is difficult to transfer to a REA prototype underwater. Thus, the choice was made that the prototype has separate lines for updrafts and downdrafts. Potential small flow rate differences between the lines have no consequence on the concentrations, contrary to variations of flow rate in time on each of the line which would occur with an active system.

4.4.5 Prototype frame stability

The first frame for the prototype had a square table shape and was in aluminium. The problem lies in the vibration frequency of the frame. It cannot be within the turbulence frequency range. So, in order to obtain the vibration frequency of the frame, a theoretical and a practical approach were established. The vibration can be estimated, theoretically, by the Strouhal number. The frequency (f) is calculated by

$$f = 0.2\ \bar{u}/d \quad \text{(Eq. 28)}$$

where $\bar{u}$ is the mean flow velocity and d the diameter of the stems of the frame, 0.04 m.

The frame vibration was measured in flume 12 at EDF R&D facilities in Chatou. The flume dimensions are 1.2 m width, 2 m depth and 80 m long. Mean current speed was 0.2 m s^{-1} and water depth was 1 m. Two accelerometers were installed on the frame to measure its vibration frequency.

4.4.6 Required sampling frequency to cover the turbulence range

The measurement requirements for EC and REA are very similar. The functioning basis for both techniques are the turbulence contribution to fluxes in a single point of measurement. Successful measurements require to cover the full turbulence range of different hydrodynamics of waterbodies (Figure 26).

According to Lorrai et al., (2010), the turbulence dissipation rate (ε) and the time scales of largest and smallest eddies of low and high turbulent environments are, respectively, 2.4 10^{-8} W kg^{-1}, 100 s and 7.4 s and 2.4 10^{-5} W kg^{-1}, 10 s and 0.2 s. The lowest period (0.2 s) corresponds to 5 Hz. Based on that, the sampling frequency for REA should be higher than 5 Hz. The idea is to have a device covering a

good range of eddy sizes allowing to access a good range of waterbody types with different hydrodynamics.

Taking into account the author reasoning, the required sampling frequency for each sampling height can be calculated using the time scale of the largest eddies (τ_{LE}) ,

$$\tau_{LE} = \frac{h}{u_*} \quad \text{(Eq. 29)}$$

where h is the height above the sediment and u_* is the friction velocity (Wengrove and Foster, 2014).

$$u_* = \sqrt[4]{\overline{u'w'}^2 + \overline{v'w'}^2} \quad \text{(Eq. 30)}$$

The prime denotes the fluctuation of the three velocity vectors. The time scale of the smallest eddies (τ_k) is derived from the Kolmogorov scale (L_K)

$$L_K = 2\pi \left(\nu^3/\varepsilon\right)^{1/4} \quad \text{(Eq. 31)}$$

$$\tau_k = \left(L_K^2/\varepsilon\right)^{1/3} \quad \text{(Eq. 32)}$$

where ν is the kinematic viscosity of the fluid. The turbulence dissipation rate is calculated through

$$\varepsilon = u_*^3/(\kappa h) \quad \text{(Eq. 33)}$$

where κ is the von Karman constant. Hence,

$$f_{low} = \frac{1}{\tau_{LE}} \quad \text{(Eq. 34)}$$

$$f_{high} = \frac{1}{\tau_k} \quad \text{(Eq. 35)}$$

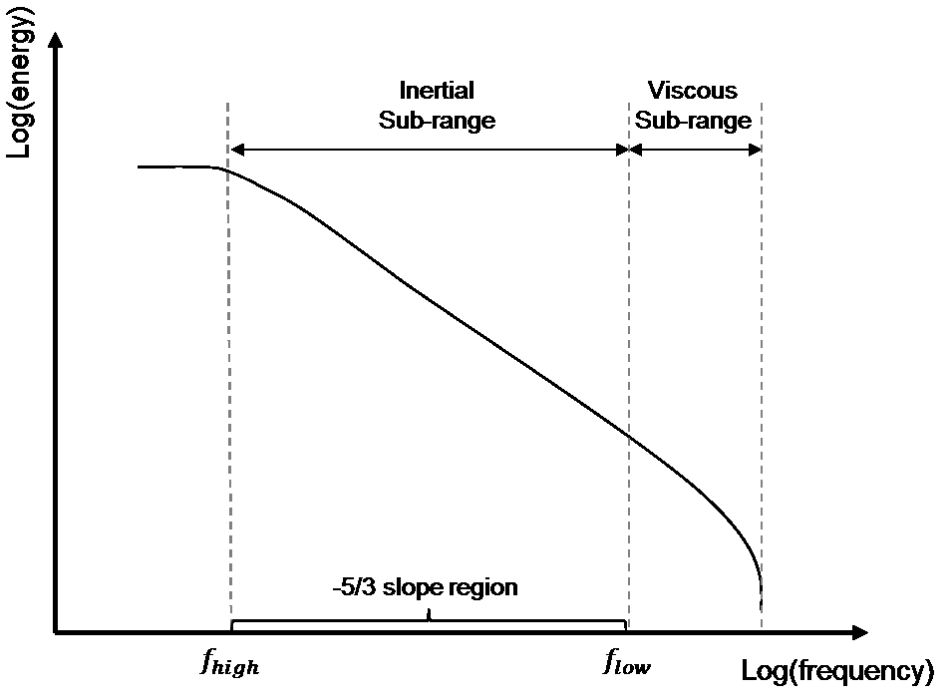

Figure 26 - Schematic of the energy spectrum of an environmental flow presenting the minimal and maximal frequencies (f_{low} and f_{high}) required to cover the inertial sub-range. Figure adapted from Borque et al., (2016).

Thus, the sampling height, the mean current and the turbulence dissipation rate at the sampling height determine the required sampling frequency to cover the whole turbulence range. But also, the duration of the running mean for the extraction of turbulent fluctuations (see at Lorke et al., 2013). In order to estimate the required sampling frequency in function of the sampling height above the sediment and the turbulence dissipation rate for REA the data, equations and reference values (e.g., turbulence rate and friction velocity) presented by Lorrai et al., (2010) were used.

4.4.7 Velocity processing for REA sampling

This subsection addresses the requirements of **axis alignment** and **turbulence fluctuation extraction**.

For REA, the sampling decision relies on the comparison between the instantaneous fluctuations of the vertical velocity to the threshold velocity. The objective of the data processing for REA is to obtain the instantaneous fluctuation of the vertical velocity in order to sample. Since REA derives from eddy covariance, the usual data processing guidelines for EC (Burba and Anderson, 2010; Lorrai et al., 2010) can be applied for REA.

The main steps on data processing to obtain the fluctuation of the vertical velocity (w') are: the removal of outliers and of anomalous velocity data, the prototype alignment with the vertical and the extraction of vertical velocity fluctuations.

The first step is required to replace low confidence velocity data measured by the ADV to reduce sampling bias. Two methods can be applied: the replacement by interpolation of velocity values of low

correlation between pulse and echo or of signal-noise-ratio (SNR) (Wahl, 2000) and the Phase-Space Threshold (PST) method presented by Goring and Nikora (2002).

The flux after Reynolds decomposition contains the contribution of advection, i.e. the flux of the compound passing along the bed with the flow ($F = \overline{\boldsymbol{wC}} + \overline{\boldsymbol{w'}}\overline{\boldsymbol{C}} + \overline{\boldsymbol{w}}\overline{\boldsymbol{C'}} + \overline{w'C'}$, see at Lorke et al., 2013). The **alignment** of the current meter coordinate system allows to find the normal to the sediment surface and to eliminate the advection contribution to the flux. All methods used to calculate alignment angles (i.e., the tilt, pitch and roll) use measured *u*, *v* and *w* to find the coordinate system of the stream line or of the main current. The output is velocities aligned to the main current direction, null average vertical velocity ($\overline{w} = 0$) and null average turbulence fluctuation ($\overline{w'} = 0$).

Finally, the fluctuation is extracted through Reynolds decomposition ($w' = w - \overline{w}$), where the average vertical velocity $\overline{w}$ is usually obtained by a running mean (Lorrai et al., 2010), useless if, ideally, $\overline{w}$ is 0. This step is a high-pass filtering in case there are low frequency oscillations (e.g., seiches in a lake).

For EC, an additional and final step used to calculate fluxes is the **synchronization** of velocity and concentration time series. A temporal delay is applied in the datasets by shifting the fluctuation compound concentration dataset (*c*') over the velocity fluctuation *w*' dataset, searching for the highest flux amplitude or the lowest probability of decorrelation (Donis et al. 2015). EC data processing is executed after the campaign. For REA this step is not possible as it bases sampling decisions on the instantaneous vertical velocity data in the field. Even without this synchronisation, in their theoretical feasibility study of subaquatic REA, Lemaire et al., (2017) found limited discrepancy between EC and simulated REA fluxes.

Figure 27 - Velocity processing steps to obtain the fluctuation of the vertical velocity.

All data processing steps executed by EC cannot be executed by REA or require adaptation. The PST executed to remove anomalous velocity outliers requires an analysis of the whole vertical velocity dataset. REA measurements does not have it. REA is limited to use the correlation and SNR measured by the ADV. The axis alignment and fluctuation extraction are possible and required by REA, but they also require an adaptation.

For the tests presented below two datasets measured by an ADV at 8 Hz were used. Both measurements were 10 cm above the sediment surface. The first dataset is a four-day measurement at lake Champs (Champs-sur-Marne – France), a survey site of the research group Leesu. Lake Champs is a shallow lake (average depth of 3 m), very eutrophic, located in an urbanized area. The lake has neither inflow nor outflow. The second dataset is a four-hour measurement from the Loge stream (Saint-Germain-sous-

Doue – France) in the Orgeval watershed, an experimental site of INRAe. The Loge stream is shallow and located in catchment with intensive agriculture. These sites will be presented in more detail in subsections 6.2.5 and 8.3.2.1.

4.4.7.1 Aligning the axes to remove the advection contribution to the fluxes

In the data processing of fluxes for EC two of the most usual methods for axis alignment are the 2-axes rotation and planar fit (Wilczak et al., 2001; Lorke et al., 2013). The use of these methods for REA has a constraint. The alignment parameters, angles or rotation matrix, are calculated before the start of the segment, during what can be called a pre-segment, and then applied to the segment (Figure 28).

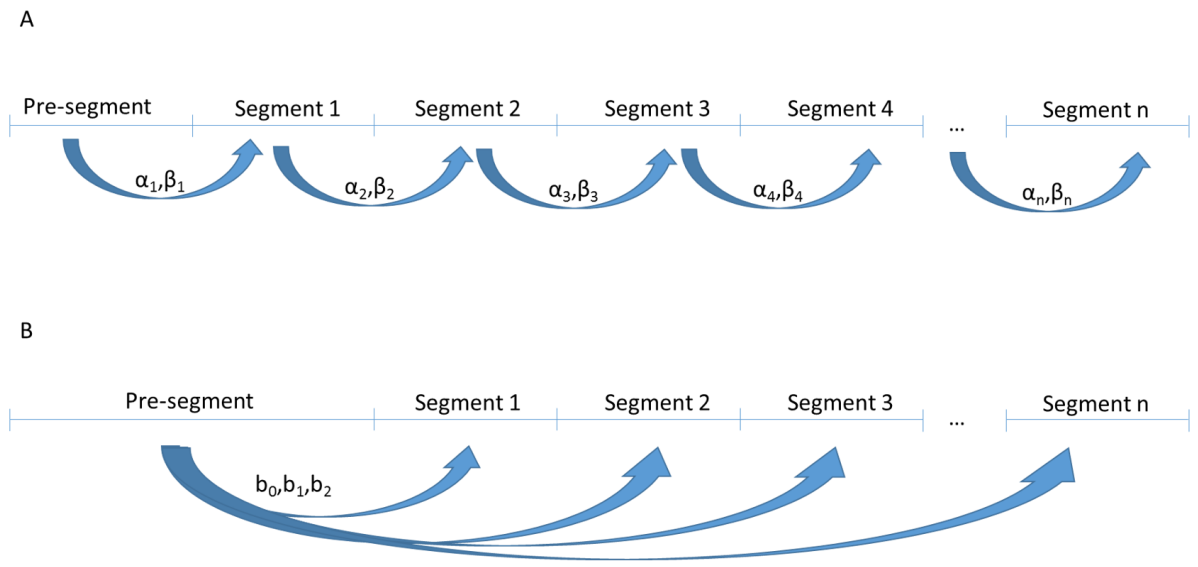

Figure 28 - Possible methods of axis alignment for REA and temporal steps of execution in field. The upper part of the figure (A) the 2-axis rotation, which for every segment there is an equal duration pre-segment to calculate the angles α and β. The bottom part of the figure (B) the planar fit method, which one pre-segment is executed for long duration resulting in the angles b_1 and b_2 and the coefficient b_0.

The 2-angles rotation uses velocities measured by the current meter (u_m, v_m and w_m) to orientate them to the main current coordinate system. Intermediary velocities (u_a, v_a and w_a) are used to calculate angles α for the rotation around the z-axis (1st column of Eq. 36) and β around the y-axis (2nd column of Eq. 36) , so that the mean of the first component $\bar{u}$ aligns with the main current and that the average vertical velocity $\overline{w}$ vanishes (Lorke et al., 2013).

$$\alpha = \tan^{-1}\frac{\bar{v}_m}{\bar{u}_m} \qquad \beta = \tan^{-1}\frac{\bar{w}_m}{\bar{u}_m}$$

$$u_a = u_m \cos\alpha + v_m \sin\alpha \qquad u = u_a \cos\beta + w_a \sin\beta$$

$$v_a = -u_m \sin\alpha + v_m \cos\alpha \qquad v = v_a$$

$$w_a = w_m \qquad w = -u_a \sin\beta + w_a \cos\beta$$

(Eq. 36)

For REA, the angles α and β are calculated with velocities measured during the pre-segment. Calculated angles are applied to measured velocities during the segment (Figure 28A).

The **planar fit** uses tens of successive periods *i* of mean velocity vectors ($\bar{u}_i$, $\bar{v}_i$ and $\bar{w}_i$) from a longer dataset to fit the following multilinear model and find the plane of the current, parallel to the sediment surface (Wilczak et al., 2001; Lorke et al., 2013).

$$\bar{w}_i = b_0 + b_1\bar{u}_i + b_2\bar{v}_i \qquad \text{(Eq. 37)}$$

Where b_0 is a potential bias on the vertical velocity due to the instrument and b_1 and b_2 are used to rotate the axes in the x-y plane. To obtain the aligned vertical velocity w we have:

$$w = -\frac{b_1}{\sqrt{b_1^2 + b_2^2 + 1}}u_m - \frac{b_2}{\sqrt{b_1^2 + b_2^2 + 1}}v_m + \frac{1}{\sqrt{b_1^2 + b_2^2 + 1}}(w_m - b_0) \qquad \text{(Eq. 38)}$$

For REA, b_0, b_1 and b_2 are calculated during the pre-segment. They are applied to the velocities over the different segments (Figure 28 B).

These methods required tests before applying them in the REA automation. The objective was to find the method which better eliminates advection in different hydrodynamic conditions. For planar fit, it is additionally important to determine the required pre-segment duration.

The indicators are the mean velocities after alignment along the vertical and along the mean current $\bar{w}$ and $\bar{u}$, computed for each method and for both sites with contrasted hydrodynamic condition (similar evaluation at Lorke et al., 2013).

The differentiation of the hydrodynamics of the two waterbodies will be made by: the frequency range of the flow turbulent domain (energy peak in velocity variance-preserving autospectra) and the turbulent kinetic energy (*k*). The turbulent kinetic energy is a proxy for turbulent diffusion and intensity (Stull, 1988) as well as the friction velocity:

$$k = \frac{1}{2}\left(\overline{u'^2} + \overline{v'^2} + \overline{w'^2}\right) \quad \text{(Eq. 39)}$$

4.4.7.2 Removing turbulence of low frequency

For this step, EC uses a centred running average over 2s+1 points (Berg et al., 2003), where $s = f.T_{RA}$, f is the sampling frequency and T_{RA} is the half-duration of the running average in seconds. Thus:

$$w_i' = w_i - \frac{1}{2s+1}(w_{i-s} + \cdots + w_i + \cdots + w_{i+s}) \quad \text{(Eq. 40)}$$

where w_i is the instantaneous measured velocity.

However, as mentioned above, REA is restricted to past velocity values. A portable REA for atmosphere presented by Sarkar et al., (2020) adapted the method above for the fluctuation extraction of the vertical velocity. Velocity data is collected before the segment starts for 30 min to provide $\overline{w}$ for the further segment. Such a duration would not eliminate low-frequency fluctuations in lentic environments, for instance. Hence, a new approach is proposed, a running mean based on past values only.

$$w_i' = w_i - \frac{1}{s+1}(w_{i-s} + \cdots + w_i) \quad \text{(Eq. 41)}$$

Tests were carried comparing simulated REA sampling action using both running averages to test if the new running average works and determine its best duration. REA sampling occurs when the fluctuation of the vertical velocity is above a threshold velocity. The simulation of REA sampling action is possible by just using any velocity dataset. The dataset used for this test were presented in the previous subsection. For this specific test, the datasets were aligned with the planar fit method.

4.5 RESULTS AND DISCUSSION

Here we present the results of the tests described on the methods section. Different tests were conducted to find best REA adaptation to aquatic environments regarding sampling mechanism, sampling flow rate regularity, the mechanical stability of the frame, and the suitability of the data processing.

4.5.1 Mechanical characteristics and choices

4.5.1.1 Only the passive mechanism produces a constant flow rate

In this subsection we present the results of the tests of the both the active and passive sampling mechanisms. A first test was conducted to verify the flow rate produced by the active and the passive mechanisms. For that, the active mechanism, operated by a peristaltic pump, sampled water for the same total duration on sequences of pump activation and deactivation with different sampling intervals. The passive system, using pressure difference between inlet and outlet of the sampling tubes, sampled water

at different hydrostatic pressure levels. The weight of the water sampled by both mechanisms was used to calculate the flow rate.

The flow rate produced by the active system decreased with the duration of and between individual activation periods (Figure 29). The standard error for each sampling interval repetition is low (n = 4). An increasing flow rate was measured because the peristaltic pump has a time response to activate and to deactivate. The smaller the sampling interval imposed, the smaller the actual time the pump rollers are static (time response > sampling interval).Thus the higher the flow rate is when the sampling interval is higher than the time response.

Transforming the number of sampling intervals (si) in frequency ($f = 1/si$) the same flow rate pattern is obviously observed, the higher the frequency the higher the flow rate. The minimum required sampling frequency to follow turbulence fluctuation is above 1 Hz. Thus, the time response of the pump at or beyond 1 Hz creates a risk of oversampling when the pump is activated for a short time (one to a few time steps at 4 Hz).

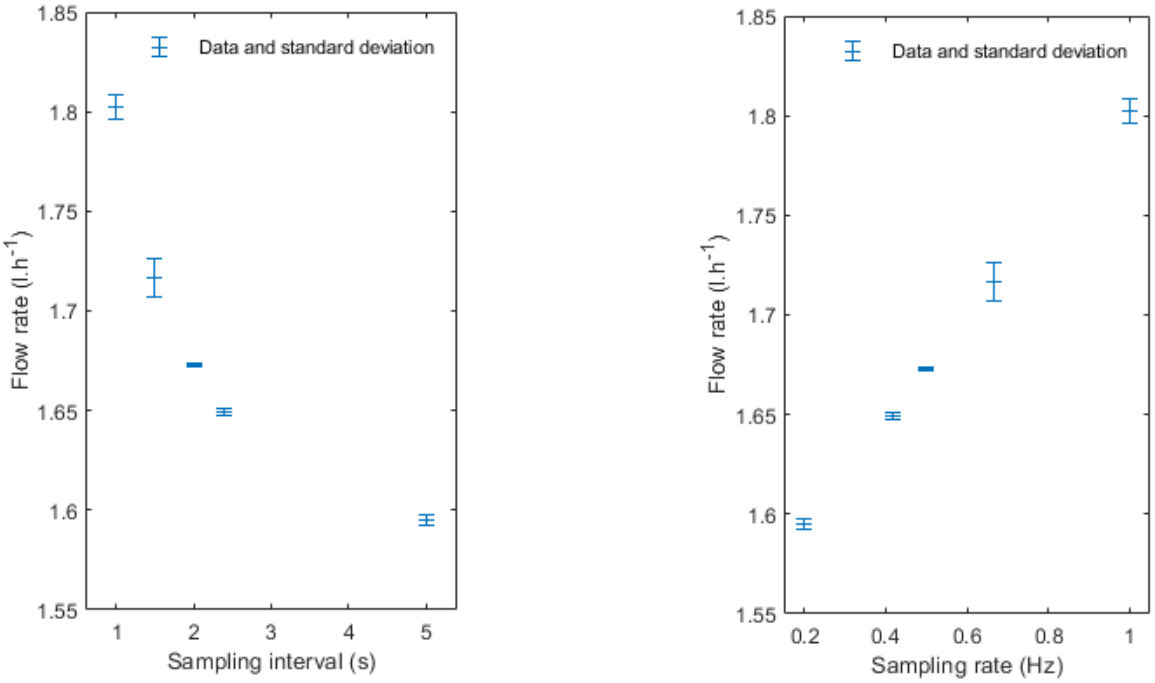

Figure 29 - Obtained flow rates using active system. On the left-hand side flow rate over the different sampling intervals and on the right-hand side the same flow rate on different sampling rate. Sampling intervals were transformed in sampling rate.

For the passive system the hydrostatic pressure difference between the tube inlet and outlet drives the water. The test shows that, as expected, the flow rate increases linearly with pressure difference (Figure 29). A pressure of around 0.3 bar led to a flow rate greater than 10 L h^{-1} and a pressure of around 0.1 bar to a flow rate greater than 3 L h^{-1} i.e. around 33 L h^{-1} bar^{-1} The expected linearity of the flow rate produced by the passive system encourages its use for REA. Also, in the passive system, as mentioned above, the sampling is triggered by the action of the solenoid valves. In the technical note provided by

the supplier of the solenoid valve the response time of the valve is 10 ms, thus the valve can sample at 100 Hz.

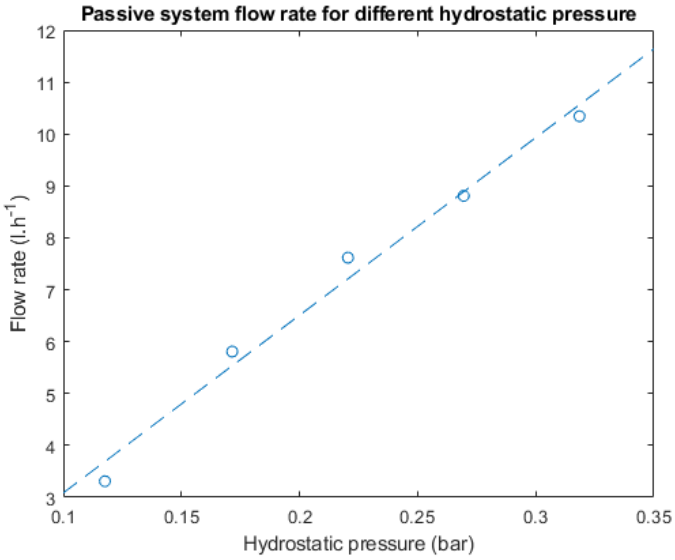

Figure 30 - Flow rate obtained by the passive system for the different hydrostatic pressures.

Taking into account the flow rate (Q) obtained for the range of hydrostatic pressure (Figure 30), the sampled volume (V) for a given accumulation period can be simulated. As mentioned before a minimal sample volume of 200 mL is the required for chemical analyses of a great range of nutrients and metallic ions (section 4.3.2). The segment duration (T) can vary from 10 to 30 min. The use of a threshold velocity (w_0) (section 4.2) by REA corresponding to 75% of the σ_w leads to an effective sampling duration of 45% for a single accumulation duration (e.g., 9 min of 20 min accumulation), thus 22.5% for each sampling line (Lemaire et al. 2017). So, the final volume should be:

$$V = Q\ T\ 0.125 \qquad \text{(Eq. 42)}$$

Comparing the obtained volume for the different segment duration and hydrostatic pressure range (Figure 31) the device can face a technical limitation. Accumulation periods shorter than 30 min at low water depth (0.2 bar for 15 min) do not sample the minimal required volume (200 mL) for chemical

analysis to explore a great range of compounds. In conclusion, the passive mechanism cannot provide capacity to REA execute measurements in shallow waterbodies (e.g., small rivers or streams).

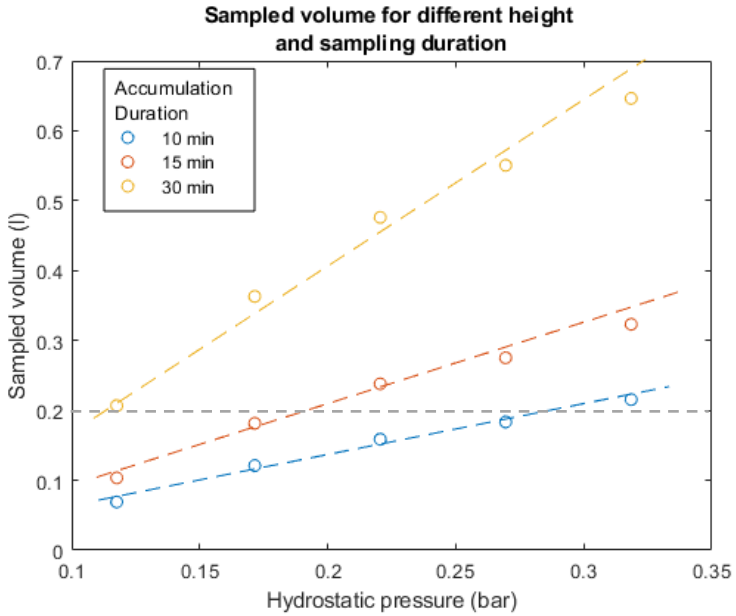

Figure 31 - Simulated sampled volume at different water depths for different segment durations. Grey dashed line is the minimal volume required for chemical analysis of the sample (200 mL).

4.5.1.2 Only the passive system produces manageable perturbation of the flow

The passive and the active mechanisms were deployed in a flume in order to test their ability to follow fast turbulence fluctuations and to observe the hydraulic perturbation by sampling. The PIV technique was used to evaluate the differences between the mechanisms. Under flow water we could not spot the sampling by REA (flow rate ≈ 4.3 L h) using the PIV. Thus: The hydraulic perturbation by sampling on running water is negligible; The experiment could not test the sampling ability of the mechanisms on running water.

In stagnant water the hydraulic perturbation of both mechanisms had 1 cm radius around the sampling tube inlet. Therefore, for the final setup the sampling tube inlets must be 1 cm away from the velocity measurement volume.

The active system samples in pulses, at a frequency which increases with the flow rate. This occurs because the rollers of the peristaltic pump mechanism squeeze the sampling tube to create a depression and, thus, make the water flow in the tube. The pulses are observed because the rollers do not press the tube constantly, and, the created depression inside the tube is not constant. The pulses, for the experiment setup, were observed at a frequency of around 2 Hz, a frequency which, depending on the hydrodynamic

conditions, can be in the turbulence range of the flow (section 4.3.3). For the passive system sampling the same problematic was not observed.

As a conclusion from these tests, the active system, normally used in atmospheric REA devices, is not suitable for the REA prototype. The sampling pump is not capable to follow high frequency turbulence fluctuation nor to produce stable flow rate for our requirements. The passive system, on the other hand, is capable to sample at high frequency (8 Hz) at reliable flow rate. However, two points require attention: The mechanism requires assistance to allow REA to measure fluxes in shallow rivers and streams, since the passive system sampling is based on hydrostatic pressure difference; The inlets of the sampling tubes is advised to be 1 cm away from the velocity measurement volume.

4.5.1.3 Sampling system adaptation for low water depths

An adaptation was required to overcome the water depth limitation for the passive system. To increase the pressure difference ΔP between the inlet and outlet of the sampling tube, a vacuum pump creates a depression in the accumulation bottle. A test was carried out to estimate the depression in the bottle and the resulting flow rate.

At 50 cm water depth and with respective depressions of -0,52 bar and -0.27 bar (total pressure difference 0.57 and 0.32 bar), the obtained average and standard deviation of the flow rates were, respectively, 12.7 ± 0.21 and 8.21 ± 0.3 L h^{-1} For the application of the passive system assisted by vacuum the required sample volume (200 mL) is obtained in 7.5 min and 12 min. Thus, the application of REA in streams and shallow rivers is solved.

4.5.1.4 A topographic tripod as a frame avoids that vibrations bias sampling

The device frame was initially thought in the shape of a metal squared table (Figure 33). However, the frame must not vibrate at a frequency within the turbulence range. A theoretical and a practical test was executed to estimate the frame vibration frequency. The former using the Strouhal number (Eq. 28) and

the latter setting up the frame in a flume with 2 accelerometers installed on an average current speed of 0.2 m s^{-1}.

The Strouhal number for the frame denotes a frame vibration at 1 Hz when the mean current speed is 0.2 m s^{-1} and the frequency doubled when the current speed also doubled (Figure 32). The accelerometers measured a frame vibration frequency of 3 Hz for an average current speed of 0.2 m s^{-1}.

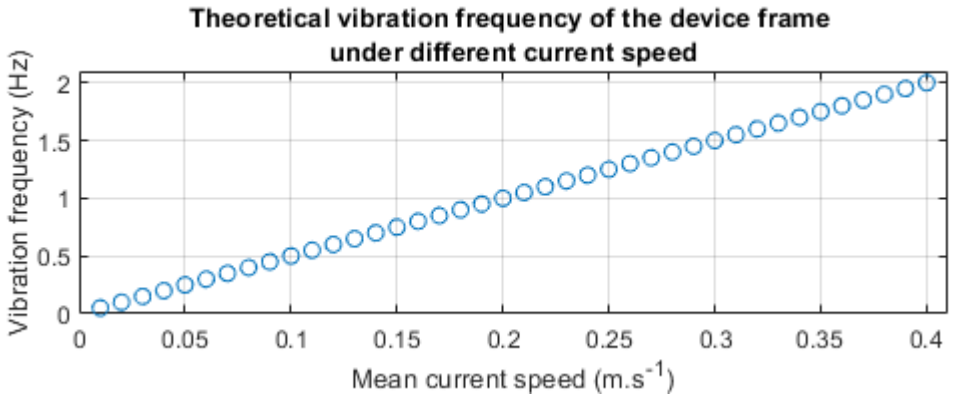

Figure 32 - Theoretical vibration of the device frame under different mean current speed

This value of current speed and above are often measured in rivers. The theoretical and practical vibration values differ because the frame is composed of T-slot profile bars in the upper part which is not considered in the computation of the Strouhal number.

The table-shaped frame is not suitable because it vibrates within the turbulence range of the flow (commonly 0.1-5 Hz, see Lorrai et al. (2010) quoted in subsection 6.4.6). The solution found was the replacement of this frame for a topographic tripod (Figure 33), as used by Lorke et al., (2019) for an eddy covariance setup (the hydrodynamic conditions are the same).

Figure 33 - Prototype frame evolution after frequency vibration tests. On the left-hand side (A) the former square shaped frame and in the right-hand side (B) the frame is a tripod.

4.5.2 Automation main functions and data processing

The development of a velocity processing specific to REA is required. The velocity processing steps used by eddy covariance to obtain the fluctuation of the vertical velocity need to be. REA is limited to past velocities unlike EC that uses the whole velocity dataset (in-line processing vs post-processing). Two steps investigated here to find the best adaptation: the axis alignment and the extraction of turbulent vertical velocity fluctuations.

4.5.2.1 Axis alignment for REA

The objective of the axis alignment step is to eliminate the contribution of advection to the flux. This step of data processing for EC is executed after field campaign unlike for REA which sampling requires vertical velocity aligned using past values (Figure 28). The objective here is to determine which axis alignment method should be privileged by REA in different hydrodynamics conditions. The methods for axis alignment used in the test are the double-axis rotation (also named 2-angles rotation) and the planar fit. A specific objective is to determine for planar fit the required duration of pre-segment according to hydrodynamics. To evaluate the alignment methods, velocity datasets collected at high frequency (8 Hz) in a shallow stream, the Loge stream in the Orgeval experimental catchment, and a shallow lake, Lake Champs-sur-Marne, were used.

The first step of the test for the two datasets is to find the required duration of pre-segment for planar fit. The second step is to align the velocity using both methods to understand which method is more reliable for the different waterbody hydrodynamics.

4.5.2.1.1 Axis alignment in highly turbulent conditions (river)

The use of a stream in the test allowed to access a waterbody whose current direction does not change and where turbulence is stable. The raw velocity dataset is divided into 14 segments of 10 min (Figure 34). The mean current speed and its standard deviation over the segments are 0.02 ± 0.009 m s^{-1}, the average vertical velocity is 0.001 ± 0.002 m s^{-1}, the friction velocity is 0.0029 ± 0.0003 m s^{-1} and the turbulent kinetic energy is 2.3 10^{-6} J kg^{-1}. From the raw data it is possible to observe that axis alignment is mandatory: the average vertical speed ($\overline{w}$) is not negligible compared to the average current speed. The standard deviation of vertical velocity (σ_w) denotes a turbulent environment, what turbulent kinetic energy and dynamics confirm (Figure 35). The turbulence was captured by measurements: the inertial subrange with a -5/3 slope is observed at high frequency in the autospectrum (Figure 37). The high cutoff frequency (f_{high}) of the turbulence domain can be seen in the variance-preserving autospectrum around 1 Hz, so that the whole turbulence domain is covered. The turbulent kinetic energy is in the same order of magnitude as in regular rivers (around 4.0 10^{-6} m^2 s^{-2}).

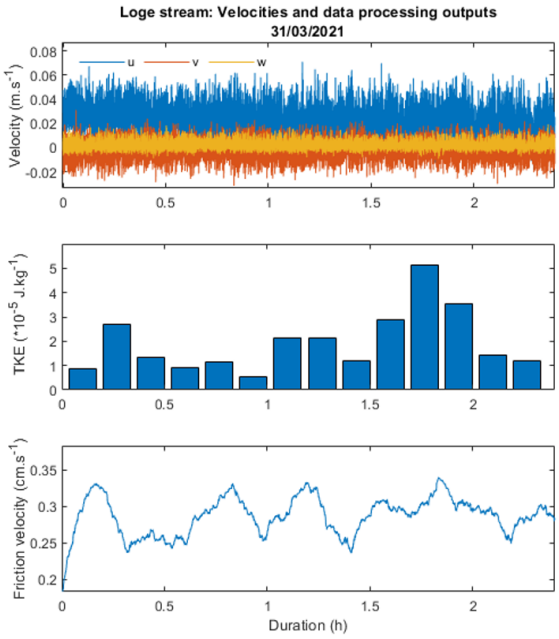

Figure 34 - Measured velocity at the Loge stream (A), the calculated turbulent kinetic energy (B) and friction velocity (C) dynamics over time.

In order to determine the required duration of pre-segment for planar fit, coefficients b_0, b_1 and b_2 of the multilinear regression were calculated for an increasing number of measured velocity points (Figure 37). The calculation started with 10 min of dataset and new velocity data were imported to the calculation of the angles in subsets of 10 min. The angles were recalculated until the end of the dataset. The idea is to empirically find when new velocities do not change the angles.

For the Loge stream the b_0, b_1 and b_2 stabilized when more than the first 1h20 min of measurements were used for the regression (Figure 36). The obtained values were used to align the velocities of the following segments. To obtain comparable temporal series the simulation of the velocities which could be used to drive REA, processed using 2-axis-rotation started 1.4 hour after the start of the dataset. Segments were also of 10 min.

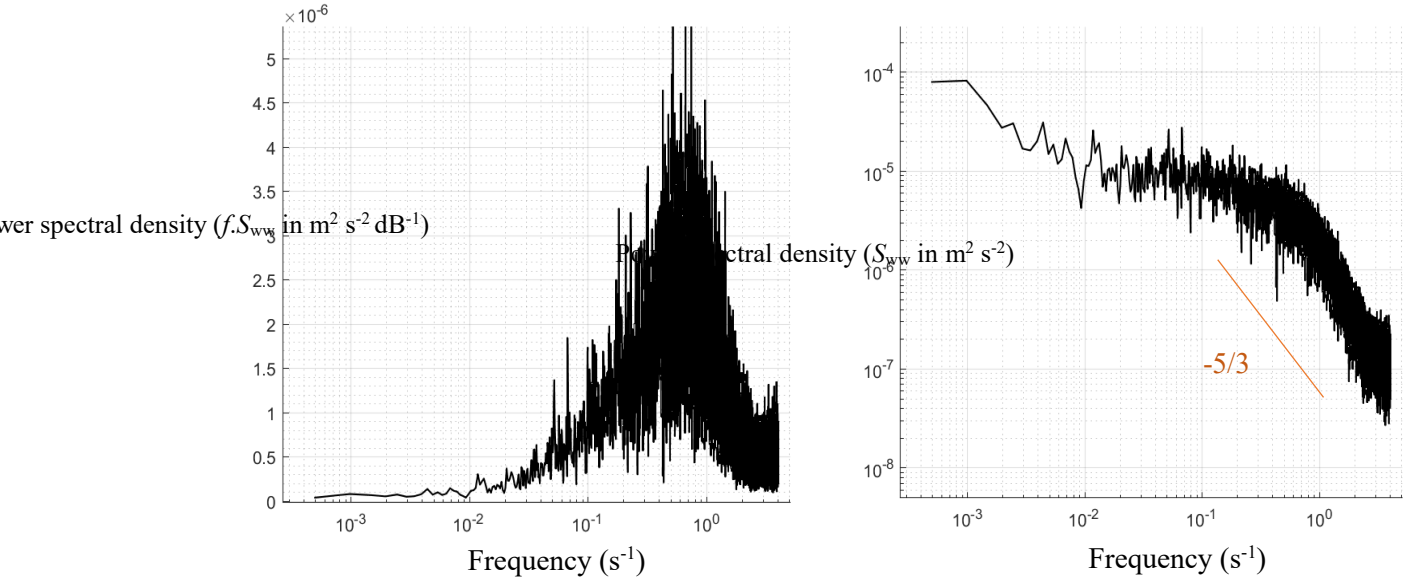

Figure 35 - Power spectral density of the vertical velocity measured at Loge stream. In the left-hand side the variance-preserving presentation and in the right-hand side the logarithmic scale presentation including (in orange) the -5/3 slope.

The first important outcome from the test is that all methods for axis alignment yielded similar mean current speeds $\bar{u}$. For the vertical velocity mean ($\bar{w}$), 2-axis rotation yielded lower values than planar fit (Table 4). However, when the axis alignment methods are applied only to past values as can be done in the field for driving REA, the values are smaller than for the raw data, but not as small as for the 2-axis rotation. The axis alignment methods adapted by REA data processing help to reduce or cancel advection contribution to the fluxes (Table 4). In fact, the conditional sampling characteristic of the technique helps. The threshold velocity (w_0) reduces the impact of advection. The output $\bar{w}$ by REA data processing was below w_0 for both axis alignment methods. Therefore, the influence of advection to the fluxes is limited by REA data processing and by REA threshold velocity.

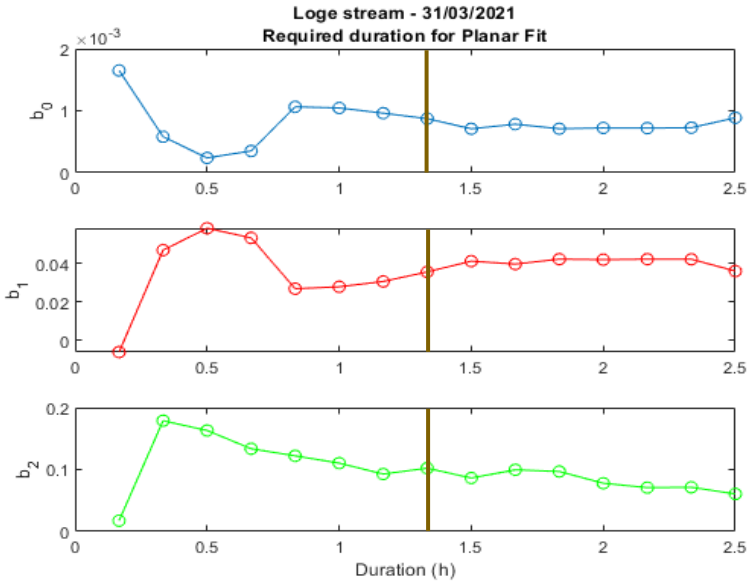

Figure 36 - Calculated b0, b1 and b2 using the Planar Fit method and, in brown, the pre-segment duration required to align prototype axes before starting the REA sampling.

Table 4 – Obtained results for mean current speed ($\bar{u}$) and mean vertical speed ($\bar{w}$) using two methods for axis alignment and applying them to REA data processing

Seg t	Raw data		w_0 (m.s^{-1})	2-axis rotation		Planar fit		REA data processing			
								2-axis rotation		Planar fit	
	$\bar{u}$ (m.s^{-1})	$\bar{w}$ (m. s^{-1})		$\bar{u}$ (m. s^{-1})	$\bar{w}$ (m. s^{-1})	$\bar{u}$ (m. s^{-1})	$\bar{w}$ (m. s^{-1})	$\bar{u}$ (m. s^{-1})	$\bar{w}$ (m. s^{-1})	$\bar{u}$ (m. s^{-1})	$\bar{w}$ (m. s^{-1})
1	0.018	1.5 10^{-3}	0.0015	0.018	-4.40 10^{-19}	0.018	-3.06 10^{-5}	0.018	2.20 10^{-4}	0.018	7.79 10^{-6}
2	0.018	1.4 10^{-3}	0.0016	0.019	-3.28 10^{-19}	0.019	-3.27 10^{-5}	0.019	-7.49 10^{-5}	0.019	5.40 10^{-5}
3	0.017	1.4 10^{-3}	0.0016	0.018	6.54 10^{-19}	0.018	-2.53 10^{-5}	0.018	7.29 10^{-6}	0.018	1.05 10^{-4}
4	0.017	1.5 10^{-3}	0.0017	0.017	-1.62 10^{-18}	0.017	1.79 10^{-4}	0.017	2.35 10^{-4}	0.017	3.12 10^{-4}
5	0.014	1.4 10^{-3}	0.0017	0.015	-1.61 10^{-18}	0.015	1.19 10^{-4}	0.015	5.62 10^{-5}	0.015	2.63 10^{-4}
6	0.018	2.2 10^{-3}	0.0020	0.018	1.13 10^{-18}	0.018	7.25 10^{-4}	0.018	4.24 10^{-4}	0.018	8.45 10^{-4}

4.5.2.1.2 Axis alignment in a low-energy environment (shallow lake)

The use of axis alignment for REA in lakes is more complex than in rivers because current speed and direction are not constant. For this test the velocity dataset captured at lake Champs was divided into 3 parts: 0 to 30 h, 30 h to 60 h and 60 h to 90 h (Figure 37). The separation is useful to observe 3 different states of hydrodynamics in the lake.

The average values characterising the hydrodynamics is presented and some points can be highlighted. The last part of the dataset presents more intense turbulence with higher values of turbulent kinetic energy, friction velocity and standard deviation of vertical velocity. The power spectra for all three parts

(Figure 39) do not clearly present the -5/3 slope of the inertial subrange and confirm that turbulence is low not only in the 3rd part, but in all of them. Also, to support the idea of low turbulence, the energy peak in the turbulence domain in the variance preserving presentation is very small (<1.5 10^{-7} m^2 s^{-2} dB^{-1}) and high noise is observed at high frequencies.

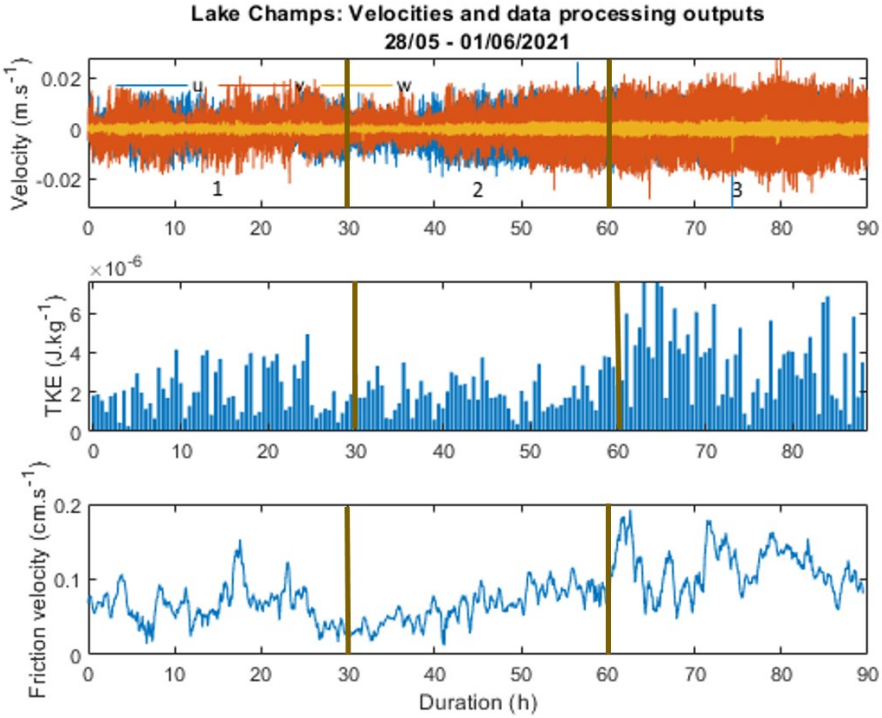

Figure 37 – Measured velocity at Lake Champs and calculated turbulent kinetic energy and friction velocity. Brown line separate the data into three subsets.

Table 5 – Average values from each part of the dataset concerning friction velocity (u_*), turbulent kinetic energy (k), mean current ($\overline{u}$), module of horizontal speed, which is resulting vector of the u and v and mean and standard deviation of the vertical speed.

Part	u_* (cm s^{-1})	k (J kg^{-1})	$\overline{u}$ (m s^{-1})	Module of horizontal speed (m s^{-1})	$\overline{w}$ (m s^{-1})	σ_w (m s^{-1})
1st	0.0653	2.04E-06	-0.00002	0.0002	-0.0001	0.0004
2nd	0.0643	2.06E-06	-0.00039	0.0004	-0.0002	0.0005
3rd	0.1129	2.83E-06	0.00017	0.0001	-0.0002	0.0007

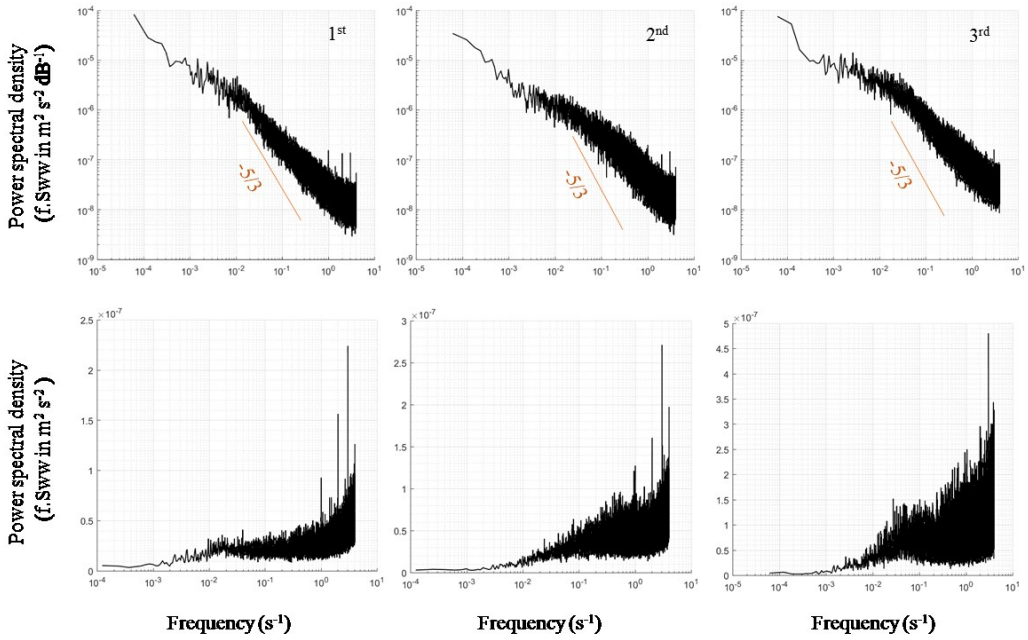

Figure 38 – Power spectral density of the vertical velocity measured at Lake Champs and separated in three parts (1,2 and 3). The figures in the top row show the log scale presentation, including the -5/3 slope (in orange), and those in the bottom row show the variance preserving presentation.

Following the same approach as for the Loge stream the pre-segment duration for planar fit was determined. As previously, a first calculation of b_0, b_1 and b_2 used 10 min of dataset and new sets of 10 min was imported for the calculation of the coefficients until the end of the dataset. The stabilization of the angles is not perfectly achieved (Figure 39). For all three parts an acceptable stabilization was achieved, in chronological sequence, after 15, 17.5 and 22h from the start of respective datasets. The higher is the complexity of the hydrodynamics of the lake, the longer the required duration for pre-segment using planar fit.

The obtained b_0, b_1 and b_2 of each part are used to align the axes for the rest of the dataset of the part. The applied equations for w alignment for each part after their pre-segment are:

1st part $\quad w = 0.015u_m + 0.0335v_m + 0.994w_m - 0.0001$

2nd part $\quad w = 0.0289u_m + 0.0115v_m + 0.995w_m - 0.0002$ (Eq. 43, 44, 45)

3rd part $\quad w = 0.0442u_m + 0.0366v_m + 0.9984w_m - 0.0002$

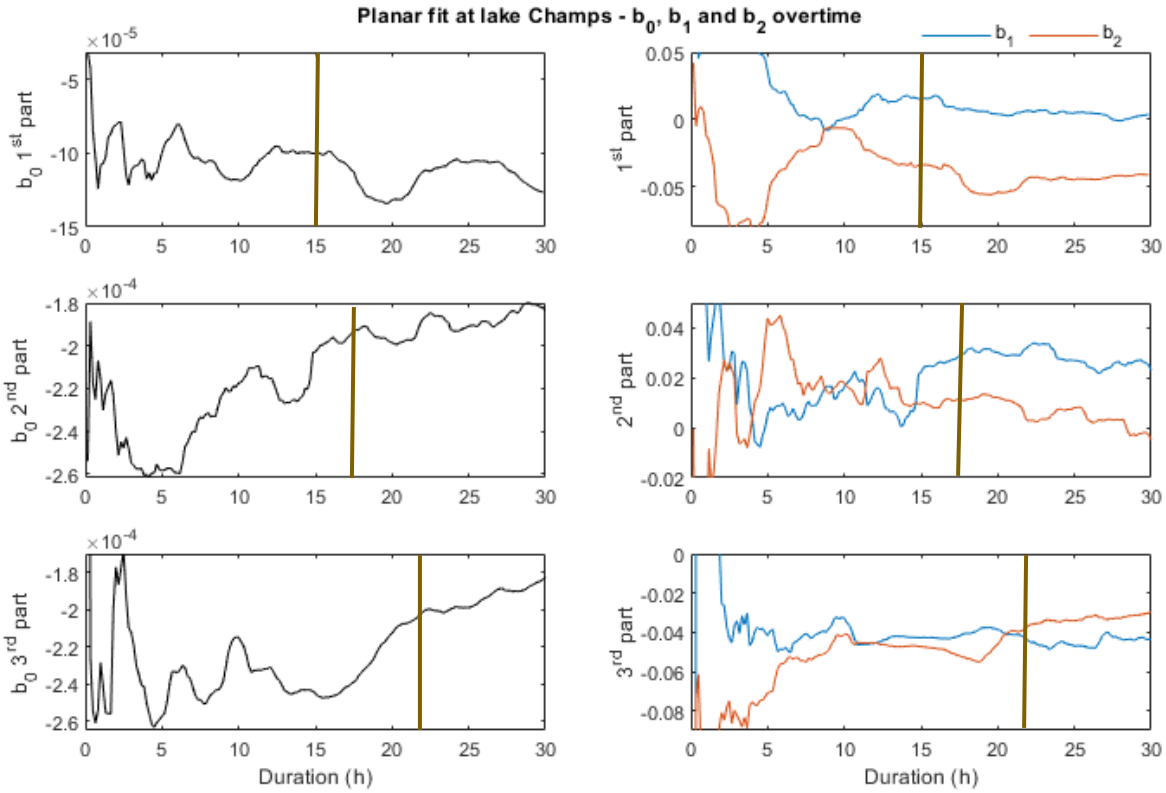

Figure 39 - Calculated b_0, b_1 and b_2 using the Planar Fit method at lake Champs for the three different parts of the dataset (up – first part; middle – second part; bottom – third part). In brown, the duration required for each part before starting the segments due to the stabilization of the calculated values.

For 2-axis-rotation the simulation of REA data processing also started at the same time as planar fit, with segments of 20 min. The calculated angles α, around z-axis and β, around y-axis were calculated for each segment (Figure 40). The angle α, which follows the current direction, is not constant within the segments for the three parts. Such fact was already expected due to lake hydrodynamics. For applying this method for REA sampling, flow conditions should remain constant for two subsequent segments, which cannot be expected. The angle β, which in an inclination of the vertical axis, also varies over the segments, but on a lesser magnitude order than α.

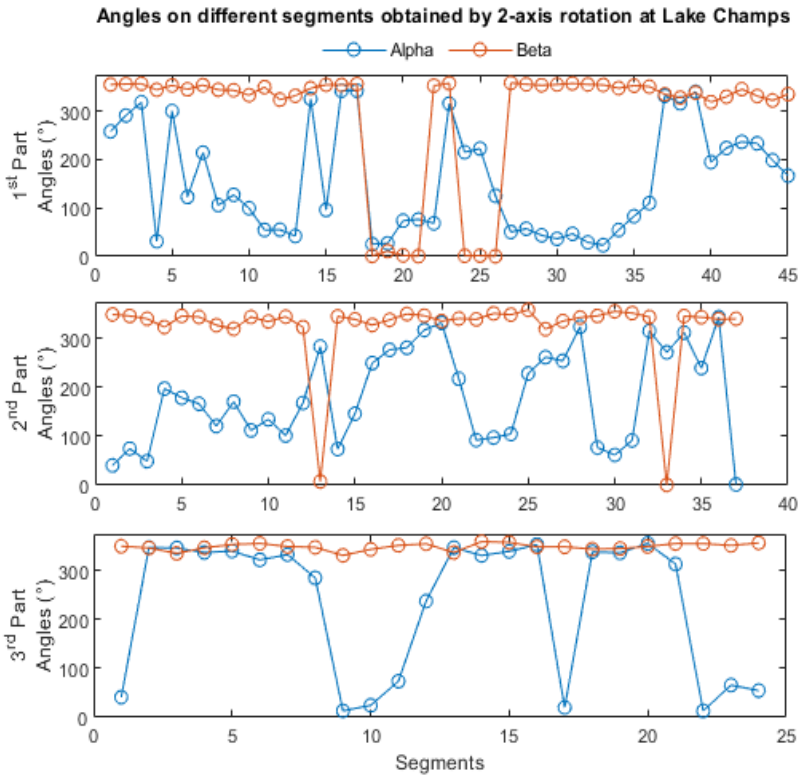

Figure 40 - The angles α and β calculated and used by REA data processing among the different segments in the different parts of the dataset of lake Champs.

Some conclusions came up from the different parts of the datasets in the lake (Figure 41 and 42). These are:

i) For all turbulent conditions there is a bias for aligned vertical velocity (*w)* between planar fit and REA data processing (REA planar fit) (Figure 42). However, the aligned vertical velocities ($\overline{w}$) are comparable

ii) The use of planar fit to align main current in all turbulent conditions (1^{st},2^{nd} and 3^{rd} parts) of the lake was similar between planar fit and REA data processing (REA planar fit) (Figure 42).

iii) The average vertical velocity $\overline{w}$ aligned by 2-axis rotation is 10^{-14} smaller than the alignment executed by REA data processing (REA 2-axis rotation). In fact, the average vertical velocity aligned by REA data processing is often close to raw data (Figure 41).

iv) The average vertical velocity aligned by REA data processing using 2-axis rotation does not follow in any of the turbulence conditions of the lake the average vertical velocity aligned by 2-axis rotation (Figure 41).

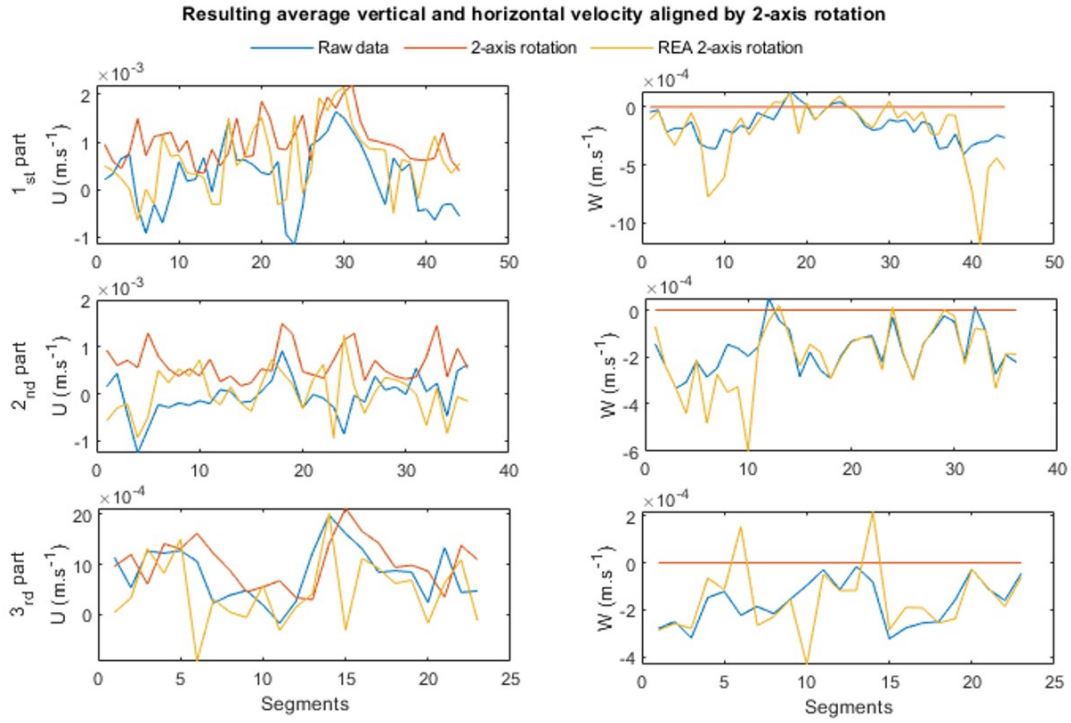

Figure 41 - Average current and current speed during each segment after use of 2-axis rotation and its adaptation for REA.

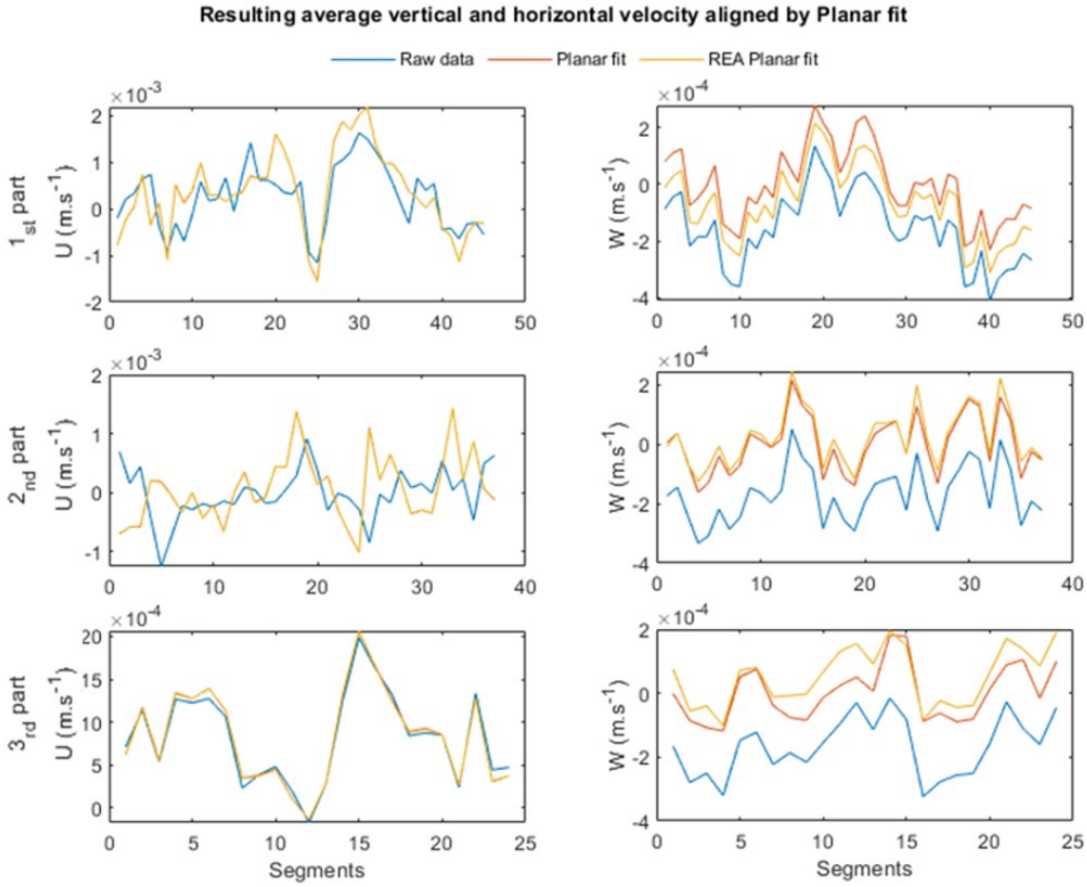

Figure 42 - Average current and current speed after use of planar fit and its adaptation for REA

The ratio of the average vertical velocity aligned by REA data processing and by the alignment methods over the threshold velocity ($\overline{w}/w_0$) was calculated for each segment. The threshold velocity was calculated for each segment. It presents two main results: Ratios of REA data processing using planar fit have less discrepancies with the ratios of planar fit than those obtained by REA data processing using 2-axis rotation and the planar fit; The smaller the ratio, the greater the ability of the conditional sampler to avoid an advection contribution to the measured flux. Thus both methods applied by REA data processing kept the average vertical velocity below the threshold velocity (Table 6).

Table 6 – Mean calculated ratios between the aligned mean vertical velocity for 2-axis rotation, planar fit and their adaptation for REA data processing and the threshold velocity (w_0)

Part	2-axis rotation		Planar fit	
	Mean ratio ($\overline{w}/w_0$)	Mean ratio ($\overline{w}/w_0$) - REA	Mean ratio ($\overline{w}/w_0$)	REA - Mean ratio ($\overline{w}/w_0$)
1st	$1.94\ 10^{-15} \pm 2.57\ 10^{-15}$	0.43 ±0.40	0.31 ±0.22	0.36 ±0.26
2nd	$9.04\ 10^{-16} \pm 7.64\ 10^{-16}$	0.27 ±0.23	0.19 ±0.13	0.18 ±0.13
3rd	$9.90\ 10^{-16} \pm 7.47\ 10^{-16}$	0.38 ±0.23	0.20 ±0.14	0.24 ±0.17

In conclusion, the axis alignment executed by REA data processing plus the conditional sampling characteristic of the technique allows to reduce advection contribution to the flux. For very turbulent environments, like, for instance, streams or rivers, both methods proved to be efficient. For less turbulent environments, like, for instance, a lake, planar fit is a more reliable and efficient method for REA data processing. The required pre-segment duration for planar fit is smaller when turbulence conditions are stable as in a river. On the contrary, environments with complex hydrodynamics such as lakes require long pre-segment durations. Further, the more complex the hydrodynamics in lakes, the longer the required pre-segment duration.

4.5.2.2 Extracting the fluctuation of the vertical velocity using REA

The fluctuation extraction of the vertical velocity for REA is important to avoid that low frequency non-turbulent flow perturbs the flux measurements. For EC, the extraction is executed through a centred running average (eq. 40), but REA is restricted on past value. Thus, a running average using only past values was adopted (eq. 41). The objective here is to determine the required size ($s = f.T_{RA}$) of the averaging window of this running average to execute the same action as a regular centred running average. The impact of poorly a selected running average size can be poor sampling by REA. The comparison between the running average of past values (also called back-looking running average) and the centred running average is made by simulating REA sampling action: REA samples when *w*' is above a threshold velocity ($w_0 = 0.75\sigma_w$). Theoretically, using this threshold, REA should sample 45% of the total duration of the segments (Lemaire et al. 2017).

Two ratios between the durations (T_{RA}) of centred and back-looking running averages were tested: 1:2 and 1:4 (30 s and 60 s, 60 s and 120 s; 15 s and 60 s, 30 and 120 s). The evaluation is based on the total sampling time (%) with the two types of running averages. In addition, the more adapted duration ratio was searched for.

For the Loge stream data, where turbulence was stable during the campaign, we observed that the sampling activity did not change with the ratio between the duration of the running averages (Figure 43). On the other hand, for Lake Champs, where turbulence intensity varies rapidly, the best ratio is 1:4 for the three periods of different turbulence intensity (Figure 44). Thus the new approach to extract the fluctuation of the vertical velocity is effective for REA data processing and a duration ratio of 1:4 is required for measurements in complex hydrodynamics. Thus, the more adapted duration for back-looking runing average is 25% of the centered running average for both hydrodynamics.

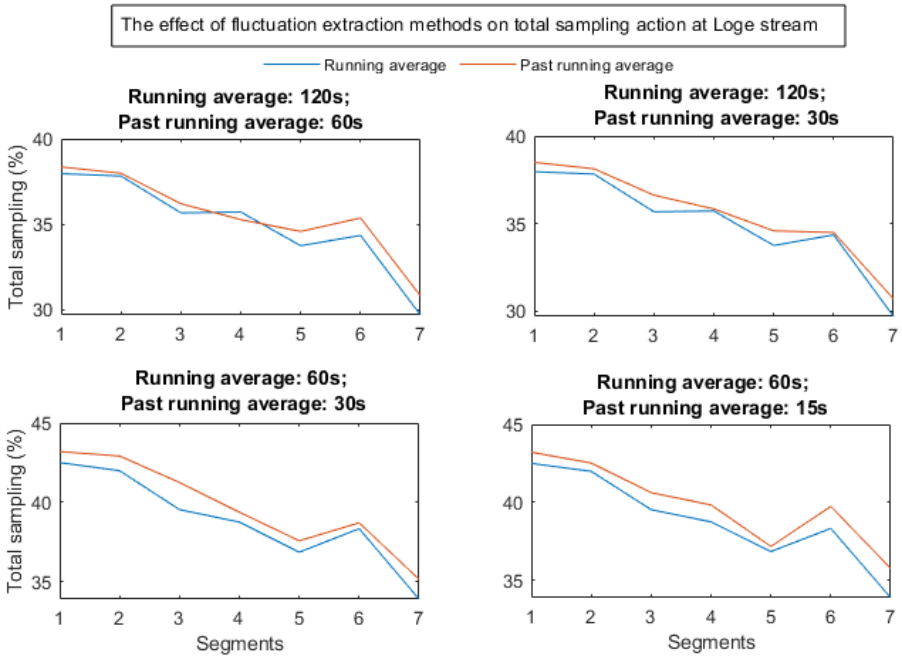

Figure 43 - Comparison of sampling time for centred and back-looking averages of different durations for extracting the turbulent velocity fluctuation (data from the Loge stream, high and stable turbulence).

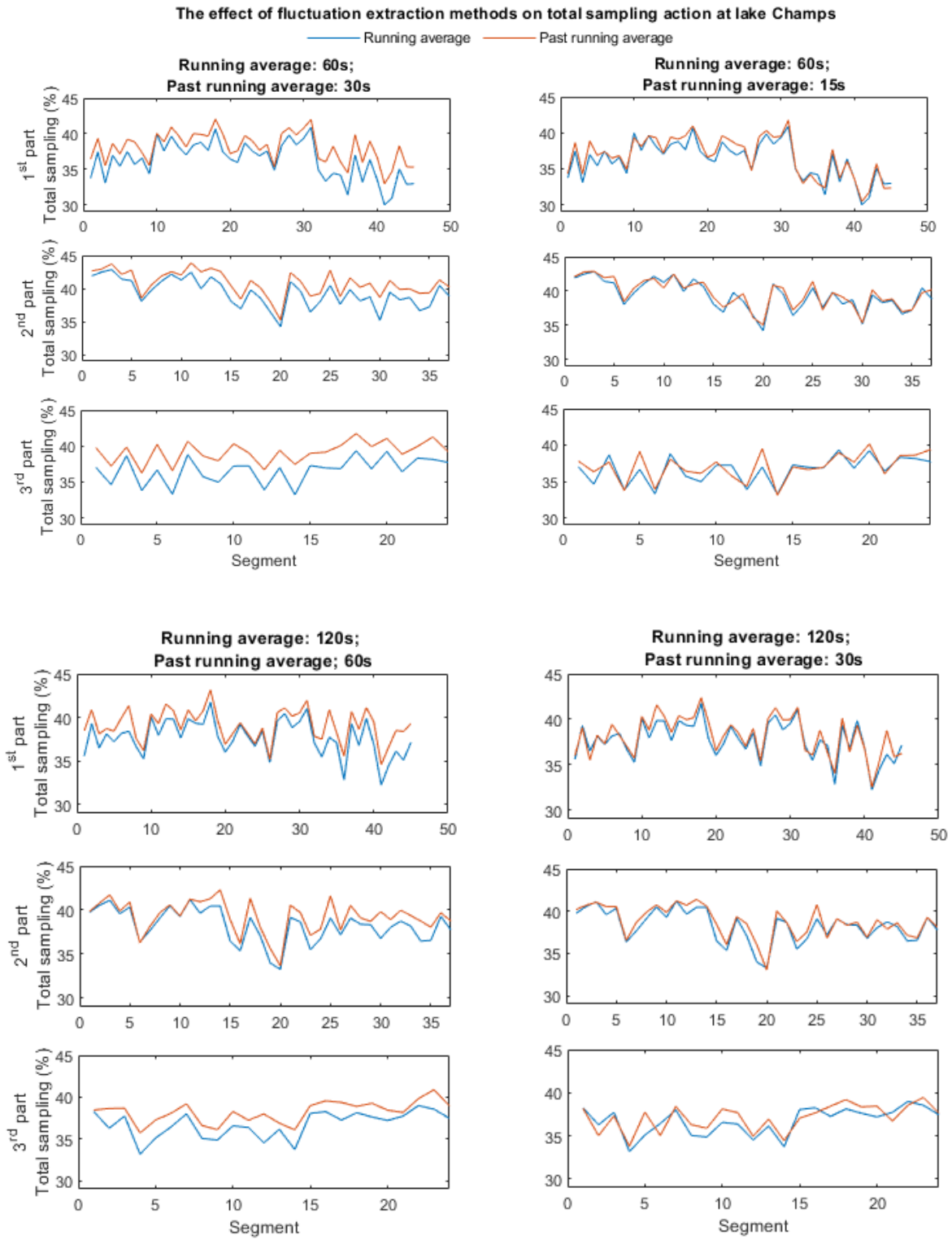

Figure 44 – Comparison of sampling time for centred and back-looking averages of different durations for extracting the turbulent velocity fluctuation (data from Lake Champs, low and variable turbulence).

4.5.2.3 *Overall action steps of REA automation containing data processing steps*

All tests and reflections concerning the velocity processing and sampling decision lead to the design of the REA automation. The resulting diagram (Figure 45) guided the coding of the automation in LabVIEW.

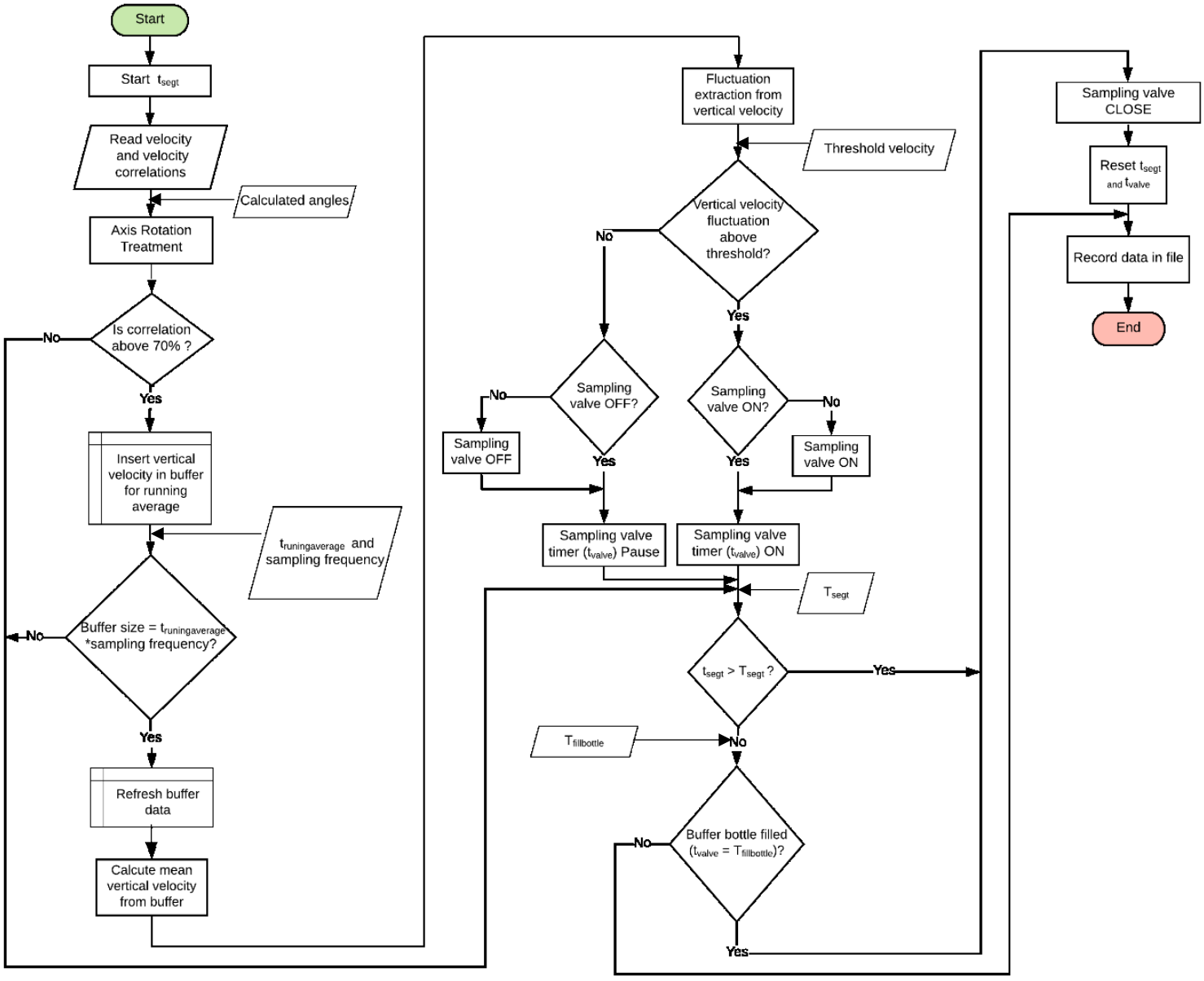

Figure 45 - Diagram representing the actions executed by REA automation. The automation runs the all the steps presented bellow for every time step, it means, it runs at desired sampling rate.

4.5.3 Required sampling frequency for REA

The sampling height is something important to measure fluxes for REA. Measurements should be executed in the turbulent boundary layer. As mentioned above different waterbodies will have different types of hydrodynamics. Turbulence above the sediment is greater in rivers and streams than in lakes. The idea of this test is to determine what is the minimum required sampling frequency to cover the turbulence range at different sampling heights. For that we used the energy dissipation in function of measurement height above the sediment, the timescale of largest and smallest eddies, the friction velocity and reference values for low and high turbulence (Table 7) (Lorrai et al., 2010).

Table 7 – Values used to calculate the required sampling frequency for different heights above the sediment

	Low turbulence	**High turbulence**
$\overline{u}_{0.1m}$	0.014 $m.s^{-1}$	0.14 $m.s^{-1}$
Friction velocity	0.001 $m.s^{-1}$	0.01 $m.s^{-1}$
Kinematic viscosity (10°C)	1.3 10^{-6} $m^2.s^{-1}$	1.3 10^{-6} $m^2.s^{-1}$

The computation of f_{high} and f_{low} for low turbulence yielded low required sampling frequencies, far below 1 Hz, at all different sampling heights (Figure 46). For high turbulence the maximum f_{low} required is 6.5 Hz when sampling height is 5 cm above the sediment.

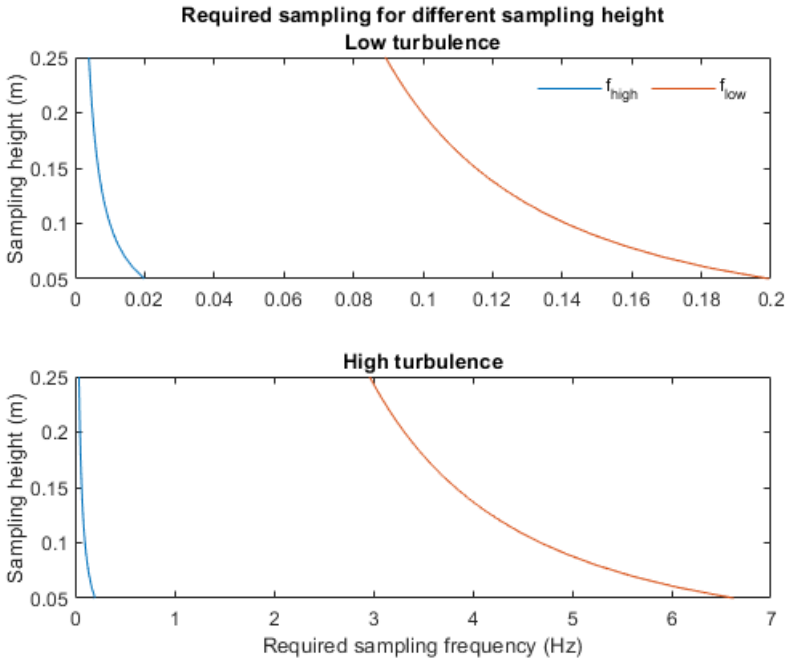

Figure 46 - Required sampling frequency calculated for different sampling heights for different turbulence conditions

The required f_{low} obtained for different heights compared to the calculated energy dissipation (Figure 47) gives a broader view of the minimum sampling frequency required by REA. From these computations we estimate that 8 Hz is sufficient to cover different types of turbulence.

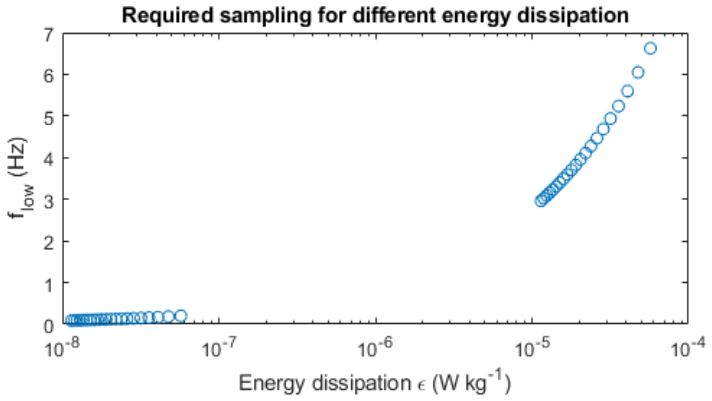

Figure 47 - Calculated f_{low} over the different energy dissipation calculated.

4.6 CONCLUSION

The test outcomes address the requirements and resulted in a prototype design that bases on REA principles and is adapted for aquatic environments. In table 8 the requirements set before starting the prototype development are presented with the solution provided by the results of the tests

Table 8 – Presented requirements in the start of the prototype development and provided solutions after obtained results from tests.

Requirement	Solution provided
Axis alignment	In aquatic environments where current direction and turbulence are constant, as rivers or streams, the axis alignment methods 2-axis rotation and planar fit can be used. In aquatic environments with varying current direction and turbulence intensity, planar fit is more adapted.
Hydraulic perturbation by sampling	The use of REA sampling mechanism in a flume analysed by PIV showed that the perturbation by the sampling action is negligible when sampling is located 1 cm away from the velocity measurement volume, even in stagnant water.
Prototype mechanical stability	The initial square-shaped table presented a vibration frequency within the flow turbulence domain. A topographic tripod of higher vibration frequencies is more adequate.
Flow rate control	The passive mechanism based on hydrostatic pressure has a regular flow rate at different depths.
Sampling based on turbulent fluctuation of vertical velocity	The flow rate test showed that the time response of the passive mechanism is short enough to sample at high frequency.
Sampling tube choice	In the sampling tubes of the prototype the samples flow in laminar regime, which make it impossible to have a common sampling tube for updraft and downdraft samples. Thus, a sampling tube is assigned to each direction.
Running average for extracting the velocity turbulent fluctuations	Simulations of REA sampling showed that a back-looking running average should be 4 times longer than a centred running mean in low turbulence environments.

The sampling engine is based on a passive system with a constant flow rate. The frame of the device is a tripod whose resonance frequency is higher than the usual range of the flow turbulence domain. The data processing required to obtain the fluctuation of the vertical velocity and to take the sampling decision is controlled by a script developed in LabVIEW. Sample accumulation is made in perfusion bags inside bottles. In addition, eddy covariance measurements can be executed at the same time as REA for complementary flux interpretations.

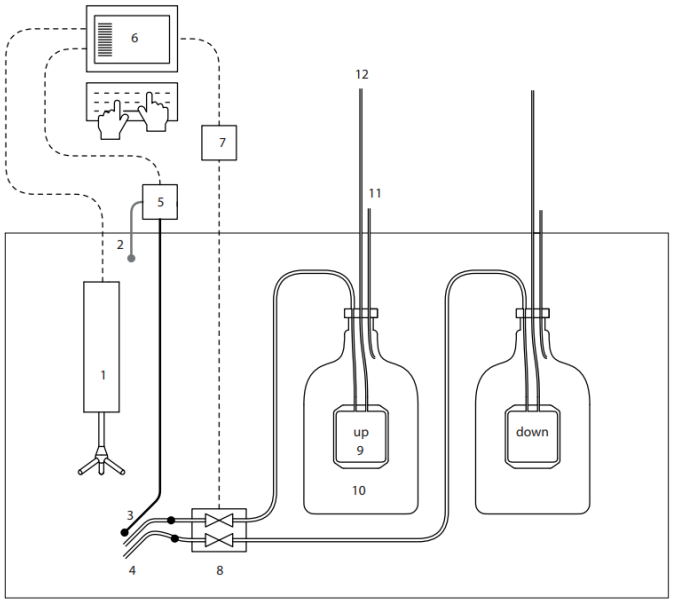

Figure 48 - The main instruments of the prototype developed to execute relaxed eddy accumulation in aquatic environments are: Acoustic Doppler Velocimeter (1), temperature probe (2), oxygen probes (3), REA tube inlets (4), oximeter (5), prototype automation (6), on/off control module (7), solenoid valves (8), accumulation bags (9), accumulation bottles (10), venting tube (11) and sample recovery tube (12).

5 AQUATIC RELAXED EDDY ACCUMULATION: A NEW TECHNIQUE TO RESOLVE BENTHIC SOLUTE FLUXES

This chapter is an article draft. The introduction and the theoretical basis summarise information already presented in the previous chapters.

5.1 INTRODUCTION

The exchange between sediment pore water and the water column plays a major **role** in regulating the water quality and ecology of aquatic ecosystems (Wang et al., 2020) and contributes to the global biogeochemical cycles. This interface is a hotspot of organic matter recycling: nutrients and greenhouse gases produced during the mineralisation of organic matter in anoxic pore water diffuse towards the water column. A wide **range of benthic fluxes** of dissolved substances have been explored: nutrients (Welch and Cooke, 1995; Søndergaard et al., 2003), metals (Giles et al., 2016), micropollutants (Ayrault et al., 2021), greenhouse gases (Guérin et al., 2016), but their **spatial variability and temporal dynamics** remains **poorly understood**. These measurements provide insights into the ecological state and dynamics and help assess restoration measures.

The organic matter content in the sediment, biological activity, concentration gradient at the water-sediment interface and near-bed currents are the main drivers of benthic fluxes (Søndergaard, 2007; Lorke and MacIntyre, 2009). **Currents** particularly reduce the thickness of the diffusive boundary layer (DBL), the thin lowest part of the benthic boundary layer and the bottleneck for solute exchange across the sediment-water interface (Lorke and Peeters, 2006). Near-bed flow **varies** in magnitude and direction in response to external forcing, including tides in coastal marine systems (Thiébaut et al., 2020), wind-generated flows and internal waves in stratified lakes and reservoirs (Reimers et al., 2020), and discharge variations in streams and rivers (Kang and Lee, 2020). Except for discharge, these variations modulate oxygen benthic fluxes at time scales of **several hours** (McGinnis et al., 2008; Murniati et al., 2015; Chipman et al., 2016).

Due to complex biogeochemical processes and fast-varying redox conditions at the sediment-water interface, the benthic fluxes of nutrients, greenhouse gases and major elements should have a different dynamic from oxygen. **Current measurement techniques** are unable to measure it at the scale of a few hours. Benthic chambers, which give access to diffusive fluxes through successive concentration measurements, were shown to underestimate fluxes in turbulent conditions (Berg et al., 2013). Even the addition of an artificial mixing fails to reproduce the turbulence conditions outside the chamber (Tengberg et al., 2004). Other techniques which measure the concentration gradient across the sediment-water interface require stable hydrodynamic conditions during their relatively long time of exposure (a few hours for dialysis chambers, e.g, Davison et al., 1991) or of operation (around 1 h for a

microprofile from a lander, e.g, Holtappels et al., 2011). All these techniques require **fine sediment** either to avoid leaks around the chamber or to be able to penetrate the sediment without damage, and they give a representation of a small sediment area at an often highly heterogeneous interface. On the contrary, aquatic **eddy covariance** also, called eddy correlation, has a large **footprint** which can reach 100 m² since its velocity and concentration are measured within the turbulent boundary layer (~ 15 cm) (Berg et al., 2007; Rheuban and Berg, 2013). EC main limitation is that it requires sensors with response time below 1 s to capture the whole range of flux-contributing eddies, and small enough to avoid perturbing them. Such sensors are only available for oxygen (Berg et al., 2022), temperature (Berg et al., 2016), colloids (Hofmann et al., 2011) and alkalinity (Long et al., 2015).

Micrometeorologists overcame these difficulties with the relaxed eddy accumulation technique in which the fast and separate sampling and accumulation of turbulent updrafts and downdrafts replace the fast measurements of EC (Baldocchi, 2014). With a simulation of REA fluxes by reanalysing EC measurements in a riverine lake, Lemaire et al. (2017) showed that it is theoretically feasible to adapt REA to the sediment-water interface.

This work aims at demonstrating the reliability of the technique in real conditions. The article presents a portable REA prototype for shallow aquatic environments, its evaluation by comparing oxygen flux measurements by REA and EC as a reference method, and the discussion of its field of use.

5.2 THEORETICAL BASIS

Assuming a steady-state mass balance, negligible divergence of horizontal advection and storage, and that the sediment surface is the only source or sink and spatially homogeneous over the measurement footprint, the vertical turbulent flux of a solute can be formulated as the covariance of the vertical velocity (w) and of the solute concentration (C) at any point of the turbulent boundary layer:

$$F = \mathrm{cov}(w, C) = \overline{w'\,C'}$$

where the overbar denotes a temporal average and the prime a turbulent fluctuation obtained by obtained by Reynolds' decomposition ($w' = w - \overline{w}$ and $C' = C - \bar{C}$). This formula is directly used in aquatic EC (Berg et al., 2003, 2007). In order to capture the whole flux-contributing frequency range of turbulence, from the turbulence production to the dissipation scales, measurement frequencies are higher than 1 Hz and the flux averaging time has to be longer than the largest eddy time scale:

$$\tau_{LE} = h/u_*$$

where h is the measurement height (usually 10-20 cm above the sediment) and u* is the current friction velocity. Averaging times, determined during post-processing, range from 5 to 30 min (Lorrai et al.,

2010; Chipman et al., 2016). High-energy flows as in rivers require shorter averaging periods than low-energy flows as in lakes; 30 min is often used by convenience.

REA is a conditional sampling technique based on turbulent velocity fluctuations (Businger and Oncley, 1990). It relies on the same assumptions about solute transport as EC. Air is pumped at a fixed flow rate. Fast-switching valves orient samples from updrafts and downdrafts into distinct accumulation compartments (e.g., Tedlar bags) according to the sign of the vertical velocity. The flux is proportional to the difference between the mean concentrations of accumulated samples ($\overline{C_{\uparrow}}$ for updrafts and $\overline{C_{\downarrow}}$ for downdrafts) most often determined in laboratory (e.g., by gas chromatograph):

$$F = b\ \sigma_w\ (\overline{C_{\uparrow}} - \overline{C_{\downarrow}})$$

where σ_w is the standard deviation of the vertical velocity during the accumulation period and b is a dimensionless empirical coefficient. A velocity threshold w_0 discards the smaller eddies; this preserves the valves and increases the mean concentration difference in accumulated samples, improving the flux quantification limit. Consequently, the coefficient b decreases exponentially from its theoretical value (b_0 = 0.63) for Gaussian distributions of w and C:

$$b = b_{\infty} + (b_0 - b_{\infty})\exp\left(-a\frac{w_0}{\sigma_w}\right) \text{ for } 0 \leq \frac{w_0}{\sigma_w} \leq 2,$$

where b_0 corresponds to a null threshold velocity, b_{∞} to an asymptotic value for $w_0 >> \sigma_w$ and a is an attenuation coefficient. Simulations of REA fluxes at the sediment-water interface yielded the following values for oxygen: b_0= 0.6, b_{∞}= 0.152, a = 1.35 (Lemaire et al., 2017).

Both in the atmosphere and in aquatic environments, the discrepancies between EC and simulated REA fluxes are minimal for a threshold velocity $w_0 = 0.75\ \sigma_w$ (Ammann and Meixner, 2002; Lemaire et al., 2017).

The main challenges for aquatic REA, the same as at the land-atmosphere interface, are to measure the concentration of accumulated samples with sufficient analytical precision and to be able to isolate a small turbulent vertical flux perpendicular to a large advective flux constituted by the passing-by of the solute in the main current over the sediment. This requires the precise alignment of the instruments with the vertical, especially with a portable device (Lemaire et al., 2017).

5.3 Materials and Methods

5.3.1 REA prototype

Inspired from atmospheric REA setups, the prototype addresses requirements concerning the stable and precise deployment of the instrument on the sediment surface at a depth up to 5 m, a sampling

frequency above 1 Hz, a stable sampling flow rate, the correct separation of updrafts and downdrafts, sufficient accumulation for chemical analysis (200 mL), and sample conservation before recovery.

In order to avoid frame vibrations within the turbulent frequency range, the instruments are fixed to a topographic tripod (Lorke et al., 2019). An acoustic Doppler velocimeter (ADV Vector, Nortek AS, 1 on Figure 1) measures three-dimensional flow **velocities** at 8 Hz at 5 to 20 cm above the sediment surface and triggers the REA control system programmed in LabVIEW (5). The latter rotates the raw velocities to compensate for the imperfect levelling of the ADV with the sediment-water interface, extracts the turbulent fluctuation of vertical velocity (w') and, if this fluctuation is larger than the velocity threshold (w_0) and according to its sign, opens one of the two fast response 2/2 solenoid valves (7) for sampling through 2.5 mm diameter PFA sampling tubes (8). Their inlets are syringe needles of 0.5 mm diameter, located 0.01 m on the side of the ADV measurement volume (14 mm height, 14 mm in diameter).

The sampling mechanism does not rely on pumps as for atmospheric REA, but on the pressure difference between the hydrostatic pressure at the inlets of the sampling tubes (8) and the atmospheric pressure in the accumulation reservoirs (10) connected to the atmosphere through venting tubes (11). Valves clamp the sampling tubes and regulate the flow rate which increases with water depth. Samples are accumulated in 250 mL PVC-free polyolefin perfusion bags (9) inserted in 2 L bottles (10); the bags fill progressively, limiting the contact of sampled water with air and avoiding external contamination. At the end of every accumulation period, the samples are collected through the recovery tubes (12). The sampled volume depends on the chemical analysis required for the target flux.

5.3.2 Adaptation of REA for technical evaluation

EC is the reference method for the technical evaluation of sub-aquatic REA. It has been used in micrometeorology to evaluate REA approaches (Oncley et al., 1993; Baker, 2000). The instruments of REA and EC were coupled to the **same frame** (Figure 49).

Oxygen was chosen for this evaluation, as its measurements by EC are robust. But sample accumulation is unsuitable for oxygen because of potential exchange with air in the accumulation bags, necessary for maintaining atmospheric pressure at the sampling tube outlet and a stable flow rate. We slightly adapted the REA setup to accurately measure oxygen REA fluxes: 50 µm diameter ultra-high speed micro-optodes (OXB50-UHS, PyroScience GmbH) continuously monitored oxygen partial pressure inside the sampling tubes during sampling (13). For EC, the oxygen probe was comparable, a 430 µm micro-optode (OXR430-UHS, PyroScience GmbH - 3). The three optodes, plugged to an oximeter (Firesting, PyroScience GmbH - 4) measured at 4 Hz. Since the oximeter deactivates its temperature measurements when it measures at high frequency, water temperature was measured (2) before every accumulation period to prepare the conversion of partial pressures into dissolved oxygen concentrations using a temperature-dependent Henry coefficient (Sander, 2015).

Contrary to EC, the duration of accumulation periods has to be fixed before REA sampling. They lasted 8 to 15 min and were longer in low-energy than in high-energy conditions.

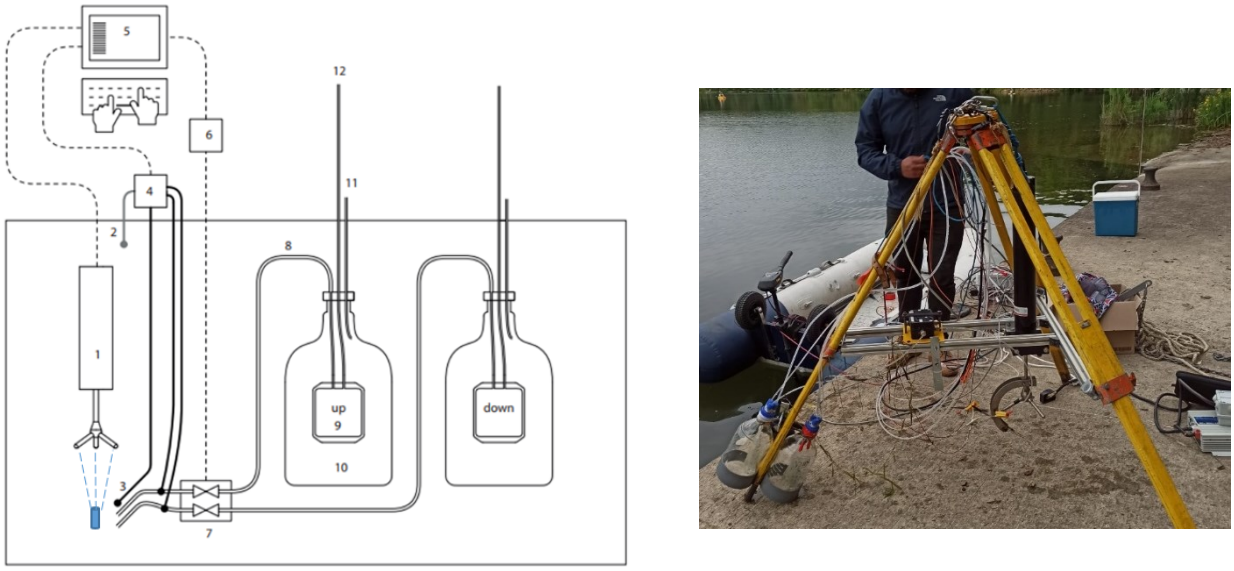

Figure 49 - Relaxed eddy accumulation setup for aquatic environments: 1) acoustic Doppler velocimeter; 2) temperature probe; 3) oxygen probes for EC and inside each sampling tube; 4) oximeter; 5) control system; 6) on/off control module; 7) solenoid valves; 8) sampling tubes; 9) accumulation bags; 10) accumulation bottles ; 11) venting tube; 12) sample recovery tubes. The blue cylinder represents the ADV measurement volume.

5.3.3 Quantification of oxygen fluxes

5.3.3.1 Quality of velocity measurements

For EC, Wahl (2000) recommended to replace by interpolation ADV velocity values with a signal-to-noise ratio below 15 dB or with a correlation between transmitted and received pulses below 70%. Velocity outliers are then commonly filtered with the Phase-Space Threshold method (Goring and Nikora, 2002). But for REA, we could only use information the ADV provides continuously namely the beam correlation. We chose to do the same for EC. When low-correlation velocities occur, REA sampling is paused, while they are replaced by linear interpolation for EC flux computation.

5.3.3.2 Reorientation of the coordination system

The prototype for aquatic REA is portable and designed for aquatic environments below 5 m depth. When it is placed on an imperfectly flat sediment or susceptible to differential settling, the coordinate system of the current meter needs to be aligned with the vertical. For aquatic EC and atmospheric REA, the double and triple angle rotations and the planar fit are the most common methods (Wilczak et al., 2001; Lorke et al., 2013). Whereas for EC the vertical velocity is aligned after the campaign, this should be done beforehand for REA since it conditions the sampling decision. For atmospheric REA, this alignment is executed once the anemometer is fixed on a “flux tower” (Pattey et al., 1993) using either 2 or 3-angles rotation for long deployments (Sarkar et al., 2020; Grelle and Keck, 2021).

Both for aquatic EC and REA, we used the 2-angle rotation to find the mean current ($\overline{u}$) direction and to cancel the mean vertical speed ($\overline{w}$). The method calculates alignment angles α (around the z-axis) and β (around the x-axis) using average velocity components ($\overline{u}$, $\overline{v}$ and $\overline{w}$) to reorient the coordinate system (Wilczak et al., 2001). Whereas for EC the rotation angles are computed from the velocities of each accumulation period, for REA, they are computed from velocities measured before each accumulation period, assuming that the current does not change direction. The angle computation period is ideally the latest accumulation period. During the prototype development phase, we used successive preparation and accumulation periods of the same duration. Hereinafter, the velocities will refer to aligned velocities.

5.3.3.3 Extraction of the turbulence velocity fluctuation

Another challenge for measuring turbulent fluxes is the presence of non-turbulent motions like waves (seiches, boat passage) which do not transport mass (Berg et al., 2003). They can temporarily drift the mean vertical velocity above the velocity threshold and perturb REA sampling. To prevent these low frequency velocities from contributing to the computed fluxes, the turbulent fluctuations of vertical velocity and concentration are extracted by subtracting running averages. For EC the extraction is performed on the entire data set after the campaign with a centred running average of 60 s after Berg et al. (2003). For REA, 30 s running averages of past values are applied. EC fluxes did not change significantly when switching from 60 s centered averages to 30 s averages of past values.

5.3.3.4 Data synchronization for EC

For EC, a synchronization between oxygen and velocity time series compensates the delay due to the distance between oxygen and velocity probes and to the time response of oxygen micro-optodes (Lorrai et al., 2010). The usual strategy is to maximise the magnitude of the Pearson correlation coefficient between time series shifted one relatively to the other within a search window of around 2 s (McGinnis et al., 2008). We used a wider search window of 5 s, since separate and imperfectly synchronised computers acquired the measurements, and we minimised the probability of decorrelation within the search window (e.g., Donis et al., (2015)).

5.3.3.5 Measuring and calculating average oxygen concentration for REA

Using the REA prototype to measure oxygen fluxes imposes an adaptation of the data processing. During the accumulation periods, dissolved oxygen concentration is measured continuously in the sampling tubes. After the campaign, to avoid including the concentration of the same sampled water several times in the average concentration, either upwards or downwards ($\overline{C_{\uparrow}}$ or $\overline{C_{\downarrow}}$), only the concentrations measured while the water is flowing through the corresponding tube are included in the average concentration. The attenuation of fluctuations, due to oxygen diffusion in the lines, is neglected. Shift tests within a 2 s window showed that it was unnecessary to synchronise the oxygen and valve opening sequences to account for the time lag between the two computers: it does not substantially change the flow.

The precision of the oxygen probes is 0.8 mmol m^{-3} at 95% of saturation. In usual conditions in rivers ($\sigma_w \approx 0.01$ m s^{-1}), the REA flux uncertainty, 200 mmol m^{-2} day^{-1}, is often large than the flux (Eq. 23). A compensation of the bias between probes drastically improves the precision of the measurement of concentration differences. To do so, before every accumulation period starts the valves open for 90 s during which the optodes of sampling lines should measure similar concentrations. At the end of this period, the average concentrations $\overline{C_{comp\uparrow}}$ and $\overline{C_{comp\downarrow}}$, yield the bias $\overline{C_{comp}}$:

$$\overline{C_{comp}} = \overline{C_{comp\uparrow}} - \overline{C_{comp\downarrow}} \quad \text{(Eq. 46)}$$

which corrects the REA flux estimates:

$$F = b\,\sigma_w \left(\overline{C_\uparrow} - \overline{C_\downarrow} - \overline{C_{comp}}\right) \quad \text{(Eq. 47)}$$

5.3.4 Selection of valid REA measurements

REA and EC techniques require fully developed turbulence and the precise alignment of the prototype with the vertical. As a first criterion, we excluded flux estimates if the power spectrum of the vertical velocity after alignment showed no turbulent inertial subrange (-5/3 slope in logarithmic scales). We computed the friction velocity (u^*) and the turbulent kinetic energy (k) to give a numerical indication for this criterion (Stull, 1988; Wengrove and Foster, 2014):

$$u^* = \left(\overline{u'w'}^2 + \overline{v'w'}^2\right)^{1/4}$$

$$k = (\overline{u'^2} + \overline{v'^2} + \overline{w'^2})/2$$

A second criterion for selecting successful REA flux measurements is when the absolute value of the mean aligned vertical velocity ($|\overline{w}|$) remains below the threshold velocity ($|w_0|$). It should vanish after 2-angle rotation but a bias can persist, e.g. when current direction can change between preparation and accumulation periods.

5.3.5 Complementary tests

For REA as for EC, the measurement point should remain in the turbulent boundary layer, above the viscous boundary layer of thickness:

$$h_{VBL} = 10\frac{\nu}{u^*} \quad \text{(Eq. 48)}$$

where $\boldsymbol{\nu}$ is the kinematic viscosity (10^{-6} m^2 s^{-1} at 20°C) (Lorke and MacIntyre, 2009). The accumulation time should also be longer than the time scale of the largest eddies.

In order to see whether the velocity processing before sampling creates a bias, we compared EC fluxes computed both with the velocities processed for REA (rotation angles from a preparation period, subtraction of running mean of 30 s of past values) and for EC (rotation angles computed on the accumulation period, 60 s centered running mean). Velocity and oxygen were synchronized in both cases since oxygen concentration and velocities were measured by separate computers.

5.3.6 Measurement sites and campaign details

5.3.6.1 River with stable and intense turbulence

REA measurements are easier at a high level of turbulence and in a unidirectional current. We first intended to investigate the range of current speed and oxygen flux suitable for the technique in a large laboratory flume (45 m long, 0.6 m wide, EDF R&D, Chatou, France). But depleting deep water by bubbling nitrogen failed at creating a vertical oxygen flux without secondary vertical currents.

We then measured oxygen fluxes in July 2020 in the Petit Morin river (modulus 3 m^3 s^{-1}) at Courcelles-sous-Jouarre (70 km east of Paris - 48.939°N, 3.149°E). The measurement point was in the middle of the river to avoid secondary currents, 20 cm above the sediment, and part of the equipment was placed on the bank. The river bed was rocky with macrophytes. The current velocity at measurement height was 0.09 m s^{-1} and the water depth 0.8 m.

5.3.6.2 Shallow lakes for strong fluxes

The challenges for REA in shallow lakes are that turbulence should be sufficient and that the prototype should be aligned with the vertical in the absence of a stable current direction. High turbulence is rare, especially in summer when thermal stratification decreases the energy transfer from the wind to near-bed currents. We investigated two shallow closed lakes. Windy days (> 8 m s^{-1}) ensured sufficient turbulence.

The first site is a reservoir at the experimental platform PLANAQUA (CEREEP-Ecotron, Saint-Pierre-lès-Nemours, France, 48.283°N, 2.670°E). The artificial lake, located on a plateau and far from obstacles, has a rectangular shape and is 126 m long, 15 m wide and 3 m deep. The sediment is sandy, homogenous and flat and the lake oligotrophic. A liner isolates it from groundwater. We measured fluxes in the middle of the lake from a footbridge in September 2020. The average current speed at measurement height (0.10 m) was 0.008 m s^{-1}.

The second lake is a former sand-pit, Lake Champs-sur-Marne (20 km East of Paris, 48.863°N, 2.597°E). It is fed by rainfall runoff and groundwater. Its surface is 0.12 km^2 and its average depth 2.5 m. The lake is strongly eutrophic and undergoes recurrent algae blooms. Trees surround the lake and grow on its central island, sheltering it from wind. During the campaigns in July and August 2020, the lake was thermally stratified only during day time, with a vertical temperature difference of 1.5°C. Macrophytes and algae covered the sediment. We measured both at two points, at shallow depth (1.2 m) from an anchored platform and in the middle of the lake (2.7 m) from a boat (Points S and M in Piccioni

et al., 2021). At shallow depth, the sediment was flat and the average velocity at measurement height (0.10 m) was 0.004 m s^{-1}. In the middle of the lake, the bathymetry was irregular with a slope of 11°. The current speed at measurement height (0.20 m) was 0.001 m s^{-1}.

5.4 RESULTS

Among 33 REA measurements at four different points, 15 respected the **criteria** of turbulence and alignment: 10 out of 24 in Lake Champs, 1 out of 6 in the artificial lake, and all 3 in the river. For these, the measurement point always remained in the turbulent boundary layer, since the maximum viscous boundary layer thickness, observed in Lake Champs, was 3 cm, below the measurement height. The accumulation period was also sufficient: the time scale of largest eddies reached 5 min in Lake Champs. For the 15 accumulation periods, the low **decorrelation probability** of oxygen and vertical velocity after synchronisation for EC ($p < 0.05$) confirms the good measurement conditions.

Flux values **range** from -150 to 50 mmol m^{-2} day^{-1}. Positive fluxes denote the production of oxygen by photosynthetic organism covering the sediment, and negative fluxes the oxygen uptake by the sediment. Fluxes varied less **in time** in the river than in the lake (coefficient of variation around 20% over 1 h vs 100% over 3 h for the four segments of July 16 2020).

The **low rate** of successfully measured fluxes can mainly be attributed to the low-energy conditions in shallow lakes. At Lake Champs, fluxes were high but turbulence was often insufficient: unvalid measurements without any inertial subrange in the vertical velocity power spectrum correspond to $u^* < 3\ 10^{-4}$ m s^{-1} and $k < 10^{-7}$ J kg^{-1}. At the artificial lake, turbulence was high (u^*= 0.9 cm s^{-1} and $k > 8.10^{-6}$ J kg^{-1}). However, ADV correlation was low (< 70%) during 6 to 60% of the duration of the accumulation periods, often above the recommended threshold of 20% (Guseva et al., 2021). This degraded the extraction of turbulent fluctuations and sampling in this reservoir, contrary to the other sites (two accumulation periods low correlation for less than 18% and the rest for less than 10%). In the **river**, the conditions were adequate for all **three accumulation periods** (moderate downward fluxes, u^* = 0.5 cm s^{-1} and $k > 1.10^{-5}$ J kg^{-1}).

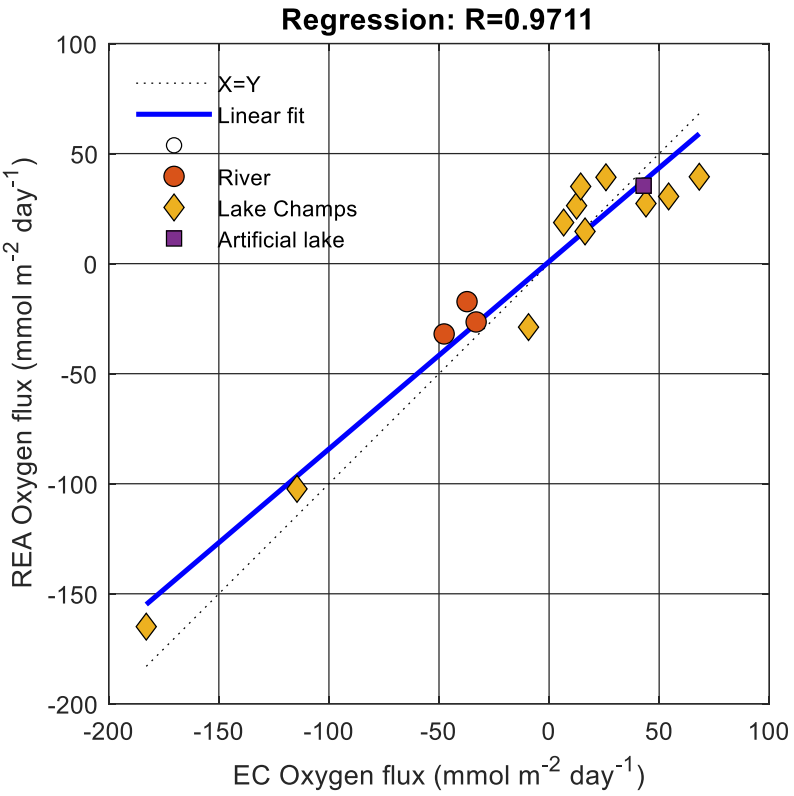

Figure 50. Comparison of fluxes measured by relaxed eddy accumulation (REA oxygen flux) and EC (EC oxygen flux) in the Petit Morin river (orange), in the artificial lake (purple) and in the Lake Champs (blue). The black line is the linear model and the grey dashed line is the 1:1 bisector line.

Fluxes measured by EC and REA present a **satisfactory agreement** ($R^2 \approx 0.97$ – Figure 50). Neither the ANOVA test found any significant difference in their median and variance ($p \approx 0.2$), nor the Student test for paired series in their mean difference of 2.3 mmol m^{-2} day^{-1} ($p = 0.6$), and differences are uncorrelated with the friction velocity.

The REA and EC measurements of the excluded accumulation periods are also correlated (in the flume, in low turbulence or when the prototype poorly functioned)**.** We found a satisfactory agreement ($R^2 = 0.77$), and a statistically not-significant difference of 24.5 mmol m^{-2} day^{-1} (paired t-test, $p = 0.13$). This shows that EC and REA, which are based on similar principles, can produce comparable results even if hydrodynamic conditions are unsuitable for their use. Therefore, on a coupled REA and EC system, comparable REA and EC oxygen flux values do not guarantee that they were measured properly.

The discrepancy between REA and EC fluxes cannot be attributed to the use of a running mean over past values and of rotation angles computed from a previous preparation period in the REA velocity processing before sampling. For the 15 accumulation periods with valid measurements, the EC fluxes computed with velocities processed for REA and for EC are highly correlated ($R^2 = 0.96$, not shown); their mean difference remains below 1 mmol m^{-2} day^{-1} and is not-significant ($p = 0.8$). Only the effect

of the lack of synchronization remains to be assessed, since the use of separate computers for sampling and for oxygen measurements imposed to synchronize the data series in this work.

5.5 DISCUSSION AND CONCLUSIONS

The fraction of successful REA measurements may appear low, but it helps understand the field of use of REA. A turbulence threshold appears to be $u^* > 3\ 10^{-4}$ m s^{-1} and $k > 10^{-7}$ J kg^{-1}. Such conditions are fulfilled in rivers and in riverine lakes (Murniati et al., 2015), but, in closed and sheltered lakes, they require either full mixing due to air cooling, or strong winds (above 8 m s^{-1} for Lake Champs), especially during periods of thermal stratification.

In order to **increase the frequency of REA flux measurement**s, an automatic multiple sampler could reduce the sample recovery time at the end of each accumulation period, and the control system could update the alignment angles from the measurements of the previous accumulation period or continuously (von der Heyden et al., 2021). This would probably be easier than to align the equipment at the beginning of each campaign with the planar fit method, which requires several hours of velocity measurements before sampling and in windy weather for lakes (Wilczak et al., 2001).

Measurements in shallow lakes are rewarded by an **intense dynamics** of oxygen fluxes. Even the flux direction **changed** in the morning of July 16, 2020 in Lake Champs probably due to the prevalence of primary production or sediment consumption. REA could cover the knowledge gap about the dynamics of nutrients, greenhouse gases and major elements at the scale of a few hours.

In the river, a defined main current direction and intense turbulence provided REA with ideal conditions. The flux values remained stable over the short deployment of 1 h. Benthic fluxes should change over the day-night cycle as observed by Berg et al. (2013) or during a flow rate increase. To prevent secondary currents from biasing flux estimation, a **straight river section** is desirable (Noss et al., 2010). It should be much broader than the width of the measurement footprint, 6.5 times the measurement height (h) (Berg et al., 2007). REA could prove very useful over stony river beds, permeable and hard sediments unsuitable for other techniques.

REA could also follow benthic flux dynamics on the coastal or estuarine shelf. The flow direction can be expected to be stable for most of the circa 6 h of tidal flood and ebb.

The aim of this work was to present a prototype and evaluate the relaxed eddy accumulation technique at the sediment-water interface in aquatic environments. The agreement with eddy covariance, an acknowledged technique, for oxygen fluxes proved the reliability of REA in rivers and shallow lakes. The prototype is readily available to measure the benthic fluxes of nutrients and major elements with accurate analytical methods. It would require adaptations for other environments like estuaries or for other substances like dissolved greenhouse gases or microplastics. REA constitutes a robust technique to understand the spatial-temporal influence of turbulence on benthic fluxes. This technical evaluation

of REA paves the way to explore finely the contribution of the sediment to local biogeochemical cycles in aquatic ecosystems.

6 EVALUATING NOVEL METHODS FOR MEASURING BENTHIC FLUXES IN A SHALLOW LAKE

This chapter is a draft of article. The introduction and the theoretical background of relaxed eddy accumulation and of eddy covariance summarise information already presented in the previous chapters.

6.1 INTRODUCTION

The impact of human activities on aquatic systems is of major concern worldwide. Large waterbodies are extensively studied, while the density of **small and shallow aquatic environments** is higher (Downing et al., 2006; Mendonça et al., 2017). Also, their importance covers social, economic and ecological aspects (Bartout et al., 2015; Biggs et al., 2017). **Shallow lakes** can be defined as lakes where wind-induced mixing is sufficient to prevent long-term stratification, enabling the bulk of the water volume to be in contact with the sediment surface (Phillips, 2004).

Eutrophic shallow waterbodies can experience **recurrent algae blooms** over a year (e.g., Guo et al., 2022), and these events can be **fast** (daily to weekly) depending on the environmental conditions (Li et al., 2021). In shallow lakes, contrary to deep lakes, phytoplankton growth can be observed for many years after a reduction in external nutrient loading. High nutrient and organic matter concentration in sediments added to the fast dynamics of thermal stratification and hydrodynamics, lead to a **high temporal variability of the water quality**.

In oxic or hypoxic environment close to the sediment surface, ferric iron limits phosphate release (section 2.3.1). In shallow lakes, bed currents driven by surface wind are often sufficient to transfer nutrients into the water column contributing to algae blooms. After a collapse of phytoplankton in a shallow lake, often due to zooplankton grazing or to nutrient shortage, phytoplankton decomposes on the sediment. Depending on the amount of carbon input, the sediment oxygen demand can increase and turn the benthic zone anoxic. In such an environment, ferrous iron can be dominant and it does not bind phosphate. The phosphate concentration in the water column can suddenly increase, opening the way for another phytoplankton bloom within a few days. The recurrent oxic-anoxic transition of the sediment surface can promote drastic changes in local nutrient fluxes (Faganeli and Ogrinc, 2009).

The diffusive transport of compounds is slow through the diffusive boundary sublayer (DBL). It is the lowest sub-layer of the benthic boundary layer, below the viscous sublayer and the turbulent sublayer (TBL) (Lorke and Macintyre, 2009 This one is considered the bottleneck of the benthic fluxes. The near-bed flow, and thus **turbulence**, trigger the **thickness of the diffusive boundary sublayer** (DBL) (Jørgensen and Revsbech, 1985; Lorke and Peeters, 2006) and, consequently, the benthic flux dynamics.

Different techniques try to quantify benthic fluxes (Viollier et al., 2003): benthic chambers (Tengberg et al., 2005), dialysis chambers (Peepers, DET and DGT) (Hesslein, 1976; Davison et al., 1991; Jézéquel et al., 2007) and the incubated sediment cores (Seitaj et al., 2017). Their main limitations concern the spatial-temporal representation of the measurements, roughly the daily scale and a few square centimetres of sediment surface. In addition, they exclude the turbulence contribution to the measured fluxes considering only diffusion as the main transport process. Aquatic eddy covariance (EC) (Berg et al., 2022) empirically quantifies the direct contribution of turbulence in a non-invasive approach (McGinnis et al., 2008; Murniati et al., 2015; and others more). EC, however, is restricted to fluxes of oxygen, alkalinity, heat, nitrate and suspended particles. EC measures at high temporal resolution (Lorrai et al., 2010) and high spatial representation due to the large footprint of its measurements (Berg et al., 2007). The spatial-temporal scales addressed by EC, extended to metallic ions and nutrient fluxes, would allow for a more precise understanding of the contribution of the sediment to, for instance, rapid algal development.

New measurement techniques are needed for a finer understanding of benthic fluxes of nutrients and of major elements, especially their turbulent part. This work assess the potential of two innovative techniques to resolve the turbulence contribution to benthic fluxes in a shallow lake, relaxed eddy accumulation (REA) and the mass transfer coefficient (MTC), and compares them with well-accepted techniques, . eddy covariance and concentration gradients measured both in thin films (DGT) and by oxygen micro-profiler. In total, the four techniques were deployed to compare measured fluxes and to follow the algae-bloom dynamics in a very eutrophic shallow urban lake. The techniques were used to compare and follow the fluxes of oxygen, ammonium, phosphate, sulphate, iron and manganese. The question relies on the turbulence contribution to these fluxes. Strengths and limitations of each technique is presented as well as the interpretation for the measured fluxes and resulting influence to the algae dynamics.

6.2 METHODS

Benthic fluxes were measured in order to test the reliability and to determine the strengths and limitations of two new techniques compared to accepted ones. In this section we present the theoretical background of the techniques, the study site, the field campaigns, the data processing and the analytical methods.

6.2.1 Theoretical background of flux quantification techniques

6.2.1.1 Aquatic eddy covariance (EC)

Aquatic eddy covariance is a technique to measure turbulent benthic fluxes. It relies on a mass balance between the sediment-water interface and the measurement depth in the turbulent boundary sublayer, neglecting molecular diffusion within this volume and assuming invariance in the horizontal plane (Huettel et al., 2020b; Berg et al., 2022). The resulting flux F of a solute is the covariance of the vertical

current velocity (*w*) and of its concentration (*C*) measured at the same point of the turbulent sublayer. The flux is

$$F = cov(w, C) = \overline{w'C'}$$

where primes indicate turbulent fluctuations computed by Reynolds decomposition ($w' = w - \bar{w}$ and $C' = C - \bar{C}$) and the overbars time averages.

6.2.1.2 Aquatic relaxed eddy accumulation (REA)

REA overcomes EC limitations to cover a broad range of benthic fluxes. REA replaces the fast response probes of EC for the fast sampling and separate accumulation of updrafts and downdrafts in the turbulent boundary layer. Sampling occurs if the fluctuation of the vertical velocity (*w'*) is larger than a velocity threshold (w_0) and according to its sign (Ammann and Meixner, 2002; Lemaire et al., 2017). The average concentration of accumulated updrafts ($\bar{C}_\uparrow$) and downdrafts ($\bar{C}_\downarrow$) yields the flux (*F*). The flux is calculated as follows:

$$\bar{F} = b\ \sigma_w\ (\bar{C}_\uparrow - \bar{C}_\downarrow)$$

where σ_w is the standard deviation of the vertical velocity, which is a proxy for the turbulent kinetic energy. The empirical coefficient *b* decreases exponentially with the ratio between the threshold velocity and the standard deviation of the vertical velocity.

$$b = b_\infty + (b_0 - b_\infty)\exp\left(-a\frac{w_0}{\sigma_w}\right) \text{ for } 0 \leq \frac{w_0}{\sigma_w} \leq 2$$

where b_0 is the value of the empirical coefficient when threshold velocity is zero and b_∞ its asymptotic value for high velocity thresholds and *a* an attenuation coefficient. The value $w_0 = 0.75\ \sigma_w$ is the best compromise and eliminates badly characterized small eddies while sampling most large eddies.
The fluxes measured by the REA and the EC have a larger spatial representation of the sediment than other techniques, due to their large footprint, the area of the sediment contributing to the measured fluxes (Berg et al., 2007; Foken, 2008). This avoids to use several similar measuring systems simultaneously as for dialysis or benthic chambers.

6.2.1.3 Mass Transfer Coefficient (MTC)

Applying Fick's first law of diffusion, the benthic turbulent flux of a solute can be expressed as the product of the difference between its concentrations measured in the diffusive boundary layer (DBL) (C_{DBL}) and in the turbulent boundary layer (C_{TBL}) and of a mass transfer coefficient (*K*).

$$F = K(C_{DBL} - C_{TBL}) \quad \text{(Eq. 49)}$$

Empirical evidence suggests that the mass transfer coefficient can be expressed as:

$$K = \alpha\, u_* Sc^{\beta} \quad \text{(Eq. 50)}$$

where α and β are empirical coefficients, u_* is the friction velocity, and Sc is the dimensionless Schmidt number expressing the ratio between water kinematic viscosity and solute molecular diffusivity *D* (Shaw and Hanratty, 1977; Lorke and Peeters, 2006). After applying the law-of-the-wall for turbulent diffusivity and assuming that the DBL thickness is equal to the Batchelor length scale, Lorke and Peeters (2006) deduced that $\alpha = 1/9$ and $\beta = -1/2$. It is unknown whether this relation is still valid for low-flow velocities, close to laminar flow. The friction velocity is calculated as (Wengrove and Foster, 2014):

$$u_* = \sqrt[4]{\overline{u'w'}^2 + \overline{v'w'}^2}$$

the primes denote the fluctuation of the velocity components *u*, *v* and *w*.

6.2.1.4 Fick's law in incubated sediment cores

Contrary to the three methods presented before, this is based on molecular diffusion. If the interfacial gradient of solute concentrations is known, benthic fluxes can be simply estimated by applying Fick's first law of diffusion in the diffusive boundary sublayer:

$$\bar{F} = -D\frac{\partial C}{\partial z},$$

where D is the solute molecular diffusivity, C is the solute concentration in the diffusive sublayer and z is the vertical coordinate (Lorke and Macintyre, 2009).

6.2.2 Sampling strategy and data processing for each technique

6.2.2.1 Techniques comparison

The four techniques presented here work at different time scales and different locations in the benthic boundary layer (Figure 51). The interface peeper used by MTC (C_{DBL}) is located in the diffusive sublayer (DBL). In the turbulent sublayer (TBL), current speed is measured at high-frequency for EC (w'), REA (w', σ_w and w_0) and for MTC (u_*), as well as dissolved oxygen concentration for EC (C'); water is also sampled at high frequency for REA ($\bar{C}_{\uparrow}$ and $\bar{C}_{\downarrow}$), but only once for MTC (C_{TBL}).

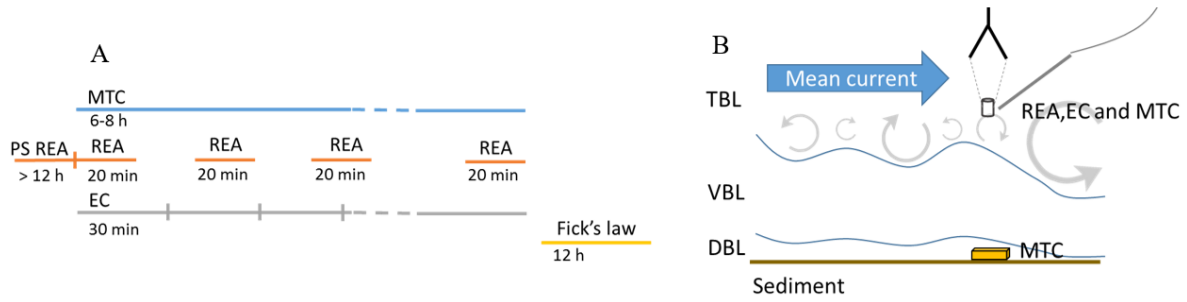

Figure 51 - On the left-hand side of the figure (A) the sampling time-scales and temporality of the techniques. On the right-hand side of the figure (B) the positioning of each in-situ measurement through the benthic boundary layer.

6.2.2.2 Eddy covariance

Eddy covariance and REA pieces of equipment were coupled to the same frame for the common use of the Doppler current velocimeter (ADV Vector – Nortek A.S., resolution 0.1 mm s^{-1}). Eddy covariance requires to measure the vertical velocity and dissolved oxygen at high frequency and at the same point. Velocity was measured at 8 Hz at a height of 15 cm above the sediment in order to cover the turbulence inertial sub-range (Kaimal et al., 1972). Dissolved oxygen concentration was measured 1 cm away from the ADV sampling volume (McGinnis et al., 2008a), using micro optodes (OXR430-UHS - PyroScience GmbH) sampling at 4 Hz.

After each campaign, the data processing for EC flux estimation begins by replacing by interpolation unreliable velocity measurements with a beam correlation below 70% or a signal-to-noise ratio below 15 dB, and velocity outliers with the 3D phase space method (Goring and Nikora, 2002). In order to measure only the vertical turbulent flux without any advection contribution, the coordinate system of the ADV is aligned to the local flow plane with the planar fit method (Wilczak et al., 2001). For that the time series of more than 14 h was divided into 100 s segments (see at Lorke et al., 2013). The turbulent fluctuations w' and C' are extracted by subtracting a 60 s centred running average from the time series. This avoids interference by low-frequency non-turbulent flow (e.g., waves caused by involuntary boat movement). The data synchronization is applied by shifting the oxygen concentration over the vertical velocity datasets to compensate the distance between velocity measurements and oxygen concentration measurements and the response time of the micro-optode (Lorrai et al., 2010). Within a shifting window of 2 s, the time shift yielding the lowest probability of decorrelation between velocity and concentration is selected (Pearson's correlation coefficient, Donis et al., 2015). Finally, the oxygen flux is computed with the right hand side of Eq. 20 with an averaging period of 30 min after Murniati et al. (2015).

6.2.2.3 Relaxed eddy accumulation

This method mainly requires to measure the vertical velocity w, from which its turbulent fluctuation w' and the velocity threshold for sampling w_0 are computed, and the concentrations of accumulated samples, $\bar{C}_{\uparrow}$ and $\bar{C}_{\downarrow}$.

REA works in-situ in two separated phases, a pre-sampling period and successive accumulation periods. During the pre-sampling period, a long series (> 12h) of velocities is recorded at 8 Hz. The first steps of the data processing are common to eddy correlation: low-quality velocity values are replaced by interpolation; the coordinate system is aligned with the normal to the sediment-water interface with the planar fit method; the vertical velocity fluctuation is extracted with a centred running average of 60s. The velocity fluctuation time series over the pre-sampling period is then used to compute the velocity threshold w_0 for the first accumulation period.

During each accumulation period, at the sampling frequency of 8 Hz of the ADV, the automation: (i) recovers velocities and correlations from the ADV; (ii) discards velocities whose correlation is below 70% (the ADV does not provide the signal-to-noise ratio at each time step); (iii) aligns the vertical velocity with the normal to the lake bottom and corrects any vertical velocity bias using the coefficients provided by the planar fit method during the pre-sampling period ; (iv) extracts the fluctuation of the vertical velocity by using a 30 s back-looking running average. Simulations presented a good agreement between a 30 s back-looking running average and the 60 s centred running average (often used for eddy covariance, section 4.5.2); (v) compares the instantaneous fluctuation of the velocity to the threshold velocity and decides on which line to sample or whether the velocity fluctuation is too low for sampling. Fast response solenoid valves control the opening of the sampling tubes placed close to the oxygen probe used by EC. The hydrostatic pressure difference between the inlet and the outlet of the sampling line drives samples to the accumulation reservoirs. Accumulation periods last around 20 min. At the end of each accumulation period, the automation updates the threshold velocity in order to follow the fast-varying current conditions of a shallow lake; The accumulated samples are carefully recovered with a syringe through a tube installed inside each accumulation bag, immediately filtered with a syringe on a 0.45 µm cellulose acetate filter and refrigerated at 6°C for transportation and storage before their chemical analysis described later.

6.2.2.4 Mass Transfer Coefficient (MTC)

As presented in Eq. 49 and 50, applying this method requires to measure the average concentrations within the DBL (C_{DBL}) and in the turbulence boundary sub-layer (C_{TBL}), the friction velocity u_* and water temperature T. The last mentioned affects the mass transfer coefficient through water viscosity, water density, and solute diffusivity.

Solute concentrations in the DBL were measured with a version of the diffusive equilibrium thin-layer (DET) (Krom et al., 1994) adapted to measure the interfacial concentration only. The gel-mini-peepers, from now on called "interface peepers", are deployed horizontally on the sediment bed. Two 5 x 20 x 4 mm pieces of BPA-I gel (Zhang and Davison, 1999) were sandwiched between two 0.4 µm thick dialysis membranes and mounted inside a plastic frame. Besides preventing the intrusion of particles into the gel, this setup allows vertical diffusion through both sides of the gel. This approach allows to average the concentrations of the bottom and the top of the DBL. In situ deployment was assisted with an aquatic camera to ensure contact with the sediment surface. Deployment lasted for 6 to 8 h. For each campaign, five interface peepers were randomly distributed on the sediment surface around the REA and EC device.

Solute concentrations in the overlying water were estimated with 2.5 mL. Samples were taken 15 cm above the sediment surface averaging REA accumulated samples or collecting with the help of a self-made benthic water sampler (12V, 10 L min^{-1} pump). All samples were immediately filtered and conserved at 6 °C before their chemical analysis.

Friction velocities u_* were estimated from ADV measurements. The probe was set in a side-looking position. ADV sampling volume was around 7 cm above the sediment bed. The sampling rate was 16 Hz. Velocity dataset was processed after the campaign as for EC. The centred running average window for the extraction of turbulent velocity fluctuations had a duration of 5 min.

6.2.2.5 Fick's law in incubated sediment cores

The contribution of molecular diffusion to the fluxes and the oxygen sediment demand were accessed using incubated sediment cores. On two different dates, three sediment cores per day (8.5 cm in diameter, 60 cm in length – around 50% sediment and 50% lake water) were retrieved from the studied site near the MTC, REA and EC sampling area.

The objective was to reproduce a natural environment where oxygen is not a limiting factor and without any thermal stratification. Thus, oxygen diffusion was favoured by not sealing the cores and lake water was recirculated in the cores in order to avoid stratification. This recirculated water was collected from the surface, the middle and the bottom of the water column on the days of sediment coring. The recirculated water volume, 56 L, is equivalent to the volume of the water column over the sediment cores while they were still in the lake (surface 0.017 m^2, water depth 3.3 m). This avoided the accumulation of solutes in the water overlying the sediment. For each incubation period, the three cores were connected to the same water recirculation system using polyethylene tubes (4 mm diameter) and a pump (10 L h^{-1}). The inflow tube poured water over each core water surface, while the outflow tube was placed at mid water depth, 15 cm below water surface. The efficiency of water recirculation was confirmed after DET removal by rhodamine tracing. The current velocity induced by recirculation was

estimated to ca. 1 mm s^{-1}.

The durations of the first and second incubations were 48 and 12 h, respectively, and performed in an air-conditioned lab at 20°C. After incubation, microprofiles of oxygen concentration were measured with a micro-optode (PSt7, PreSens, Germany) and a micromanipulator in order to determine the sediment oxygen demand.

Then DET probes (also called gel minipeepers) were placed into the sediment, paying attention to position the sediment-water interface in their middle, and exposed for 8 h. After recovery, each minipeeper was washed and the gel was partitioned at the SWI. The two gel phases, above and below the SWI, were sliced into 5 mm layers. Each slice was placed in pre-weighted glass vial and diluted with 2.5 mL mili-Q water. Vials were stored horizontally for 12 to 24 h to keep gels saturated. Then gels were transferred to other vials with a 2.5 mL 1% nitric acid solution and let back-diffuse into the solution for another 12-24 h before being discarded. The solution is analysed to determine the concentration of the compounds.

6.2.3 Chemical analysis (REA, MTC and mini-peepers in sediment cores)

The target fluxes of this comparison were sulphate, phosphate, ammonium, iron and manganese. REA samples were analysed using ion chromatography (Compact flex 930 – Metrohm AG) to determine anion concentrations. –Analytical precision, 3% for this apparatus, was estimated to 1% for concentration differences between waters sampled in the same aquatic environment and in similar conditions. UV-visible spectrophotometry (Lambda 35, Perkin Elmer Inc., accuracy 5%) was used to quantify ammonium concentrations for REA. Samples for MTC and from the sediment cores were analysed for major anions and NH_4^+ concentrations using ion chromatography (ICS 3000 Dionex – Thermo Fisher Scientific Inc). For Iron and manganese ions, all samples were analysed by inductively coupled plasma mass spectrometry (ICP-MS – Agilent 8800 ICP-QQQ – Accuracy 15% – Agilent Technologies Inc.). Samples obtained after acid dilution were analysed only in ICP-MS.

6.2.4 Flux quality analysis for REA and EC

EC and REA both require sufficient turbulence. The first quality criterion is that the power spectral analysis of the vertical velocity during each measurement period fully covers the turbulence inertial subrange (-5/3 slope of the autospectrum in logarithmic scales and clear smooth peak in variance-preserving autospectrum). For REA only, two criteria are added: the average vertical velocity fluctuation processed by REA automation during an accumulation period ($|\overline{w'}|$), ideally zero, should not be larger than the velocity threshold (w_0); and the solute concentration difference between accumulated samples ($\overline{C_\uparrow} - \overline{C_\downarrow}$) should remain above the analytical precision of their average concentration; else the confidence level for the flux values is considered as low.

6.2.5 Study site

Lake Champs-sur-Marne is a small, shallow, urban lake located in the east of Paris, France. Originally formed as a sand-pit and now used for recreational purposes, it has a surface area of 0.12 km^2, a mean depth of 2.5 m, and a maximum depth of 3.5 m. It is very eutrophic with recurrent algal blooms, and its proximity with the Marne river (≈100 m) opens the hypothesis that its water quality is affected by the river's water quality. However, the only connection to the river is via groundwater flow as the lake has no direct inflow nor outflow.

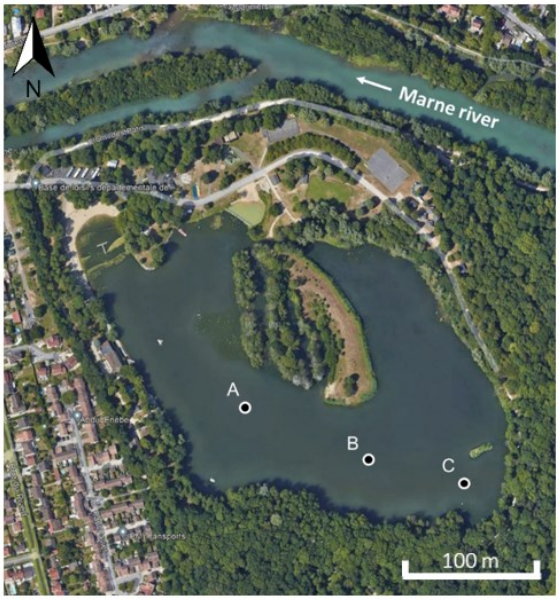

Figure 52 - Satellite photo of Lake Champs-sur-Marne (source: Google) presenting the location of the measurements (B and C) and the location of the surveillance instruments of the lake (A and B).

The lake is equipped with a high-frequency measurement system monitoring continuously different parameters including water temperature at different depths (0.5, 1.5 and 2.5 m) at points A and B and hourly profiles of oxygen, chlorophyll, conductivity and temperature from a profiling buoy (Prol'Eau buoy equipped with BBE Fluoroprobe) at point B. On the top of the buoy a meteorological station measures the wind speed and direction which are recorded hourly. More information about this lake and the instruments can be found in Piccioni et al., (2021) and Tran Khac et al., (2018).

Measurements to compare the techniques were executed from a boat in two different locations of the lake at points B and C (Figure 52). The locations were selected for the lower abundance of macrophytes than at point A. Measurements occurred on June 5, 2021 at point B and on June 13, 18, and 29, 2021 at point C. MTC was deployed for all campaigns. REA and EC were deployed during the first 3 campaigns. Sediment cores were extracted on June 18 and 29.

6.3 RESULTS

6.3.1 Adequate hydrodynamic limiting conditions for EC and REA measurements

The turbulence contribution to nutrient and major metallic ion fluxes was measured using different techniques on different dates in Lake Champs. Among all four measurement days the comparison of techniques could be done only for the campaign of **June 13**. At 15 cm above the sediment the turbulence was too weak on June 5, 18 and 29. The turbulent kinetic energy (k), calculated as $1/2\left(\overline{u'^2}+\overline{v'^2}+\overline{w'^2}\right)$ (Stull, 1988) remained below 10^{-7} J kg^{-1} and friction velocity below the velocimeter resolution, 10^{-4} m s^{-1}. The power spectra of the vertical velocity did not exhibit any turbulence inertial range.

6.3.2 Oxygen supply lower than the sediment demand

The sediment oxygen demand was greater than the oxygen supplied by the water column. The oxygen demand by the sediment was measured ex situ through the micro-profile in sediment cores extracted on June 18 and the oxygen supply in situ by eddy covariance on June 13. Assuming no significant change in the organic matter content of the sediment between these dates, the sediment oxygen demand, 36 mmol m^{-2} day^{-1}, was larger than the actual oxygen supply to the sediment, -14.6 ± 4.3 mmol m^{-2} day^{-1} (n = 12, daily average and standard deviation, Figure 53A). Moreover EC fluxes are significantly correlated with the friction velocity (Figure 53B, R^2 = 0.48) which shows that they are triggered by turbulence, as formerly observed by McGinnis et al. (2008) in Lake Wohlen (Switzerland) and Murniati et al. (2015) in Lake Langersee on the Havel river (Germany).

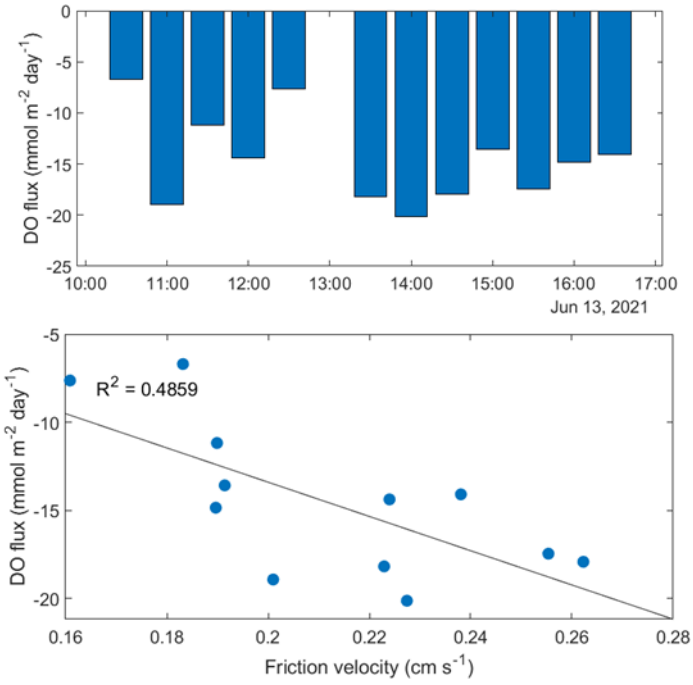

Figure 53 - A) turbulent benthic oxygen fluxes (eddy covariance) during the June 13 2021 campaign. B) Relation between oxygen fluxes and the friction velocity.

6.3.3 Different dynamics for oxygen and for nutrient and metallic ion fluxes

Few nutrient and metallic ion fluxes presented a high confidence level after flux quality evaluation (Figure 54). The low confidence level is mostly due to concentration differences below analytical precision, and once to a too high vertical average velocity (at 13:57). Most fluxes measured with REA were directed upwards (positive sign): phosphate, ammonium, iron and manganese fluxes. The direction of sulphate fluxes remains uncertain due to a high concentration in water as opposed to the other studied ions, and hence a high uncertainty on concentration differences (data not shown).

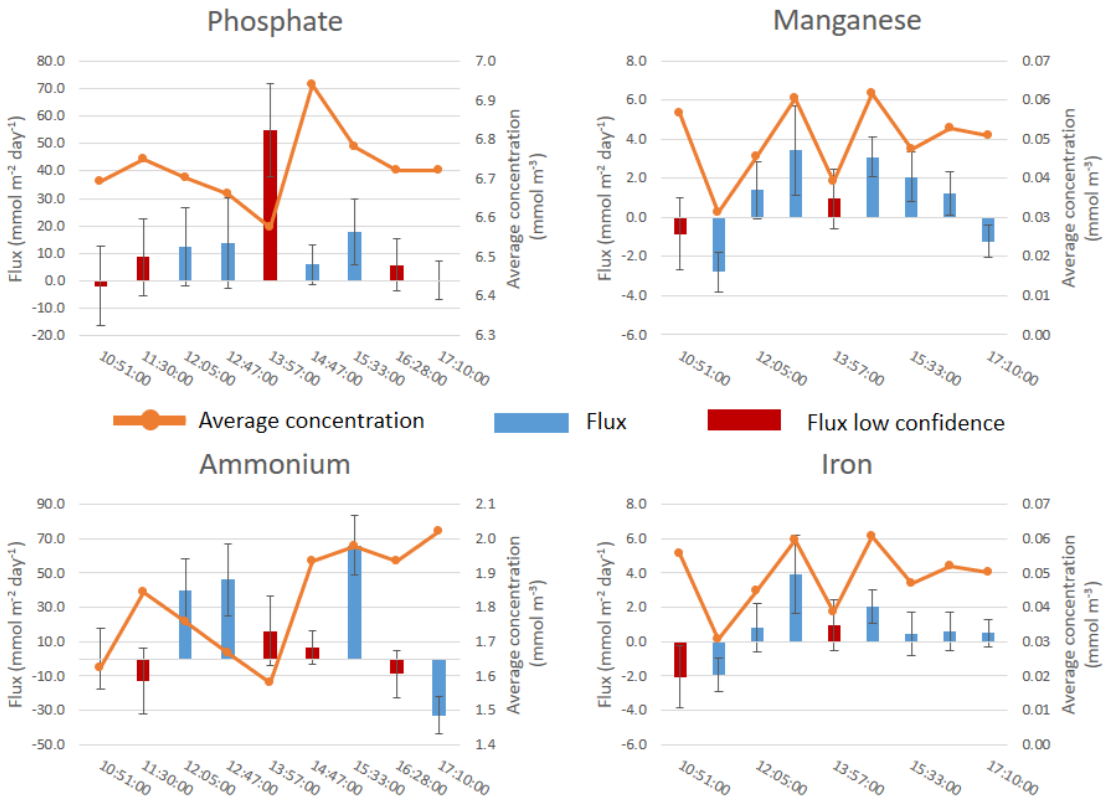

Figure 54 - Nutrient and metal flux dynamics and temporal concentrations measured by REA at Lake Champs. Fluxes with low confidence (LC) are marked in black. Black line highlight a null flux.

Contrary to oxygen fluxes, no significant correlation was found between the fluxes measured by REA and the friction velocity (Figure 55). However, excluding the segment biased by REA (13h57), an increasing trend was found between the fluxes of phosphate, ammonium, iron and manganese and the friction velocity.

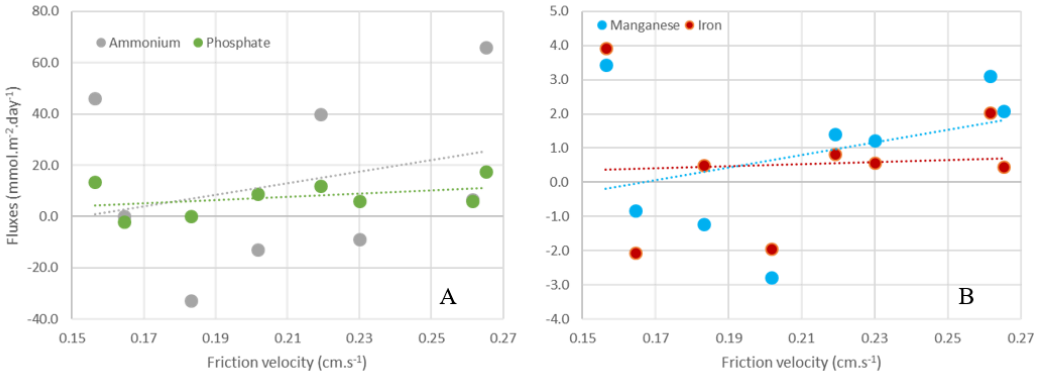

Figure 55 - Fluxes measured by REA on June 13 compared to the friction velocity (except sulphate): A) ammonium and phosphate; B) manganese and iron.

Planar fit, the alignment method used for REA, did not completely eliminate the **advection bias** in the flux measurements. The perturbation of flux measurement by advection due to misalignment is proportional to the average concentration of the solute in the benthic zone, and is major for sulphate (around 900 mmol m^{-3}), while it remains limited for the other solutes, mostly reduced compounds more concentrated in sediment pore water than in the benthic boundary layer (2-6 mmol m^{-3} for ammonium and phosphate, 0.05 mmol m^{-3} for iron and manganese ions).

6.3.4 Comparable turbulent fluxes by REA and MTC, larger than diffusive fluxes

The comparison of fluxes measured in the cores with the others techniques must be done with caution. The incubation experiment was designed to have no oxygen limitation, contrary to what was measured in-situ. However, vertical profiles measured with mini-peepers in sediment cores after incubation showed agreement with interface concentrations measured in-situ for phosphate (Figure 56). Phosphate fluxes measured in the sediment cores and by MTC were, respectively, 0.01 and 0.08 mmol m^{-2} day^{-1}.

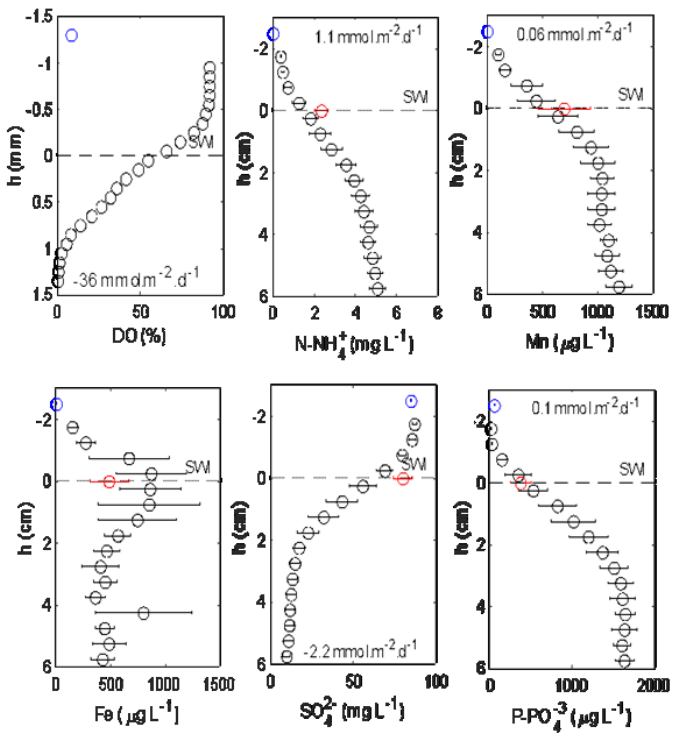

Figure 56 - Concentration profiles of chemicals dissolved in porewater (and overlying water) from sediment core incubations. Upper-left panel: Dissolved Oxygen (DO) measured with a micro-optode. Other panels include P-phosphate, N-ammonia, manganese, iron, and sulphate all measured with minipeepers. Black circles correspond to the average of a certain layer out of six minipeepers deployed in different sediment cores taken from Lake Champs. As a reference, blue and red circles represent in-situ concentrations measured 15 cm above the sediment and at the interface, respectively.

Averaging the concentrations of the six mini-peepers of both incubations and computing the interface gradients enabled the estimation of fluxes based on Fick's law for phosphate, ammonium, manganese and sulphate (Table 11). The gradient was not clear for iron, which could be due to reactions with sulphur in anoxic sediment (1.5 cm below sediment surface).

As expected, diffusive fluxes of ammonium, manganese and iron in the sediment cores are much smaller than turbulent fluxes estimated by MTC and REA (Table 12).

Table 9 - Parameters involved on the calculation of fluxes by MTC for the June 13, 2021 campaign.

Compounds	**u_* (cm s^{-1})**	**Schmidt no.**	**MTC (m s^{-1})**	**C_{TBL} (µmol l^{-1})**	**C_{DBL} (µmol l^{-1})**	**Flux (mmol m^{-2} d^{-1})**
Phosphate	0.1	1221	$3.3.10^{-6}$	1.7 ± 0.3	2.0 ± 1.4	0.08 ± 0.31
Ammonium		558	$5.2.10^{-6}$	1.2	176.5	78.7
Iron		924	$4.0.10^{-6}$	0.05	3.7	1.27
Manganese		922	$4.0.10^{-6}$	0.02	3.5	1.21

Unlike for phosphate, MTC and REA measured comparable fluxes for ammonium, iron and manganese: iron and manganese fluxes present similar values , ammonium fluxes are twice larger for MTC. The

discrepancy is much larger for phosphate.

Table 10 – Daily fluxes measured by EC, REA, MTC and in the sediment cores on June 13th at Lake Champs. REA and EC daily averaged fluxes are presented with the standard deviation.

	Fluxes (mmol m^{-2} day^{-1})				
	Ammonium	**Phosphate**	**Iron**	**Manganese**	**Oxygen**
REA	27.1 ± 38.0	12.3 ± 4.9	0.9 ± 1.8	1.0 ± 2.2	
EC	-	-	-	-	-14.6 ± 4.3
MTC	61 ± 20	0.08 ± 0.31	1.27 ± 4.4	1.21 ± 6.9	-
Sediment cores	1.1	0.1	-	0.06	-36

6.4 DISCUSSION

6.4.1 Reliability of REA and MTC fluxes

The downwards fluxes measured by REA do not necessarily denote the consumption of the compounds by the sediment. Measured negative fluxes for manganese and iron at 11:30 AM occur after an important decrease in their concentrations. Precipitation of these compounds in hypoxic conditions can occur at low turbulence levels (Canfield et al., 2005a). Metallic ions can also bind to calcium carbonate (Nealson and Saffarini, 1994). Ammonium fluxes towards the sediment is not usual. This was observed on environments with an alternation of oxic and anoxic conditions (Faganeli and Ogrinc, 2009). The daily averaged fluxes of these three compounds measured by REA are reliable. Such measurements could help understand the dynamics of low temporal scale fluxes in shallow eutrophic lakes.

The footprint of REA measurement is a possible source of difference with fluxes measured MTC. Computed after Berg et al., (2007), it covered a sediment surface area of 37 m^2, while MTC covered only a few square centimetres. In addition, ammonium is more reactive and sustains the food web in the lake. Total dissolved iron and manganese concentrations are stable and they may be spatially uniform. Comparable nutrient and metallic fluxes driven by turbulence show the reliability of the new techniques.

6.4.2 Oxygen and ammonia fluxes enhancing algae growth and contributing to anoxia

The weather conditions on June 2021 favoured an algal bloom then its recession. It caused rapidly varying oxygen conditions in the water column. Most of the days of June the lake presented daily thermal stratification (Figure 57B). The monthly average temperature difference in the water column at PtA was 3°C and its maximum 7°C. Algae fluorescence (Figure 57C) began to increase on June 15 and quickly reached a peak on June 18 (increase by ≈ 21 µg L^{-1} day^{-1} in chlorophyll A equivalent unit).

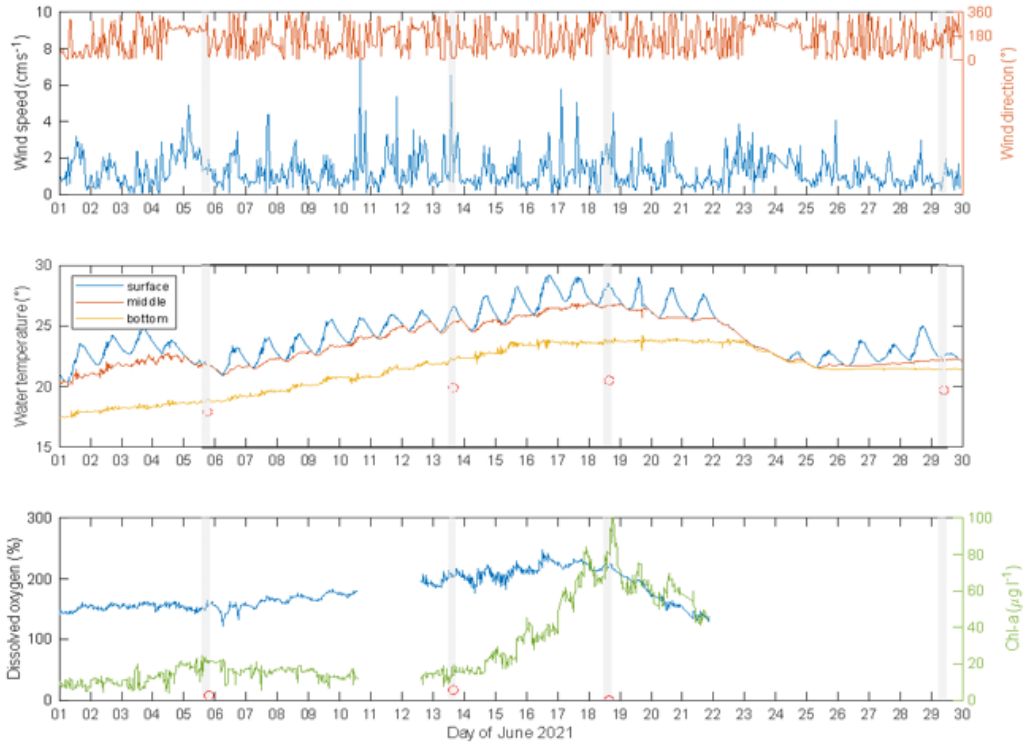

Figure 57 - Temporal changes of wind, water temperature, dissolved oxygen (DO), and chlorophyll-a (Chl-a) measured in Lake Champs during June 2021 (VINCON-LEITE, et al., in-prep). Water temperature were recorded in point A. Wind speed and direction, DO and Chl-a were recorded in point B (buoy), at depths 2.25 m and 0.25 m, respectively. Areas shaded in grey represent sampling days. Bottom temperature (7 cm above sediment) and bottom DO (15 cm) at the sampling spot are presented by red circles.

As shown by the low benthic oxygen concentrations, the oxygen demand by the sediment was greater than the supply from the surface during the whole month. In the pelagic zone dissolved oxygen measured at mid-depth sustainably increased (up to 245%) until the algae bloom (mostly composed by *Dolichospermum circinale*), because of algae growth and of macrophyte presence (Figure 57 C). However, the benthic zone remained hypoxic and maybe anoxic (<15% DO during sampling campaigns 15 cm above the sediment) due to the limited diffusion of oxygen in the hypolimnion in low turbulence conditions.

Before the bloom peak the oxicline, the oxic-anoxic boundary was very likely moving along the vertical at the daily time scale. During the day photosynthetic organisms caused the super-saturation of oxygen above the thermocline, around 50 cm above the sediment surface. During the night the water column was partially mixed due to surface cooling and there was no oxygen production but consumption by respiration so that oxygen concentration should have decreased in the benthic zone and the oxicline moved upwards. However, the thermocline does not disrupt and its position is stable in the daily scale, as well as, the oxicline. After senescence of the bloom algae there is increased oxygen demand by the sediment (not measured) leading to strong anoxia (data not shown).

REA and MTC measurements gave insights in the understanding of the ecological dynamics of Lake

Champs. Recurrent high phosphorus concentrations is measured in the lake (Molar N:P ratio$_{(2020-2021)}$ = 16 ± 5 at VINCON-LEITE et al., in-prep), leading to the hypothesis that nitrogen is the limiting nutrient for flora and fauna. Just before the algae bloom dynamic started, in-situ probes measured a great ammonium release from the sediment. The flux measurements strengthen the nitrogen-limiting hypothesis.

6.4.3 Suitable techniques for different environmental situations

Benthic flux quantification presents limitations inherent to the used technique. The new techniques presented in this work do not differ in these terms. REA, for instance, lacks a reliable technique to successfully align the coordinate system of the current meter and avoid advection perturbing the measured fluxes. A possible solution for future use would either be to reduce the sampling duration (around 3 min), apply 2-angles rotation successively and refresh alignment angles every 3 min or continuously with a back-looking moving window calculating the angles (von der Heyden et al., 2021). The precision of the analytical methods determining the concentration of the accumulated samples limits the range of solutes and of measurable flux values. In the present work we empirically found a minimal rate of turbulence ($k > 1.10^{-7}$ J.kg^{-1} and $u_* > 0.01$ cm.s^{-1}) below which the technique does not work. Thus REA can have difficulties in waterbodies where the bed currents are mainly driven by surface wind. However, REA can explore the dynamics of benthic fluxes at a small time step while covering a great sediment surface as opposed to other techniques like MTC.

MTC presents similar limitations as DET or DGT considering the exposure time and the spatial representativeness (a few square centimetres). The use of the interface peepers on sediment partially covered by biofilm is not recommended (Woodruff et al., 1999). Such a technique can be applied in different hydrodynamics conditions, as far as turbulence is present, and it takes into account the turbulence effect on the fluxes.

6.5 CONCLUSIONS

Two innovative techniques to measure benthic nutrient fluxes were assessed in a very eutrophic shallow lake and compared to well-established techniques. The use of MTC and REA allowed to access the turbulence contribution to nutrient and metallic ion fluxes. Similar scales of daily ammonium, manganese and iron fluxes were measured by both techniques. In addition, REA measured the short-time variation of these fluxes, giving insights to understand ecological dynamics at short time scale. Both techniques require improvements but they promise to be powerful tools towards a better empirical understanding of benthic fluxes and of the biogeochemistry of shallow aquatic ecosystems.

7 MAIN CONCLUSION AND PERSPECTIVES

Freshwater quality in natural environments is of major concern for the agricultural, industrial, and domestic sectors. Despite decades of efforts to reduce the pollutant inputs, water quality recovery can be slow, due to the pollutant stock in the sediment of aquatic ecosystems. For example, the so-called internal load presents a notable contribution to the dynamics of eutrophication. Such benthic fluxes (i.e. at the interface between the sediment and the water column) result from microbiological and chemical activity in the sediment. They have different drivers including hydrodynamics. Turbulence affects the benthic boundary layer, more specifically fluxes through the thickness of the diffusive sublayer (DBL). Different techniques are widely used to quantify benthic fluxes (e.g., benthic chambers, dialysis chambers, concentration profilers or eddy covariance). No technique is capable to measure turbulent benthic fluxes over a large sediment area without perturbing the bed flow for a great range of fluxes. The adaptation to the aquatic environment of relaxed eddy accumulation (REA), a micrometeorology technique, was shown to be theoretically feasible. The objectives of this work were: To develop a prototype that reproduces and adapts the REA facility to aquatic environments; To perform a technical validation of the prototype with a reference method; And to use the prototype to measure nutrient and metallic ion fluxes on a small time scale in a natural aquatic environment.

All the work presented here was possible thanks to the Ecole des Ponts ParisTech financing the doctoral scholarship, AgroParisTech for operational costs of the AquaREA project, the UPEC for the use of their facilities, but also, the synergy between the Laboratoire d'Hydraulique Saint Venant and the Laboratoire Eau, Environnement et Systèmes Urbains. Over the years, various partners have contributed to the design and implementation of the project including the Institute for Environmental Studies of the University of Koblenz-Landau (Germany), the Soil and Water Research Infrastructure (SoWa) of the University of South Bohemia (Czech Republic), the Laboratoire des sciences du climat et de l'environnement (LSCE, France) and the research unit Continental Hydrosystems - Resources, Risks, Restoration (HYCAR) of the French National Research Institute of Science and Technology for the Environment and Agriculture (INRAE).

The prototype development was based on the principles of REA and adapted the data processing and the sampling to shallow aquatic environments. The following topics were investigated: the mechanical stability of the frame, the sampling mechanism, the control of the sampling rate and the required sampling frequency. Several simulations were performed to select options and optimal parameter values for the data processing in different hydrodynamic regimes:

- the method and the duration for aligning the velocimeter with the vertical to avoid that advection perturbs flux measurements;
- the duration of the back-looking running average required to extract the turbulent fluctuation of the vertical velocity and to avoid that low frequency flow structures perturb flux measurements.

At high frequencies, the prototype is now able to process velocity data, make sampling decisions and accumulate upstream and downstream samples in separate tanks.

The REA prototype was submitted to a technical validation with a reference method: Eddy covariance (EC). EC was chosen as the reference method because of the similarity of sampling requirements and measurement principles with REA. Both techniques measured oxygen fluxes simultaneously on four different types of water bodies. REA was adapted to perform oxygen measurements, as accumulation tanks are not able to retain dissolved gases in the samples. The presence of turbulence and the proper functioning of the REA were the main evaluation parameters for selecting comparable fluxes. Positive and negative fluxes, respectively, oxygen production by the benthic community and oxygen uptake by the sediment, were measured by the techniques. With a good agreement between REA and EC oxygen fluxes, the REA technique was validated.

In a small, shallow, and highly eutrophic urban lake, four techniques were deployed with the aim of comparing measured fluxes during an algal bloom to identify the substances whose fluxes can be measured. The techniques deployed were the new Mass Transfer Coeffcient (MTC), REA, diffusive gradients in thin films and microprofiles in ex-situ sediment cores and EC. The fluxes selected for comparison were ammonium, phosphate, sulphate, oxygen, iron and manganese. The measurements allowed the quantification of significant ammonium fluxes to the water column a few days before the onset of algal bloom dynamics. The comparisons also revealed larger sediment oxygen demand, as measured by the sediment cores, than the oxygen supply, as measured by EC. Among the four days of the field study, REA and EC discriminated favourable turbulence levels for only one day. On this day, MTC and REA measured similar values of daily average fluxes of ammonium, iron and manganese. The fluxes measured by REA showed a marked temporal dynamic over the day. The variability of the oxygen, ammonium, manganese and iron fluxes tended to increase when the friction velocity was higher. As expected, the turbulent fluxes measured by REA and MTC were higher than the diffusive fluxes measured in the sediment cores (ammonium, iron and manganese).

The field campaigns allowed us to understand the conditions under which the technique is used. In running water systems, hydrodynamics is not a limiting factor since the occurrence of turbulence can be considered constant. In lakes, on the other hand, bottom currents often vary according to wind, air temperature, inflows and outflows. Turbulence is intermittent in lakes where wind is the main driver of shear stress in the benthic zone. Thermal stratification reinforces turbulence low energy and intermittence. REA can measure fluxes from a wide range for friction velocity higher than 0.02 cm s^{-1} and a turbulent kinetic energy above 10^{-7} $J.kg^{-1}$. The uncertainty of the measured fluxes is correlated to the accuracy of the analytical method used to determine the concentration differences between accumulated samples. Uncertainty based on analytical precision reduces the confidence of measured fluxes when the concentration of the solute in the water column is high. Under the present operating and

processing conditions, REA cannot measure dynamics in which the flux is towards the sediment (for example, sulphate), except for oxygen for which REA was adapted. To overcome this problem, an analytical protocol derived from REA is needed to significantly increase the accuracy of the analysis. The process of selecting the water body of interest and the measurement point must take into account the flux footprint. The length and width of the footprint should not exceed the dimensions of the water body. Otherwise, the measured fluxes will be biased.

REA has a great potential for monitoring the spatial-temporal dynamics of benthic fluxes. However, challenges are still to overcome. The adapted planar fit and 2-angle rotation methods for aligning the coordinate system with the vertical still need improvement. The alignment angles were not always similar between those calculated for both REA and EC. Recent papers have presented non-constant alignment angles during the accumulation period. The duration of the running average used by REA (back-looking) needs further study. When the duration is too long compared to the time scale of the largest eddies, the resulting fluxes tend to be very high. In complex hydrodynamic water bodies, such as the Lake Champs, machine learning could be used to automatically refresh the moving average duration taking into account the instantaneous friction velocity and the measurement height. In addition, the autonomy of the system could be increased with a higher number of accumulation periods during a sampling campaign.

A wider use of the REA for estuarine ecosystems can be imagined minding the turbidity and the clogging of the sampling system. The tide should provide hydrodynamics compatible with the requirements of REA and the technique could help to understand the importance of hydrodynamics for biogeochemical processes. A future application requiring instrumental development of the device would open up the possibility of exploring fluxes of, for example, dissolved gases (e.g., greenhouse gases), organic micropollutants, microplastics and isotopes.

8 APPENDICES

8.1 APPENDIX 1 – ADDITIONAL INFORMATION FOR REA TECHNICAL VALIDATION

Supplementary figures of the REA technical validation (section 5) are presented here. These concerns: The Lake Champs (France) location in the Île-de-France, measurement points and survey system point (Figure 58); The PAR at Lake Champs during June 16th (Figure 59); Examples of the log-log representation of the power spectra of the vertical velocity (Figure 60); Finally, the location and illustrative picture of the sampling locations in the Île-de-France (Figure 61).

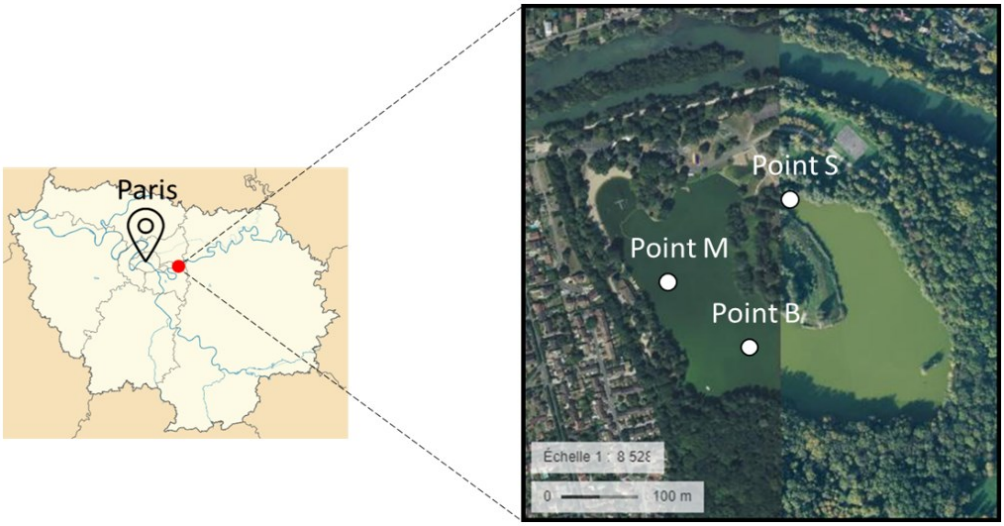

Figure 58 - On the left-hand side of the figure, there is the localization of the Lake Champs in the Paris suburban area. On the right-hand side of the figure, measurement points S and M used in REA validation, as well as, Point B where the micrometeorological station is located.

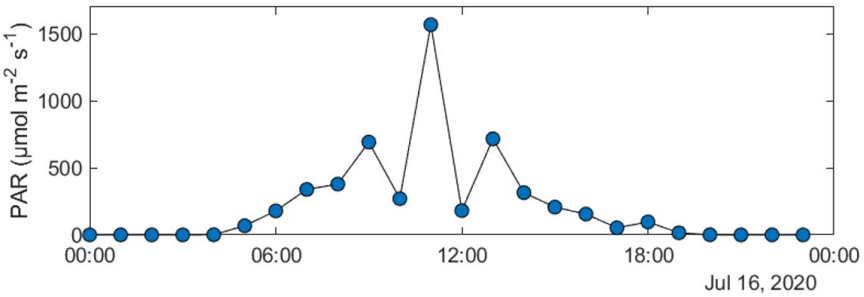

Figure 59 - PAR at Lake Champs during the July 16th of 2020.

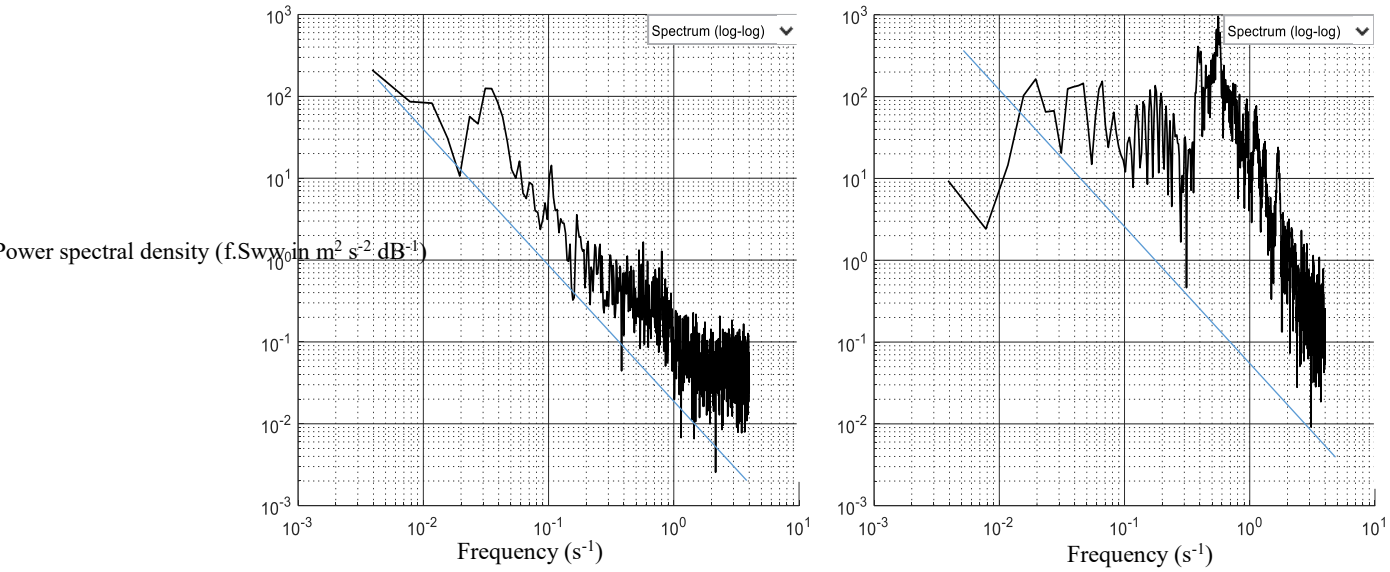

Figure 60 - On the left-hand side the log scale presentation of the power spectral density of the vertical velocity measured at Lake Champs at 16/07/2020 (12:38) where turbulence range was covered. Right-hand side power spectrum of the vertical velocity for the at Lake Champs at 17/07/2020 (14:32) where turbulence range was disturbed. The figures include the -5/3 slope (blue line).

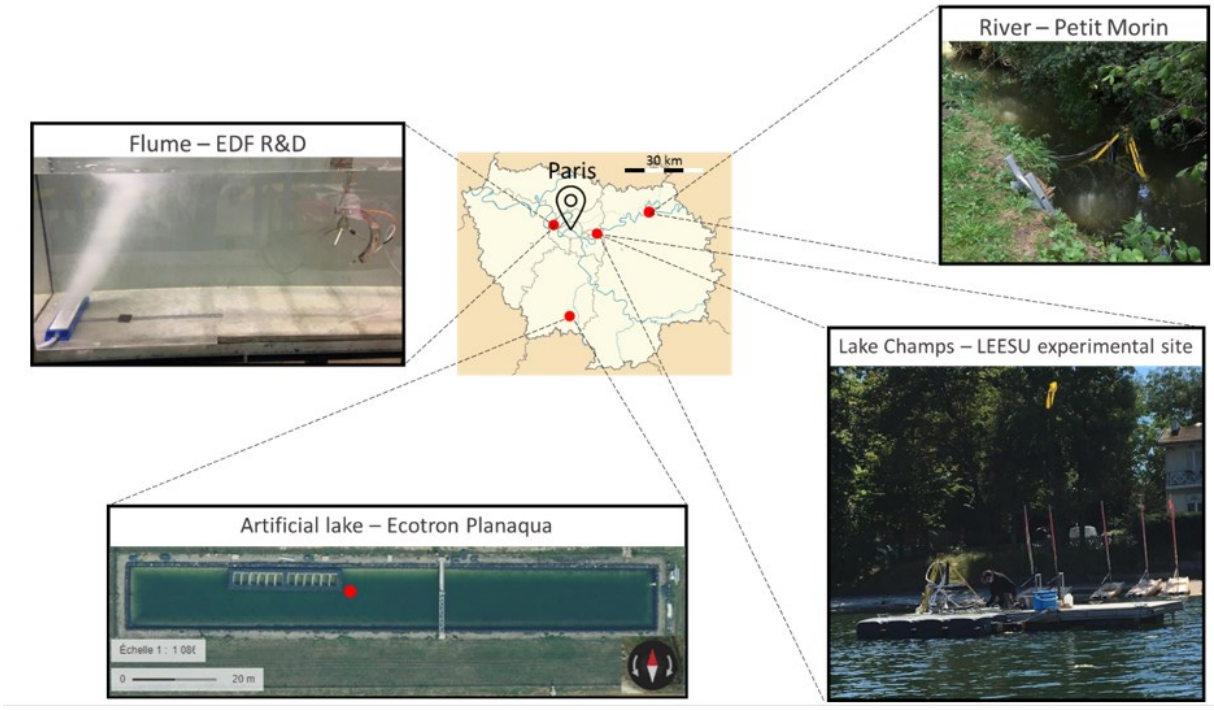

Figure 61 - Different measurement sites where EC and REA were deployed for the validation of REA. Site details in the "methods" section of the chapter. Red dot in the artificial lake indicate specific measurement point (Source: Google maps).

8.2 APPENDIX 2 – COMPILATION OF PROBLEMS ENCOUNTERED USING REA

Not all campaigns led to reliable flux measurements. Different problems were faced among different campaigns. Those are presented in the different annexes below.

Table 11 - Problems faced on different campaigns not presented in the chapters

Site	Waterbody type	Date	Objective	Faced problems
Stream Loge	Shallow stream	April, 2021	To follow nitrate and ammonium flux dynamics	- Analytical method low accuracy - High nitrate concentration in the water - Low quantity of ammonium fluxes
Stream Loge	Shallow stream	July, 2021	To compare nitrate, ammonium and phosphate fluxes with benthic chamber	- Technical problems with REA - Poor REA use conditions (Footprint, etc.) - Different environmental conditions between REA and benthic chambers
Planaqua	Artificial oligotrophic shallow lake	May, 2021	To follow nutrient fluxes in an oligotrophic lake	- Poor hydrodynamics in the lake - Footprint larger than the sediment borders
Lake Champs	Eutrophic shallow lake	August and September, 2020	To follow ammonium and phosphate flux dynamics in the lake.	- Lack of support measurements to interpret fluxes

8.3 APPENDIX 3 - MEASUREMENTS IN A SMALL STREAM IN AN AGRICULTURAL SUB-CATCHMENT: A STUDY OF THE DYNAMICS OF NITRATE FLUXES

8.3.1 Introduction

In Europe, several **policies** have been implemented to try to reduce the concentration of nitrates in inland aquatic ecosystems. Some policies, such as the Water Framework Directive 2000/60/EC, include a Nitrate Directive that recommends a nitrate level below 50 mg L-1 in freshwater. However, some authors consider this threshold to be questionable and too high (Aubert, 2021). In rural areas, **agriculture** covers most of the surface. These agricultural areas often follow the dominant agricultural model with intensive fertilisation. Nitrogen and phosphorus are widely applied to the soil during the growing season and during certain physiological stages depending on the cultivation type. Nitrogen is highly mobile in the soil and the application excess is flushed to drains or groundwater. The available nitrogen plays a role in the trophic status of the whole river network and of coastal waters.

The importance of studying small agricultural catchments for a bottom-up approach is not new. Various observatories monitor nitrate dynamics to work on alternatives to help legislators and decision-makers. The **Orgeval observatory** is one of them. The catchment area has been studied since the 1970s and is monitored at high frequency. Several studies have been carried out there, because the contribution of the network of small rivers has an impact downstream on the water supply of the Paris metropolitan area (about 9 million inhabitants).

Denitrification has gained ground as a solution to the nitrate problem. The uptake of nitrate by the sediment occurs in the sediment over a reducing environment (hypoxic or anoxic). Eriksson, (2001) presented experimental work in which he observed a weak influence of current velocity on denitrification in river sediments; the main driving factors were solar radiation and oxygen concentration. The lower the oxygen concentration and the brighter the sunlight, the more efficient the denitrification. Billen et al. (2015) present a biogeochemical model for rivers, validated by field measurements and experiments, in which the high concentration of oxygen in the water column transforms the ammonium flux into nitrate in the benthic boundary layer (BBL). However, the BBL thickness of running waters tends to be thinner than in a lentic environment (e.g., lake) (Lorke and Peeters, 2006). Thus, the diffusive boundary sublayer, the deepest of the BBL sublayers, often considered as the bottleneck of the exchange between sediment and water column, is thinner. In such an environment, the oxic-anoxic boundary, depending on the oxygen concentration in the well-mixed water column, can be located in the sediment. An oxic sediment in the subsurface cannot effectively perform denitrification, since nitrate is not required to replace oxygen as an electron acceptor. Since early diagenesis occurs in the first few millimetres of the sediment subsurface, an oxic sediment surface promotes ammonification and nitrification.

Invasive **techniques** do not provide easy access to such measurements as deployment is complicated and turbulence is required. Relaxed eddy accumulation and eddy covariance are a good option as they are non-invasive and take into account the contribution of turbulence to the fluxes.

This chapter presents measurements of the contribution of turbulence to nitrate and ammonium fluxes at high temporal scales in the Loge stream located in the Orgeval observatory.

8.3.2 Methods

8.3.2.1 Study site and environmental conditions during measurements

The **Loge stream** is located in the Orgeval experimental catchment, a critical zone observatory (Île-de-France region – around 60 km on East direction of Paris). The observatory is maintained by INRAe and as an historical experimental site (total surface are of around 100 km^2). The streams and rivers in there are instrumented for high-frequency survey of chemical and physical parameters. The Loge stream is located at Saint-Germain-sous-Doué. The stream was classified as intermittent since 2016. There is no water running during summer months. The surface of the catchment of the measurement point is around 4 km^2. Half of the total surface area is covered by forest and the other half covered by intensive, drained and irrigated cereal agriculture.

The stream width in the measurement point was around 1.7 m and depth was around 0.4 m. Upstream of the measuring point, the reach is straight for more than 350 m. The measuring point was purposely selected by avoiding meanders to diminish secondary currents. These disturb the measurements of turbulence contribution to the fluxes. The monitoring system of the stream installed by INRAe was around 10 m downstream the measurement point.

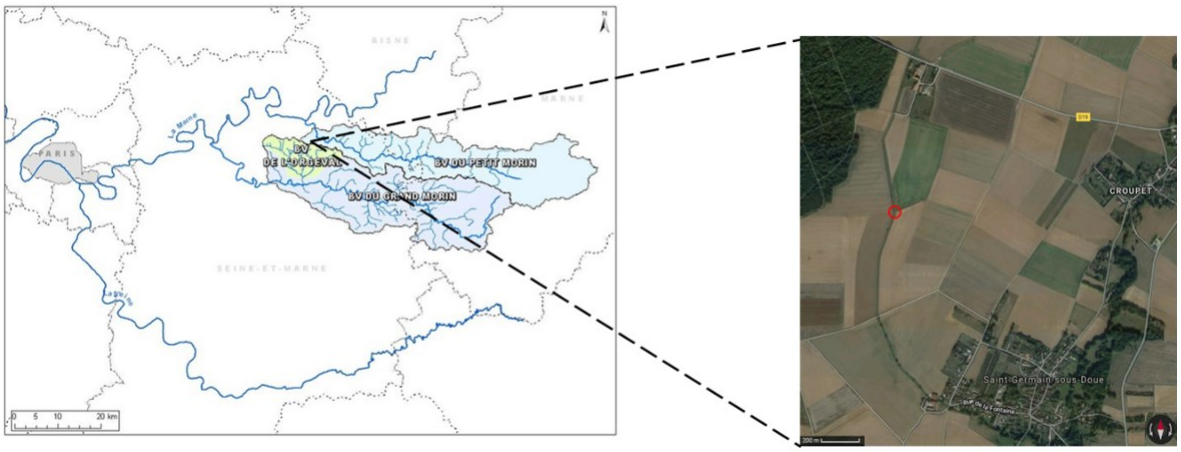

Figure 62 - The Orgeval watershed (green) in the Île-de-France region (left-hand side) (Source: https://gisoracle.irstea.fr/). The satellite image of the Loge stream (right-hand side) (Source: Google). The red circle indicates the measurement point.

The physical and chemical conditions in the water varied largely during the measurement campaign on April 29, 2021. Meteorological conditions were slightly cloudy and air temperature was around 12°C. The flow rate during the day was 11 L s^{-1} and it is not measured at high frequency. The water temperature

was slightly higher than the air temperature (~1°C). It increased after 12:00 from 12°C until 14°C at 18:00. The water depth decreased during the measurement day (5 mm) above the precision of the probe (1 mm). In fact, the same depth decrease was observed during the other days of the week. It might be related to water evaporation or upstream water use for irrigation. Calculations to estimate the average flow speed indicated small variation by depth decrease (around 2%). On the stream bed there were macrophytes, algae and biofilm (Figure 63).

Figure 63 - In the left-hand side the REA and EC placed in the Loge stream. The black arrow denotes the stream flow direction. Water turbidity in the left-hand side photo was the result of prototype deployment. Turbidity was very low during the measurements. On the right, macrophytes and algae in detail on the sediment upstream of the measurement point.

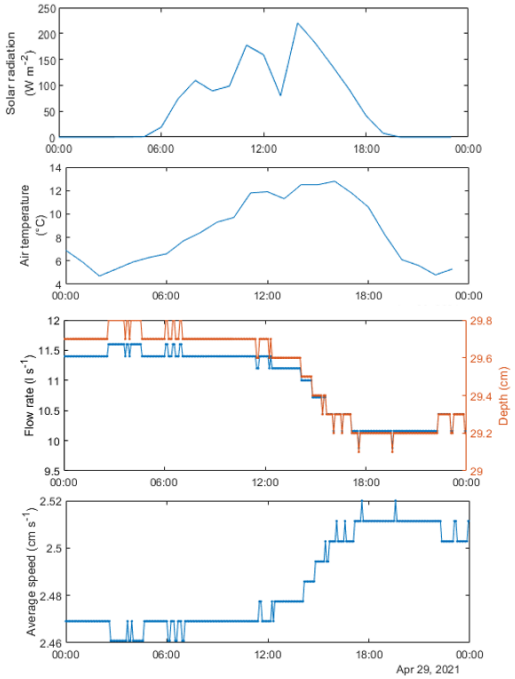

Figure 64 - Hydrological and meteorological conditions during measurements in the Loge stream and in the Orgeval watershed. The solar radiation (A) and Air temperature (B) were measured at the meteorological station at Boissy-le-Chatel (5 km south from the measurement location). The water depth and flow rate (C) was measured by the survey system in the stream.

8.3.2.2 *Techniques and data processing*

The techniques deployed to explore the turbulent contribution to the fluxes were the REA and EC. The instruments and data processing are the same as in the other chapters. REA and EC sampling devices for the concentration ($\bar{C}_{\uparrow}$, $\bar{C}_{\downarrow}$ and $\overline{C'}$) were coupled to the same frame to use same Doppler **velocimeter** and measure the fluxes in similar spatio-temporal scales. REA prototype changed compared to the setup presented in the previous chapters. **Sampling** is assisted by depression in the accumulation reservoirs forcing accumulation bags to suck samples when the sampling valves open. Vacuum pump was connected to the reservoirs at 0.2 bar. The **sampling height** was 8 cm above the sediment surface. EC **averaging periods** were of 7 min and REA accumulation duration of 10 min. Fast segments are linked to greater turbulence range in the stream (k = 1.55 10^{-5} J kg^{-1}). Main equations used here were already presented in the previous chapters.

The **alignment** of the coordinate system of the Doppler currentmeter were performed by Planar Fit (Wilczak et al., 2001). The angles for REA were calculated from a dataset collected for 1 hour just before the start of the measurements.

8.3.2.3 *Physical and chemical parameter*

This chapter is a study of the oxygen, nitrate and ammonium flux dynamics**. Samples** were retrieved from the accumulation bags through the sample recovery tube by gently using syringes. The samples were immediately filtered with a 0.45 µm cellulose acetate filter and refrigerated at 6°C for transportation and storage. To quantify the nitrate concentration an UV spectrometer (Trios-OPUS – Accuracy 5%) was used. The spectrophotometry at visible UV (Lambda 35 – Accuracy 5% – Perkin Elmer Inc.) was used to determine the ammonium concentration. **Oxygen flux** was exclusively measured by EC.

Flux uncertainty take into account the accuracy of the analytical method. This one is applied to every concentration and the resulting error is propagated. It is multiplied by the standard deviation of the vertical velocity and the empirical coefficient *b*. As in the previous chapter, for high average concentration the flux uncertainty is high.

8.3.3 Results and discussion

8.3.3.1 *Oxygen dynamics strongly affected by photosynthetic organism*

Oxygen concertation was increased by large presence of photosynthetic organisms covering the stream bed. The **oxygen concentration** in the water during the sampling period increased by almost 150 mmol m^{-3}. In mg L^{-1}, the oxygen concentration at deployment started was around 13 mg L^{-1} (≈110% DO) and finished with around 17 mg L^{-1} (≈150 % DO). **Temperature** measured by REA temperature probe matches the INRAe survey system. **Oxygen fluxes** measured by EC present positive fluxes (from the bed to the water column); their daily average and standard deviation were 73 ± 45 mmol m^{-2} day^{-1}.

Strange phenomenon with occurs after 12:00 changing physical and chemical parameters (Figure 64). The **water temperature** also increases in 3°C from midday until 14:00. The water depth decreases during the period. The components of the **velocity** (*u*, *v* and *w*) increase and the effect is noted in the friction velocity, and, thus in the oxygen flux. The **variability of the oxygen flux** increased also. In the linear fit comparing the oxygen fluxes with the **friction velocity** the coefficient of determination is good for the whole measurement period ($R^2 = 0.68$). However, it is very low for measurements before mid-day ($R^2 = 0.01$). The lower and less variable friction velocity (0.4 ± 0.01 cm s^{-1}) leads to a stable oxygen flux before noon (42.1 ± 5 mmol m^{-2} day^{-1}), which is expected in such stream. After mid-day the average and the variability of the friction velocity and of the oxygen flux increases (respectively 91.6 ± 48.2 mmol m^{-2} day^{-1} and 0.6 ± 0.15 cm s^{-1}) improving the linear model quality ($R^2 = 0.54$).

The sudden **increase of the water temperature** was not related to the net solar radiation. The last significant rainy event occurred more than 15 days ($Q = 21$ L s^{-1}) before the measurement day. Therefore, no water input from the drains was expected. Certainly there is an upstream contribution changing the thermic regime of the water which is unknown. This one changed the hydrodynamics and the effect on the fluxes. Since the friction velocity increased the thickness of the diffusive boundary layer changed decreased. In such super saturated running water, the oxygen concentration is well mixed in water column. Add to an almost negligible DBL the oxygen supply to the sediment is unlimited. In fact, it is supposed that oxic-anoxic boundary is not in the DBL, but in the first millimetres or centimetres below sediment surface. This changes the biogeochemical cycle of the nitrogen.

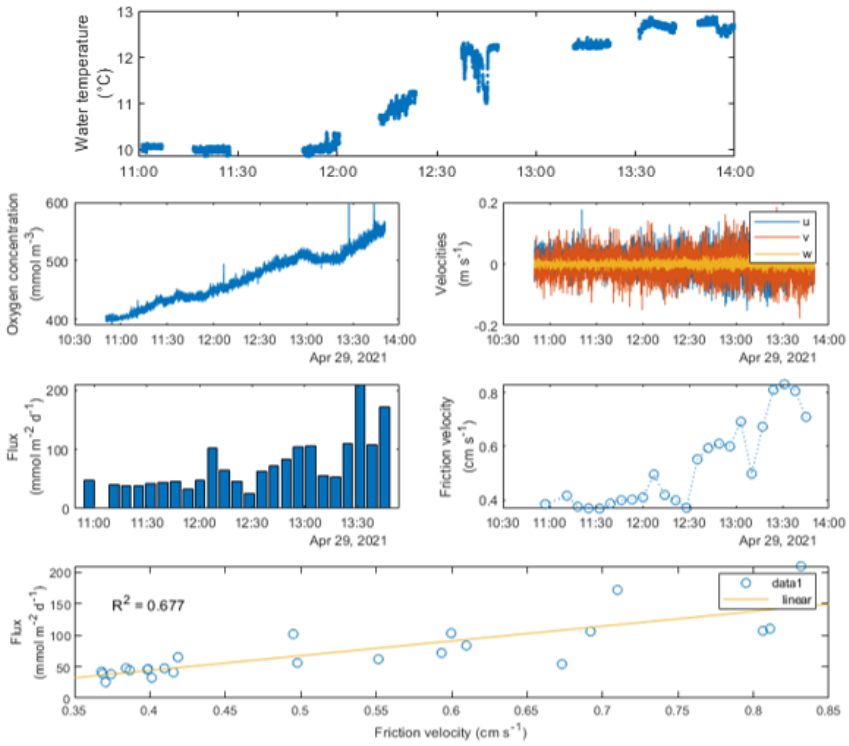

Figure 65 - Water temperature (A), oxygen concentration (B), velocities (C), oxygen fluxes (D) and friction velocity (E) measured during sampling. Linear fit of fluxes compared to the friction velocity (F).

The **measurement footprint** of the flux covered a great surface of the sediment. Until midday, in oval shape, the width was 0.5 m (between the stream shores) and length was 123 m covering 50 m^2 of the sediment surface. The density of covered sediment was not measured, however, visually, the macrophytes and algae were well distributed on the sediment and covering half surface of the surface.

8.3.3.2 Fluxes uncertainty a limitation of REA

The oxygen flux and oxygen mixing enhance a changes in the expected nitrogen cycle. The oxic surface of the sediment enhance ammonification and the nitrification. Thus nitrate and ammonium fluxes were expected to be released by the sediment. Using REA, these fluxes were measured.

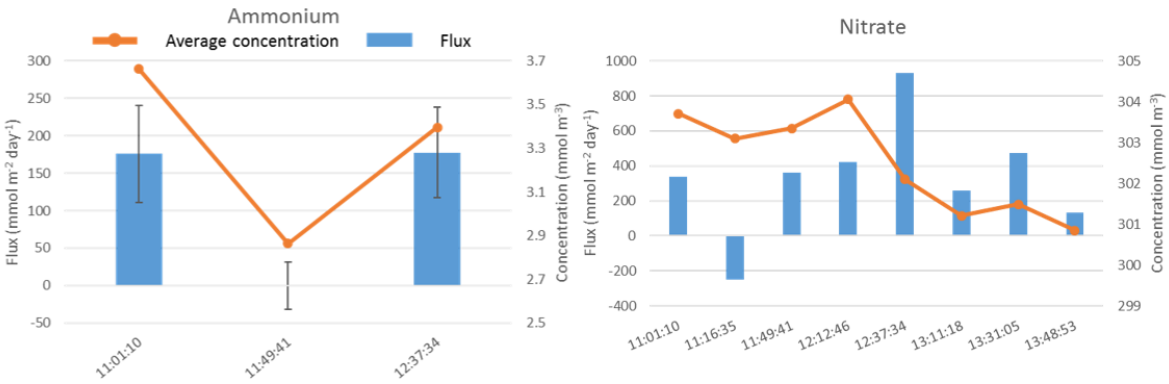

Figure 66 - Nitrate and ammonium fluxes measured by REA. Errors bars at ammonium fluxes take into account accuracy of the analytical method.

Great daily fluxes of nitrate and ammonium were measured, respectively 334 ± 331 and 117 ± 102 mmol m^{-2} day^{-1} (Figure 66). Removing accumulation periods that the uncertainty is greater than the flux, daily averages for nitrates was 547± 259 mmol m^{-2} day^{-1} and 177 ± 1 mmol m^{-2} day^{-1} for ammonium. The uncertainty of the nitrate flux is in average ten folds higher than the measured flux. Nitrate fluxes cannot be considered as well succeeded.

8.3.4 Conclusion

The objective was to better understand the drivers of nitrogen fluxes in small streams. REA and EC were deployed to quantify the turbulence contribution to oxygen, ammonium and nitrate fluxes at high temporal scale and wide sediment representation. Both techniques share similar footprint measurement and measurement timing. The EC measurements followed the photosynthetic activity enhancing the oxygen super-saturation of the stream. REA measurements helped to access resulting fluxes of ammonification. Resulting nitrate fluxes were not considered to be accurate as the uncertainties were greater than the measured fluxes. REA requires very high accuracy to better quantify the fluxes.

8.4 APPENDIX 4 – COMPARING REA TO BENTHIC CHAMBER IN A STREAM

8.4.1 Objective

To compare measurements of REA and benthic chamber to estimate turbulence contribution to the benthic fluxes.

8.4.2 Material and methods

8.4.2.1 Studied site and period

Figure 67 - On the left-hand side of the figure the benthic chamber deployed in the Loge stream. The mixing system is presented by red circle. On the right-hand side, upstream the benthic chamber, REA was deployed. Upstream REA measurement point the stream was no longer straight.

Measurements were executed in the Loge stream (details on previous annex) on 07/07/2021. Environmental conditions changed from the campaign in April 2021. The stream no longer presented a straight section. Stream flow velocity at measurement point was around 0.005 m s^{-1} and depth was around 0.3 m and width around 1.5 m.

8.4.2.2 Techniques deployed

REA setup is the same presented on the previous annex. The only change was the method to align the coordinate system. For this campaign we used the 2-angle rotation. REA measurement height was around 10 cm above the sediment. The accumulation duration was of 10 minutes.

The deployed benthic chambers belong to the Laboratoire des Sciences du Climat et de l'Environnement (CEA - CNRS - UVSQ - Université Paris-Saclay). The sediment overlying water is enclosed and it is sampled in regular time-step. The chamber featured an agitator driven by the external flow of water (Figure 67).

8.4.2.3 *Analytical methods and fluxes*

The fluxes explored were the ammonium, the nitrate and the phosphate. To determine nitrate and phosphate concentrations for both techniques we used the Ion Chromatography (Compact flex 930 – Metrohm AG – Adapted accuracy of 1% for concentration differences analysis). The spectrophotometry at visible UV (Lambda 35 – Accuracy 5% – Perkin Elmer Inc.) was used for the ammonium.

8.4.3 Results

8.4.3.1 *Benthic chambers*

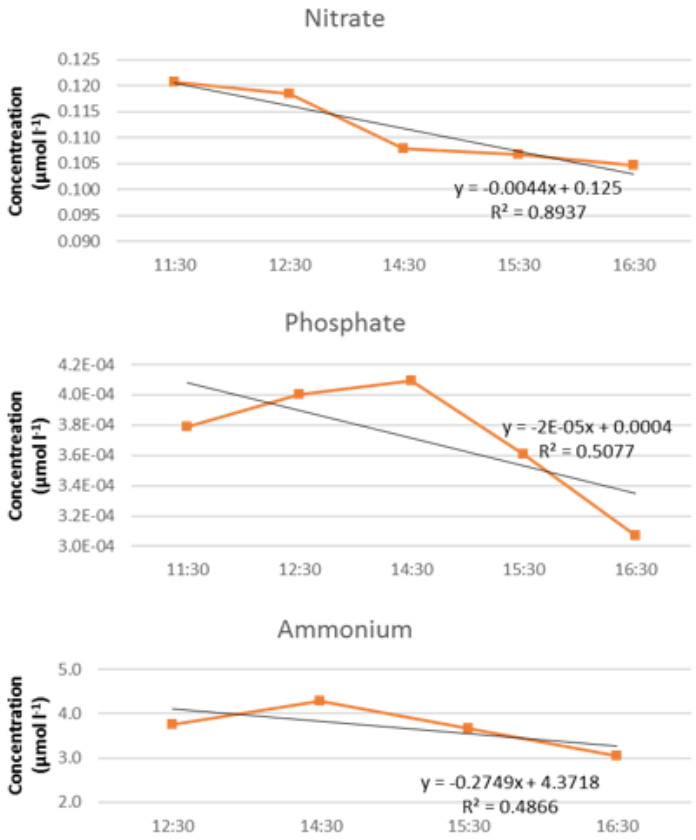

Figure 68 - The concentration overtime of nitrate, phosphate and ammonium (all in orange) from the benthic chamber. The linear fit of the concentration evolution and the R^2 and the linear equation.

The obtained fluxes from the benthic chambers were: -0.002 mmol m^{-2} day^{-1} for nitrate; - 8.10^{-6} mmol m^{-2} day^{-1} for phosphate; and - 0.1 mmol m^{-2} day^{-1} for ammonium. Only the nitrate presents a reliable measurement as the linear fit presents good quality (R^2 = 0.89). Thus, demineralization was measured by the technique.

8.4.3.2 *REA*

REA presented functioning problems and during the measurement day. It worked in the final half of benthic chambers deployment.

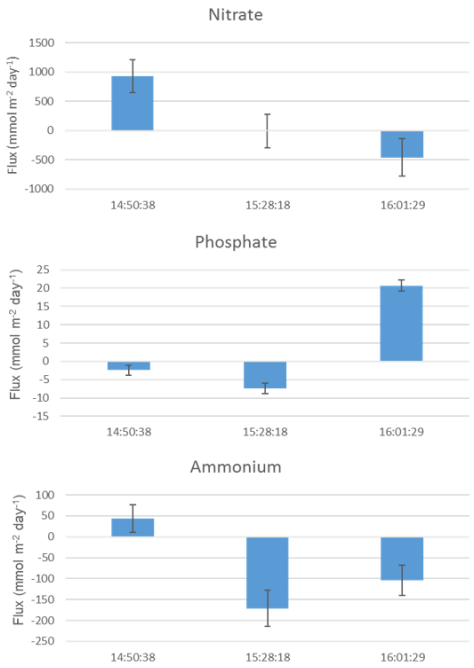

Figure 69 - Temporal dynamics of nitrate, phosphate and ammonium fluxes measured by REA.

8.4.3.3 Comparing fluxes

The comparison of benthic chamber fluxes can be compared just for the same period as REA run correctly. Benthic chamber fluxes were recalculated for the same period (assuming linear fit) as REA and REA fluxes were averaged giving.

Table 12 – Compared fluxes of ammonium, phosphate and nitrate measured by REA and benthic chambers.

	Benthic chamber	**REA**
Ammonium flux (mmol m^{-2} day^{-1})	-0.37	- 77
Phosphate flux (mmol m^{-2} day^{-1})	-3.10^{-5}	3.6
Nitrate flux (mmol m^{-2} day^{-1})	-0.001	153

The order of magnitude and direction of the fluxes measured by the techniques are not the same. The comparison failed for different reasons. The benthic chamber was set up in different environmental conditions from those of the REA. It was deployed under a bride with very low sunlight. The footprint of REA was in the complete opposite situation. Also, for REA the conditions of use were not respected. The footprint was not only covering sediment surface, it transposed the borders of the stream.

8.4.4 Conclusion

To achieve good measurement of REA the good conditions need to be respected. On this case the footprint needs to be just on the stream bed.

8.5 APPENDIX 5 – EXPERIMENTS IN OLIGOTROPHIC ARTIFICIAL LAKE

8.5.1 Objective

To follow nutrient dynamics in an oligotrophic and experimental lake.

8.5.2 Methods

8.5.2.1 Measurement site

Measurements were executed in the experimental site Planaqua at 20/05/2021. Same experimental place is presented in the Chapter 3 of this work. However, for this time we used one of the small lakes of 750 m^3, length 30m, width 15m and depth 2,80m (Lake 9). The average speed measure in the sampling depth was - 0.14 cm s^{-1}. The currents were coming from the backwards of the prototype.

Figure 70 – Artificial lake used for the measurements.

8.5.2.1 Analytical methods

The fluxes searched were for nitrate, phosphate and ammonium and for these we used the Ion Chromatography (Compact flex 930 – Metrohm AG – Adapted accuracy of 1% for concentration differences analysis).

8.5.2.2 REA

Measurements were executed 15 cm above sediment surface. The accumulation duration was 15 minutes. Same REA setup and data processing as in Chapter 4.

8.5.3 Results

8.5.3.1 REA fluxes

The only compound not out of range of the analytical technique was ammonium. Those fluxes were very high (Figure 71). The daily average and standard deviation was 156 ± 325 mmol m^{-2} day^{-1}.

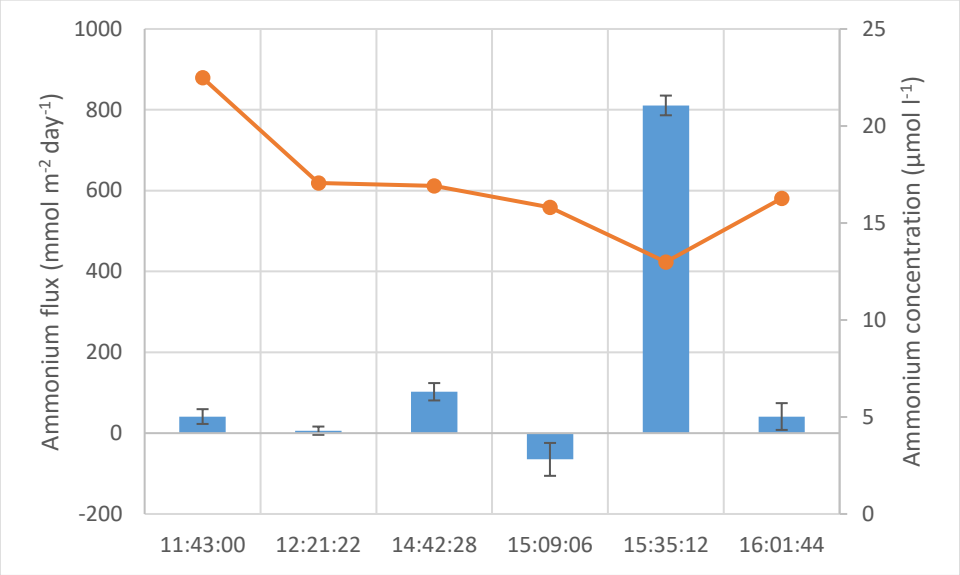

Figure 71 - Ammonium flux (blue bars) and average concentration (orange line) measured by REA in the artificial lake.

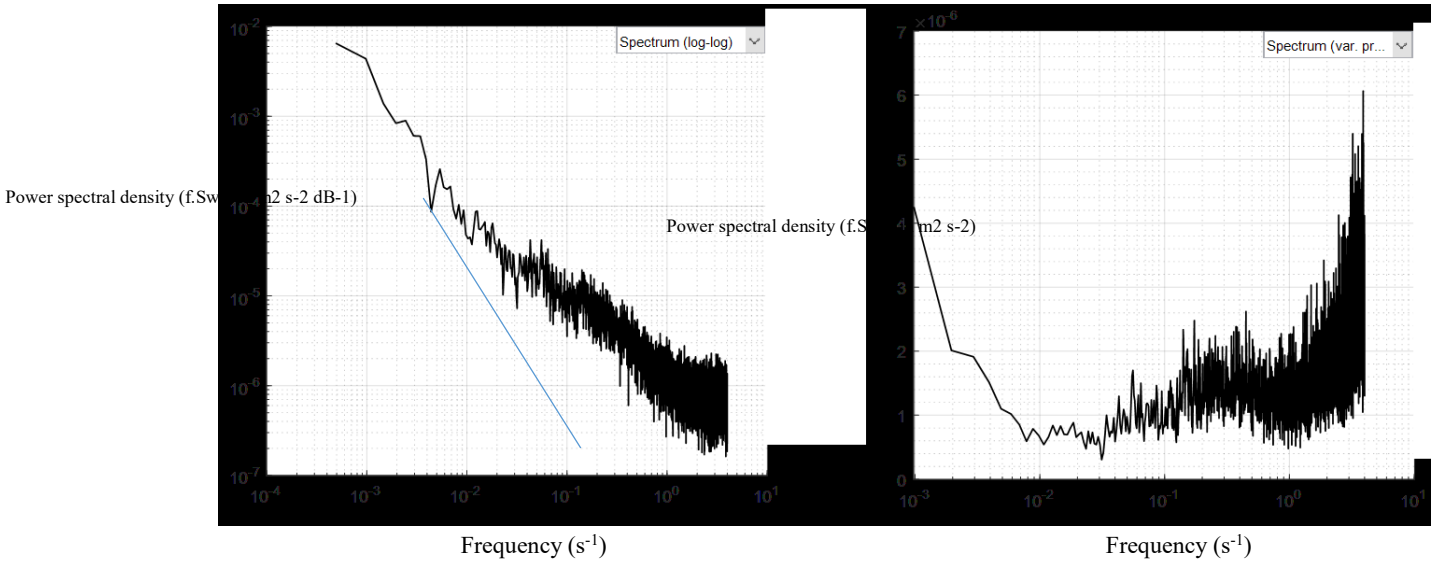

Figure 72 - The log-log (left-hand side) and the variance preserving (right-hand side) representation of the power spectrum of the vertical velocity during the whole REA deployment. The blue line is the -5/3 slope.

High ammonium fluxes were led by bad sampling conditions. The footprint was not only covering sediment surface, it transposed the borders of the lake. In addition, the main current speed was coming from backwards. It biases the measurement. Finally, the turbulence was not strong and the turbulence range was not followed.

8.5.4 Conclusion

REA conditions of use were not respected regarding the positioning, the footprint and the turbulence level and the measured fluxes were completely biased.

8.6 APPENDIX 6 – NUTRIENT FLUXES MEASURED BY REA LAKE CHAMPS ON 2020

8.6.1 Objective

Follow the phosphate and ammonium dynamics in the Lake Champs.

8.6.2 Methods

8.6.2.1 Site

The measurements were executed 26 August and 2nd of September 2020. REA was deployed on the Point A of the Lake Champs (Descriptions on the Chapter 3). During the measurement campaigns low thermal stratification was measured (1°C difference between bottom and top) and oxygen concentration was 110% DO homogeneously through the whole water column. The mean current speed at sampling height was 0.002 m s^{-1}, for the first day, and 0.007 m s^{-1} for the second day. Lake bed was covered by a phylamentous algae.

8.6.2.2 REA

REA setup and data processing were the same as in the Chapter 3. The sampling height above the sediment was around 15 cm. The accumulation duration was of 15 minutes. No oxygen measurements by EC or REA measurements. Some kind of technical problem made the data unavailable.

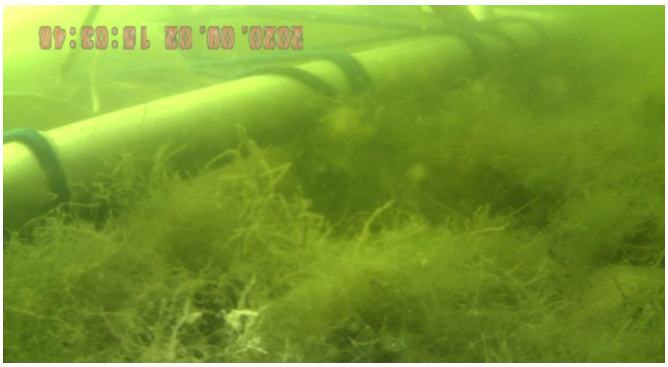

Figure 73 - Sediment bed covered by phylamentous algae. (Photo: Eric Viollier)

8.6.2.3 Analytical method

To determine the ammonium and phosphate concentration we used the spectrophotometry at visible UV (Lambda 35 – Accuracy 5% – Perkin Elmer Inc.).

8.6.3 Results

The fluxes of ammonium and phosphate were followed for both days.

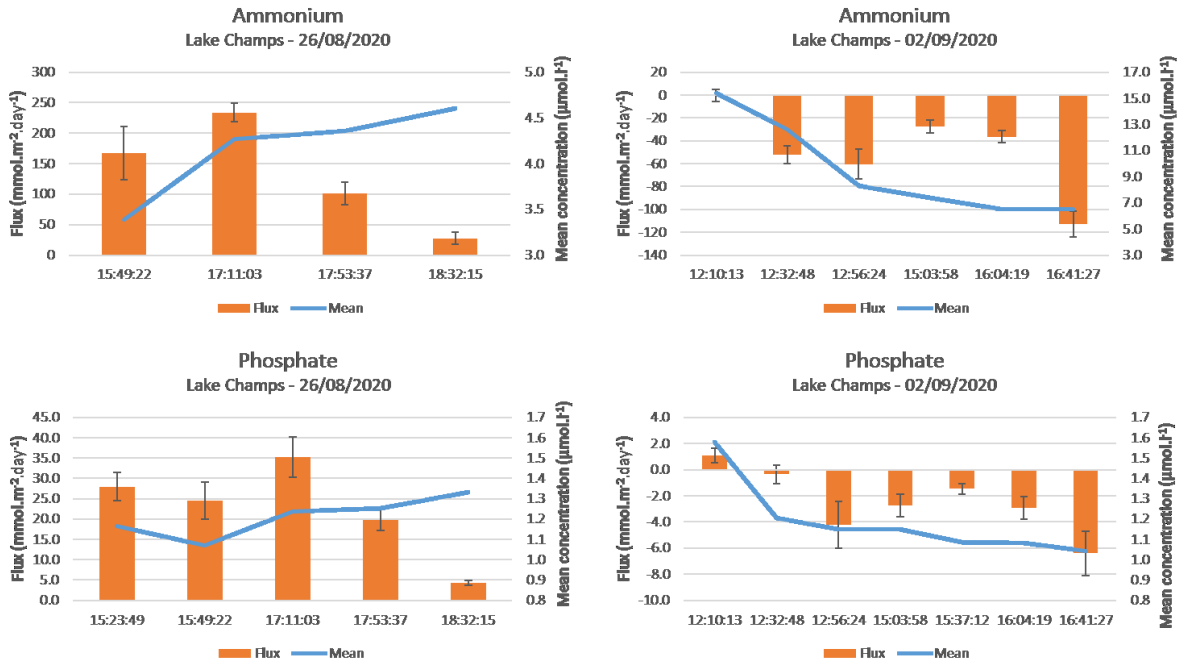

Figure 74 - The fluxes (orange bars) and average concentration (blue line) for ammonium and phosphate. On the left-hand side measurements on 26 of August and on the right-hand side measurements on 2nd of September, both of 2020.

For the 26/08 the fluxes of both nutrients were from the lake bed towards the water column and the average concentration of the compounds increased. On the 02/09 the measured fluxes were mostly towards the lake bed and the concentration of the compounds decreased.

No further exploration of the data was executed as no support measurements were functioning, nor for oxygen fluxes and nor from the lake surveillance system. The lack of additional data makes impossible the interpretation of the fluxes.

8.6.4 Conclusion

The measurements were not accounted as valuable due the lack of supplementary measurement to ensure an interpretation.

8.7 APPENDIX 7 – HOW TO USE REA: THE MANUAL

8.7.1 Introduction

The objective of the document is present the required steps to proceed before field campaign start. The document is under development and a specific part for REA automation will be developed.

8.7.2 Check list for field campaign

1. Computer with automation
    a. Charger
    b. USB stick
2. Oxymeter
    a. USB cable connector
3. ADV
    a. Charger
    b. Converter ADV cable - USB
4. Power cable valves and thermometer (grey box)
5. 2 Supplementary perfusion bags
6. Battery charged
7. 12v – 220w converter
8. Lab analysis
    a. Syringes
    b. Filters
    c. Icebox with ice
    d. Vials
    e. Permanent marker
    f. Pen and adhesive tape
9. Vacuum pump (if measurements are executed in stream)
10. Weight to compensate bottles buoyancy

8.7.3 Overall verification of the prototype in the laboratory before the field

1. Check if the caps of the accumulation bottles are well sealed with parafilm
2. Put the weight in the tripod leg which the bottles are
3. Attach the box containing the valves to the metallic frame
4. Test valves action using automation software
5. Test the ADV measurements using the automation software
6. Positioning the tube inlets and oxygen probe (needles) 1 cm far (horizontal axis) of the ADV sampling volume (use the fake sampling volume)

7. In case of measuring oxygen fluxes, check the positioning of the oxygen probes in the T close to the tube inlets.

8.7.4 In situ, before positioning REA on the sediment

1. Check and correct the alignment of the ADV with a level. Like for a topographic tripod.
2. Slide away the oxygen probe tip
3. Connect power cable of ADV to a source of power

8.7.5 In situ, after positioning REA on the sediment

1. Open ADV Vector
    a. Check the sampling height above the sediment and if the probes and/or sampling tube inlet: On-line → start probe check. When it is done ADV is ready to run.
    b. Set deployment → configuration → 8 Hz; XYZ; lake or river; nominal range depends on the expected current speed. Bad nominal range leads to high SNR and low correlation.
    c. Click on "Start Recorder data Collection" → Fill the name of the deployment
2. Open LabVIEW script for REA

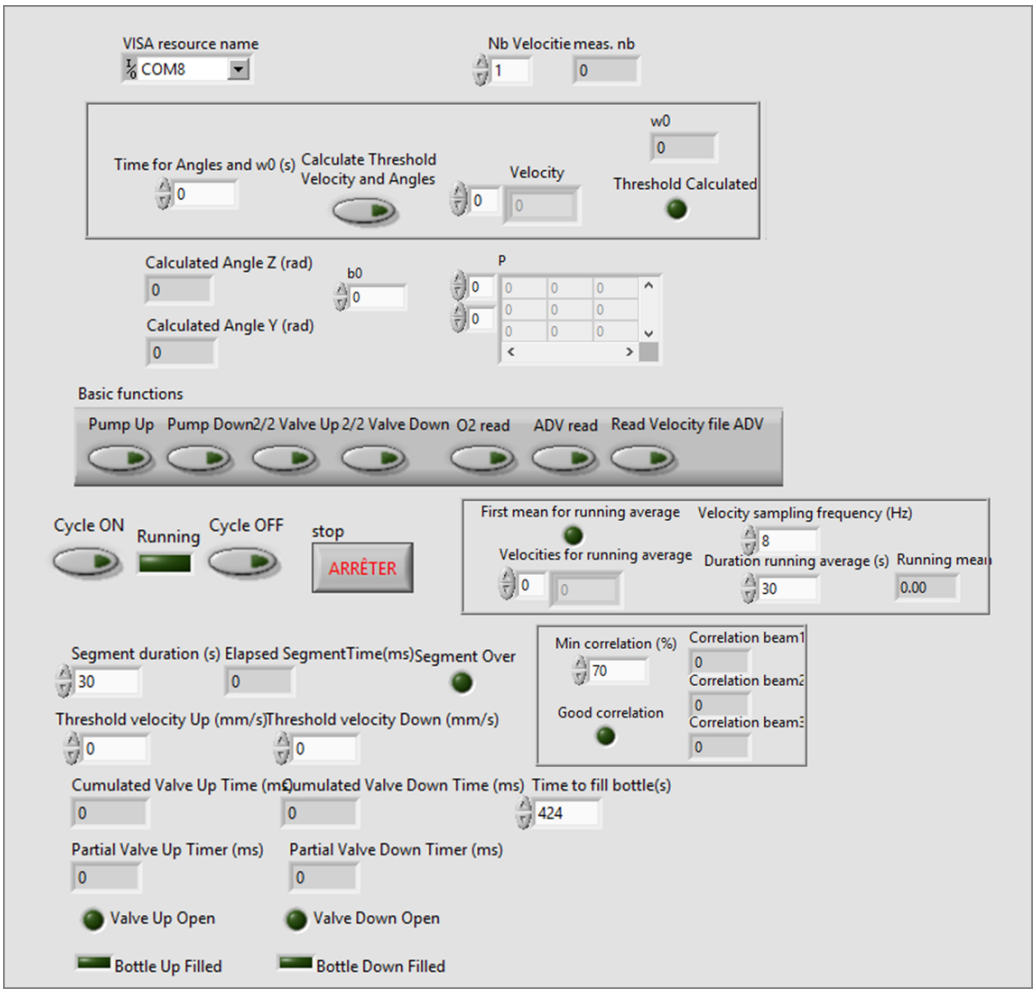

Figure 75 - User interface of the automation of REA using LabVIEW.

a. Check if ADV cable is connected to the good "COM" in the "Visa resource name";
b. Test if all the components of the prototype are being controlled by the script;
c. If the alignment of the coordinate system previously selected, you must fill the b_0, the P matrix and the threshold velocity previously calculated.
d. If the alignment of the coordinate system previously selected is the 2-angle rotation insert the selected "Time for angles and w0 (s)" and press the button "Calculate threshold velocity and angles. When it is finished the angles will be displayed as well as, the threshold velocity.
e. On "Segment duration (s)" insert the total accumulation period in seconds.
f. On "Duration running average (s)" insert the required duration in seconds and the sampling frequency on the above space named "Velocity sampling frequency (Hz)".
g. Select the correlation threshold on "Min. Correlation (%)".
h. Select the duration that the bottles are completely filled on "Time to fill bottles".
i. Press "Cycle ON" to start sampling.

9 REFERENCES

Ahmerkamp, S., Marchant, H.K., Peng, C., Probandt, D., Littmann, S., Kuypers, M.M.M., and Holtappels, M. (2020). The effect of sediment grain properties and porewater flow on microbial abundance and respiration in permeable sediments. Sci Rep *10*, 3573. https://doi.org/10.1038/s41598-020-60557-7.

Aller, R.C., and Aller, J.Y. (1998). The effect of biogenic irrigation intensity and solute exchange on diagenetic reaction rates in marine sediments. Journal of Marine Research *56*, 905–936. https://doi.org/10.1357/002224098321667413.

Aller, R.C., Hall, P.O.J., Rude, P.D., and Aller, J.Y. (1998). Biogeochemical heterogeneity and suboxic diagenesis in hemipelagic sediments of the Panama Basin. Deep-Sea Research Part I: Oceanographic Research Papers *45*, 133–165. https://doi.org/10.1016/S0967-0637(97)00049-6.

Ammann, C., and Meixner, F. (2002). Stability dependence of the relaxed eddy accumulation coefficient for various scalar quantities. Journal of Geophysical Research: Atmospheres *107*, ACL7-1-ACL7-9. https://doi.org/10.1029/2001JD000649.

Andersen, T.J., Fredsoe, J., and Pejrup, M. (2007). In situ estimation of erosion and deposition thresholds by Acoustic Doppler Velocimeter (ADV). Estuarine, Coastal and Shelf Science *75*, 327–336. https://doi.org/10.1016/j.ecss.2007.04.039.

Andersen M.R., Kragh T., and Sand-Jensen K. (2017). Extreme diel dissolved oxygen and carbon cycles in shallow vegetated lakes. Proceedings of the Royal Society B: Biological Sciences *284*, 20171427. https://doi.org/10.1098/rspb.2017.1427.

Aubert, C. (2021). Les apprentis sorciers de l'azote. La face cachée des engrais chimiques (Terre Vivante Editions).

Ayrault, S., Meybeck, M., Mouchel, J.-M., Gaspéri, J., Lestel, L., Lorgeoux, C., and Boust, D. (2021). Sedimentary Archives Reveal the Concealed History of Micropollutant Contamination in the Seine River Basin. In The Seine River Basin, N. Flipo, P. Labadie, and L. Lestel, eds. (Cham: Springer International Publishing), pp. 269–300.

Baker, J.M., Norman, J.M., and Bland, W.L. (1992). Field-scale appliction of flux measurement by conditional sampling. Agricultural and Forest Meteorology *62*, 31–52. https://doi.org/10.1016/0168-1923(92)90004-n.

Baker, M.A., Dahm, C.N., and Valett, H.M. (2000). Anoxia, Anaerobic Metabolism, and Biogeochemistry of the Stream-water–Ground-water Interface. In Streams and Ground Waters, J.B. Jones, and P.J. Mulholland, eds. (San Diego: Academic Press), pp. 259–283.

Baldocchi, D. (2014). Measuring fluxes of trace gases and energy between ecosystems and the atmosphere – the state and future of the eddy covariance method. Global Change Biology *20*, 3600–3609. https://doi.org/10.1111/gcb.12649.

Bartout, P., Touchart, L., Terasmaa, J., Choffel, Q., Marzecova, A., Koff, T., Kapanen, G., Qsair, Z., Maleval, V., Millot, C., et al. (2015). A new approach to inventorying bodies of water, from local to global scale. DIE ERDE – Journal of the Geographical Society of Berlin *146*, 245–258. https://doi.org/10.12854/erde-146-20.

Bauerfeind, S. (1985). Degradation of phytoplankton detritus by bacteria: estimation of bacterial consumption and respiration in an oxygen chamber. Marine Ecology Progress Series. Oldendorf *21*, 27–36. .

Berg, P., and Pace, M.L. (2017). Continuous measurement of air–water gas exchange by underwater eddy covariance. Biogeosciences *14*, 5595–5606. https://doi.org/10.5194/bg-14-5595-2017.

Berg, P., Røy, H., Janssen, F., Meyer, V., Jørgensen, B.B., Huettel, M., and de Beer, D. (2003). Oxygen uptake by aquatic sediments measured with a novel non-invasive eddy-correlation technique. Marine Ecology Progress Series *261*, 75–83. https://doi.org/Berg, P. , Røy, H. , Janssen, F. , Meyer, V. , Jørgensen, B. , Huettel, M. and de Beer, D. (2003) Oxygen uptake by aquatic sediments measured with a novel non-invasive eddy-correlation technique , Marine Ecology Progress Series, 261 , pp. 75-83 . doi:https://doi.org/10.3354/meps261075 <https://doi.org/10.3354/meps261075> , hdl:10013/epic.50540.

Berg, P., Long, M.H., Huettel, M., Rheuban, J.E., McGlathery, K.J., Howarth, R.W., Foreman, K.H., Giblin, A.E., and Marino, R. (2013). Eddy correlation measurements of oxygen fluxes in permeable sediments exposed to varying current flow and light. Limnology and Oceanography *58*, 1329–1343. https://doi.org/10.4319/lo.2013.58.4.1329.

Berg, P., Koopmans, D.J., Huettel, M., Li, H., Mori, K., and Wüest, A. (2016). A new robust oxygen-temperature sensor for aquatic eddy covariance measurements. Limnology and Oceanography: Methods *14*, 151–167. https://doi.org/10.1002/lom3.10071.

Berg, P., Delgard, M.L., Polsenaere, P., McGlathery, K.J., Doney, S.C., and Berger, A.C. (2019). Dynamics of benthic metabolism, O_2, and pCO_2 in a temperate seagrass meadow. Limnology and Oceanography *64*, 2586–2604. https://doi.org/10.1002/lno.11236.

Berg, P., Huettel, M., Glud, R.N., Reimers, C.E., and Attard, K.M. (2022). Aquatic Eddy Covariance: The Method and Its Contributions to Defining Oxygen and Carbon Fluxes in Marine Environments. Annual Review of Marine Science *14*, 431–455. https://doi.org/10.1146/annurev-marine-042121-012329.

Berg, P.E., Røy, H., and Wiberg, P.L. (2007). Eddy correlation flux measurements: The sediment surface area that contributes to the flux. Limnology and Oceanography *52 (4)*, 1672–1684. https://doi.org/10.4319/lo.2007.52.4.1672.

Berner, R.A. (1971). Principles of Chemical Sedimentology (McGraw-Hill).

Berner, R.A. (1980). Early Diagenesis: A Theoretical Approach (Princeton University Press).

Berry, D.W. (1950). Geological Survey Water-supply Paper (U.S. Government Printing Office).

Biggs, J., von Fumetti, S., and Kelly-Quinn, M. (2017). The importance of small waterbodies for biodiversity and ecosystem services: implications for policy makers. Hydrobiologia *793*. https://doi.org/10.1007/s10750-016-3007-0.

Billen, G., Garnier, J., and Silvestre, M. (2015). A simplified algorithm for calculating benthic nutrient fluxes in river systems. Annales de Limnologie - International Journal of Limnology *51*, 37. https://doi.org/10.1051/limn/2014030.

Bloesch, J. (2009). Sediments of Aquatic Ecosystems. In Encyclopedia of Inland Waters, G.E. Likens, ed. (Oxford: Academic Press), pp. 479–490.

Boehrer, B., and Schultze, M. (2008). Stratification of lakes. Reviews of Geophysics *46*. https://doi.org/10.1029/2006RG000210.

Bonhomme, C., Jézéquel, D., Poulin, M., Saad, M., Vinçon-Leite, B., and Tassin, B. (2016). Lake Pavin Mixing: New Insights from High Resolution Continuous Measurements. In Lake Pavin: History, Geology, Biogeochemistry, and Sedimentology of a Deep Meromictic Maar Lake, T. Sime-Ngando, P. Boivin, E. Chapron, D. Jezequel, and M. Meybeck, eds. (Cham: Springer International Publishing), pp. 177–184.

Boudreau, B.P. (1996). The diffusive tortuosity of fine-grained unlithified sediments. Geochimica et Cosmochimica Acta *60*, 3139–3142. https://doi.org/10.1016/0016-7037(96)00158-5.

Boudreau, B.P., and Jørgensen, B.B. (2001). The Benthic Boundary Layer: Transport Processes and Biogeochemistry (Oxford, New York: Oxford University Press).

Bowen, H.J.M. (1979). Environmental chemistry of the elements (London; New York: Academic Press).

Bowling, D.R., Turnipseed, A.A., Delany, A.C., Baldocchi, D.D., Greenberg, J.P., and Monson, R.K. (1998). The use of relaxed eddy accumulation to measure biosphere-atmosphere exchange of isoprene and other biological trace gases. Oecologia *116*, 306–315. https://doi.org/10.1007/s004420050592.

Brady, D.C., Testa, J.M., Di Toro, D.M., Boynton, W.R., and Kemp, W.M. (2013). Sediment flux modeling: Calibration and application for coastal systems. Estuarine, Coastal and Shelf Science *117*, 107–124. https://doi.org/10.1016/j.ecss.2012.11.003.

Broström, G., and Nilsson, J. (1999). A theoretical investigation of the diffusive boundary layer in benthic flux chamber experiments. Journal of Sea Research *42*, 179–189. https://doi.org/10.1016/S1385-1101(99)00031-3.

Bruins, J., Petrusevski, B., Slokar, Y., Kruithof, J., and Kennedy, M. (2014). Manganese removal from groundwater: Characterization of filter media coating. Desalination and Water Treatment *55*, 1–13. https://doi.org/10.1080/19443994.2014.927802.

Brune, A., Frenzel, P., and Cypionka, H. (2000). Life at the oxic–anoxic interface: microbial activities and adaptations. FEMS Microbiology Reviews *24*, 691–710. https://doi.org/10.1111/j.1574-6976.2000.tb00567.x.

Buchholtz-ten Brink, M.R., Gust, G., and Chavis, D. (1989). Calibration and performance of a stirred benthic chamber. Deep Sea Research Part A. Oceanographic Research Papers *36*, 1083–1101. https://doi.org/10.1016/0198-0149(89)90079-4.

Burba, G., and Anderson, D. (2010). A Brief Practical Guide to Eddy Covariance Flux Measurements: Principles and Workflow Examples for Scientific and Industrial Applications.

Businger, J.A. (1986). Evaluation of the Accuracy with Which Dry Deposition Can Be Measured with Current Micrometeorological Techniques. Journal of Applied Meteorology and Climatology *25*, 1100–1124. https://doi.org/10.1175/1520-0450(1986)025<1100:EOTAWW>2.0.CO;2.

Businger, J.A., and Oncley, S.P. (1990). Flux Measurement with Conditional Sampling. J. Atmos. Oceanic Technol. *7*, 349–352. https://doi.org/10.1175/1520-0426(1990)007<0349:FMWCS>2.0.CO;2.

Camara, M., Jamil, N.R., and Abdullah, A.F.B. (2019). Impact of land uses on water quality in Malaysia: a review. Ecological Processes *8*, 10. https://doi.org/10.1186/s13717-019-0164-x.

Canfield, D.E., Kristensen, E., and Thamdrup, B. (2005a). The Iron and Manganese Cycle. In Advances in Marine Biology, (Academic Press), pp. 269–312.

Canfield, D.E., Erik Kristensen, and Bo Thamdrup (2005b). The Sulfur Cycle. In Advances in Marine Biology, (Academic Press), pp. 313–381.

Cannon, D.J., and Troy, C.D. (2018). Observations of turbulence and mean flow in the low-energy hypolimnetic boundary layer of a large lake. Limnology and Oceanography *63*, 2762–2776. https://doi.org/10.1002/lno.11007.

Chen, X., Andersen, T.J., Morono, Y., Inagaki, F., Jørgensen, B.B., and Lever, M.A. (2017). Bioturbation as a key driver behind the dominance of Bacteria over Archaea in near-surface sediment. Sci Rep *7*, 2400. https://doi.org/10.1038/s41598-017-02295-x.

Chipman, L., Berg, P., and Huettel, M. (2016). Benthic Oxygen Fluxes Measured by Eddy Covariance in Permeable Gulf of Mexico Shallow-Water Sands. Aquatic Geochemistry *22*, 529–554. https://doi.org/10.1007/s10498-016-9305-3.

Cooksey, B., Cooksey, K., Miller, C.A., Paul, J., Rubin, R., and Webster, D.R. (1984). The Attachment of Microfouling Diatoms. p.

Dadi, T., Völkner, C., and Koschorreck, M. (2015). A sediment core incubation method to measure the flux of dissolved organic carbon between sediment and water. Journal of Soils and Sediments *15*. https://doi.org/10.1007/s11368-015-1213-4.

Dale, A.W., Sommer, S., Lichtschlag, A., Koopmans, D., Haeckel, M., Kossel, E., Deusner, C., Linke, P., Scholten, J., Wallmann, K., et al. (2021). Defining a biogeochemical baseline for sediments at Carbon Capture and Storage (CCS) sites: An example from the North Sea (Goldeneye). International Journal of Greenhouse Gas Control *106*, 103265. https://doi.org/10.1016/j.ijggc.2021.103265.

Dar, N., Pandit, A., and Ganai, B. (2014). Factors affecting the distribution patterns of aquatic macrophytes. Limnological Review *14*. https://doi.org/10.2478/limre-2014-0008.

D'Autilia, R., Falcucci, M., Hull, V., and Parrella, L. (2004). Short time dissolved oxygen dynamics in shallow water ecosystems. Ecological Modelling Volume 179, Issue 3, 30 November 2004, Pages 297-306 *179*, 297–306. https://doi.org/10.1016/j.ecolmodel.2004.02.009.

Davison, W. (1993). Iron and manganese in lakes. Earth-Science Reviews *34*, 119–163. https://doi.org/10.1016/0012-8252(93)90029-7.

Davison, W., Grime, G.W., Morgan, J.A.W., and Clarke, K. (1991). Distribution of dissolved iron in sediment pore waters at submillimetre resolution | Nature. Nature 323–325. .

Dawson, R.N., and Murphy, K.L. (1972). The temperature dependency of biological denitrification. Water Research *6*, 71–83. https://doi.org/10.1016/0043-1354(72)90174-1.

Dearmont, D., McCarl, B.A., and Tolman, D.A. (1998). Costs of water treatment due to diminished water quality: A case study in Texas. Water Resources Research *34*, 849–853. https://doi.org/10.1029/98WR00213.

Desjardins, R.L. (1977). Description and evaluation of a sensible heat flux detector. Boundary-Layer Meteorol *11*, 147–154. https://doi.org/10.1007/BF02166801.

Donis, D., Holtappels, M., Noss, C., Cathalot, C., Hancke, K., Polsenaere, P., Wenzhoefer, F., Lorke, A., Meysman, F.J.R., Glud, R.N., et al. (2015). An Assessment of the Precision and Confidence of Aquatic Eddy Correlation Measurements. p.

Donis, D., McGinnis, D.F., Holtappels, M., Felden, J., and Wenzhoefer, F. (2016). Assessing benthic oxygen fluxes in oligotrophic deep sea sediments (HAUSGARTEN observatory). Deep Sea Research Part I: Oceanographic Research Papers *111*, 1–10. https://doi.org/10.1016/j.dsr.2015.11.007.

Downing, J.A., Prairie, Y.T., Cole, J.J., Duarte, C.M., Tranvik, L.J., Striegl, R.G., McDowell, W.H., Kortelainen, P., Caraco, N.F., Melack, J.M., et al. (2006). The global abundance and size distribution of lakes, ponds, and impoundments. Limnology and Oceanography *51*, 2388–2397. https://doi.org/10.4319/lo.2006.51.5.2388.

Drews, G. (2000). The roots of microbiology and the influence of Ferdinand Cohn on microbiology of the 19th century. FEMS Microbiology Reviews *24*, 225–249. https://doi.org/10.1111/j.1574-6976.2000.tb00540.x.

Ebenstein, A. (2012). The Consequences of Industrialization: Evidence from Water Pollution and Digestive Cancers in China. The Review of Economics and Statistics *94*, 186–201. https://doi.org/10.1162/REST_a_00150.

Eriksson, P.G. (2001). Interaction Effects of Flow Velocity and Oxygen Metabolism on Nitrification and Denitrification in Biofilms on Submersed Macrophytes. Biogeochemistry *55*, 29–44. .

Faganeli, J., and Ogrinc, N. (2009). Oxic-anoxic transition of benthic fluxes from the coastal marine environment (Gulf of Trieste, northern Adriatic Sea). Marine and Freshwater Research - MAR FRESHWATER RES *60*. https://doi.org/10.1071/MF08065.

Foken, T. (2008). Micrometeorology (Berlin Heidelberg: Springer-Verlag).

Forja, J.M., and Gómez-Parra, A. (1998). Measuring nutrient fluxes across the sediment-water interface using benthic chambers. Marine Ecology Progress Series *164*, 95–105. https://doi.org/10.3354/meps164095.

Froelich, P.N., Klinkhammer, G.P., Bender, M.L., Luedtke, N.A., Heath, G.R., Cullen, D., Dauphin, P., Hammond, D., Hartman, B., and Maynard, V. (1979). Early oxidation of organic matter in pelagic sediments of the eastern equatorial Atlantic: suboxic diagenesis. Geochimica et Cosmochimica Acta *43*, 1075–1090. https://doi.org/10.1016/0016-7037(79)90095-4.

Gächter, R., and Meyer, J. (1993). The role of microorganisms in mobilization and fixation of phosphorus in sediments | SpringerLink.

Gallagher, J., and Daiber, F. (1974). Oxygen consumption at the soil-water interface in a Delaware salt marsh. Chesapeake Science *15*, 248–250. https://doi.org/10.2307/1350979.

Giles, C.D., Isles, P.D.F., Manley, T., Xu, Y., Druschel, G.K., and Schroth, A.W. (2016). The mobility of phosphorus, iron, and manganese through the sediment–water continuum of a shallow eutrophic freshwater lake under stratified and mixed water-column conditions. Biogeochemistry *127*, 15–34. https://doi.org/10.1007/s10533-015-0144-x.

Golterman, H.L. (1975). Stratification in Deep Lakes. In Developments in Water Science, (Elsevier), pp. 145–173.

Gomez, E., Fillit, M., Ximenes, M., and Picot, B. (1998). Phosphate mobility at the sediment–water interface of a Mediterranean lagoon (etang du Méjean), seasonal phosphate variation. Hydrobiologia *373/374*, 203. https://doi.org/10.1023/A:1017092226396.

Goring, D.G., and Nikora, V.I. (2002). Despiking Acoustic Doppler Velocimeter Data. Journal of Hydraulic Engineering *128*, 117–126. https://doi.org/10.1061/(ASCE)0733-9429(2002)128:1(117).

Graf, W.H., and Mortimer, C.H. (1979). Hydrodynamics of Lakes (Elsevier).

Grelle, A., and Keck, H. (2021). Affordable relaxed eddy accumulation system to measure fluxes of H2O, CO2, CH4 and N2O from ecosystems. Agricultural and Forest Meteorology *307*, 108514. https://doi.org/10.1016/j.agrformet.2021.108514.

Grenz, C., Moutin, T., Picot, B., and Massé, H. (1991). Comparaison de deux méthodes de mesure de flux de nutriments à l'interface eau-sédiment:méthode des peepers et méthode des chambres benthiques. Comptes Rendus de l'Académie Des Sciences. Série III, Sciences de La Vie *313*, 239–244. .

Grüneberg, B., Dadi, T., Lindim, C., and Fischer, H. (2015). Effects of nitrogen and phosphorus load reduction on benthic phosphorus release in a riverine lake. Biogeochemistry *123*, 185–202. https://doi.org/10.1007/s10533-014-0062-3.

Guérin, F., Deshmukh, C., Labat, D., Pighini, S., Vongkhamsao, A., Guédant, P., Rode, W., Godon, A., Chanudet, V., Descloux, S., et al. (2016). Effect of sporadic destratification, seasonal overturn, and artificial mixing on CH_4 emissions from a subtropical hydroelectric reservoir. Biogeosciences *13*, 3647–3663. https://doi.org/10.5194/bg-13-3647-2016.

Guo, P. (2012). Dependency of Tortuosity and Permeability of Porous Media on Directional Distribution of Pore Voids. Transp Porous Med *95*, 285–303. https://doi.org/10.1007/s11242-012-0043-8.

Guo, H., Liu, H., Lyu, H., Bian, Y., Zhong, S., Li, Y., Miao, S., Yang, Z., Xu, J., Cao, J., et al. (2022). Is there any difference on cyanobacterial blooms patterns between Lake Chaohu and Lake Taihu over the last 20 years? Environ Sci Pollut Res https://doi.org/10.1007/s11356-021-18094-x.

Guseva, S., Aurela, M., Cortés, A., Kivi, R., Lotsari, E., MacIntyre, S., Mammarella, I., Ojala, A., Stepanenko, V., Uotila, P., et al. (2021). Variable Physical Drivers of Near-Surface Turbulence in a Regulated River. Water Resources Research *57*, e2020WR027939. https://doi.org/10.1029/2020WR027939.

Hammond, D.E., Cummins, K.M., McManus, J., Berelson, W.M., Smith, G., and Spagnoli, F. (2004). Methods for measuring benthic nutrient flux on the California Margin: Comparing shipboard core incubations to in situ lander results. Limnology and Oceanography: Methods *2*, 146–159. https://doi.org/10.4319/lom.2004.2.146.

Hargrave, B.T. (1969). Similarity of Oxygen Uptake by Benthic Communities1. Limnology and Oceanography *14*, 801–805. https://doi.org/10.4319/lo.1969.14.5.0801.

Henrichs, S.M. (1992). Early diagenesis of organic matter in marine sediments: progress and perplexity. Marine Chemistry *39*, 119–149. https://doi.org/10.1016/0304-4203(92)90098-U.

Hensen, C., Landenberger, H., Zabel, M., and Schulz, H.D. (1998). Quantification of diffusive benthic fluxes of nitrate, phosphate, and silicate in the southern Atlantic Ocean. Global Biogeochemical Cycles *12*, 193–210. https://doi.org/10.1029/97GB02731.

Hesslein, R.H. (1976). An in situ sampler for close interval pore water studies1. Limnology and Oceanography *21*, 912–914. https://doi.org/10.4319/lo.1976.21.6.0912.

von der Heyden, L., Wißdorf, W., Kurtenbach, R., and Kleffmann, J. (2021). A Relaxed Eddy Accumulation (REA) LOPAP-System for Flux Measurements of Nitrous Acid (HONO). Atmospheric Measurement Techniques Discussions 1–23. https://doi.org/10.5194/amt-2021-408.

Hicks, B., and McMillen, R. (1984). A Simulation of the Eddy Accumulation Method for Measuring Pollutant Fluxes. Journal of Applied Meteorology *23*, 637–643. https://doi.org/10.1175/1520-0450(1984)023<0637:ASOTEA>2.0.CO;2.

Hofmann, H., Lorke, A., and Peeters, F. (2011). Wind and ship wave-induced resuspension in the littoral zone of a large lake. Water Resources Research *47*. https://doi.org/10.1029/2010WR010012.

Holley, E.R. (1977). Oxygen Transfer at the Air-Water Interface. In Transport Processes in Lakes and Oceans, R.J. Gibbs, and R.P. Shaw, eds. (Boston, MA: Springer US), pp. 117–150.

Holmer, M., and Storkholm, P. (2001). Sulphate reduction and sulphur cycling in lake sediments: a review. Freshwater Biology *46*, 431–451. https://doi.org/10.1046/j.1365-2427.2001.00687.x.

Huang, J., Franklin, H., Teasdale, P.R., Burford, M.A., Kankanamge, N.R., Bennett, W.W., and Welsh, D.T. (2019). Comparison of DET, DGT and conventional porewater extractions for determining nutrient profiles and cycling in stream sediments. Environ. Sci.: Processes Impacts *21*, 2128–2140. https://doi.org/10.1039/C9EM00312F.

Huettel, M., Berg, P., and Merikhi, A. (2020). Technical note: Measurements and data analysis of sediment–water oxygen flux using a new dual-optode eddy covariance instrument. Biogeosciences *17*, 4459–4476. https://doi.org/10.5194/bg-17-4459-2020.

Idso, S.B. (1973). On the concept of lake stability. Limnology and Oceanography *18*, 681–683. https://doi.org/10.4319/lo.1973.18.4.0681.

Jacobsen, O. (1978). SORPTION, ADSORPTION AND CHEMOSORPTI.ON OF PHOSPHATE BY DANISH LAKE SEDIMENTS I.

Jensen, H.S., Kristensen, P., Jeppesen, E., and Skytthe, A. (1992). Iron:phosphorus ratio in surface sediment as an indicator of phosphate release from aerobic sediments in shallow lakes. Hydrobiologia *235*, 731–743. https://doi.org/10.1007/BF00026261.

Jézéquel, D., Brayner, R., Metzger, E., Viollier, E., Prévot, F., and Fiévet, F. (2007). Two-dimensional determination of dissolved iron and sulfur species in marine sediment pore-waters by thin-film based imaging. Thau lagoon (France). Estuarine, Coastal and Shelf Science *72*, 420–431. https://doi.org/10.1016/j.ecss.2006.11.031.

Jézéquel, D., Michard, G., Viollier, E., Agrinier, P., Albéric, P., Lopes, F., Abril, G., and Bergonzini, L. (2016). Carbon Cycle in a Meromictic Crater Lake: Lake Pavin, France. In Lake Pavin: History, Geology, Biogeochemistry, and Sedimentology of a Deep Meromictic Maar Lake, T. Sime-Ngando, P. Boivin, E. Chapron, D. Jezequel, and M. Meybeck, eds. (Cham: Springer International Publishing), pp. 185–203.

Jia, T., Zhang, X., and Dong, R. (2019). Long-Term Spatial and Temporal Monitoring of Cyanobacteria Blooms Using MODIS on Google Earth Engine: A Case Study in Taihu Lake. Remote Sensing *11*, 2269. https://doi.org/10.3390/rs11192269.

Johnson, K.S., Barry, J.P., Coletti, L.J., Fitzwater, S.E., Jannasch, H.W., and Lovera, C.F. (2011). Nitrate and oxygen flux across the sediment-water interface observed by eddy correlation measurements on the open continental shelf. Limnology and Oceanography: Methods *9*, 543–553. https://doi.org/10.4319/lom.2011.9.543.

Jørgensen, B.B. (1982). Mineralization of organic matter in the sea bed—the role of sulphate reduction. Nature *296*, 643–645. https://doi.org/10.1038/296643a0.

Jørgensen, B., and Kasten, S. (2006). Sulfur Cycling and Methane Oxidation. In Marine Geochemistry, pp. 271–309.

Jørgensen, B.B., and Revsbech, N.P. (1985). Diffusive boundary layers and the oxygen uptake of sediments and detritus1. Limnology and Oceanography *30*, 111–122. https://doi.org/10.4319/lo.1985.30.1.0111.

Jørgensen, B.B., Findlay, A.J., and Pellerin, A. (2019). The Biogeochemical Sulfur Cycle of Marine Sediments. Frontiers in Microbiology *10*. .

Kaimal, J.C., and Finnigan, J.J. (1994). Atmospheric Boundary Layer Flows: Their Structure and Measurement (Oxford University Press).

Kaimal, J.C., Wyngaard, J.C., Izumi, Y., and Coté, O.R. (1972). Spectral characteristics of surface-layer turbulence. Quarterly Journal of the Royal Meteorological Society *98*, 563–589. https://doi.org/10.1002/qj.49709841707.

King, J.N. (2011). 9.16 - Analytical Characterization of Selective Benthic Flux Components in Estuarine and Coastal Waters*. In Treatise on Estuarine and Coastal Science, E. Wolanski, and D. McLusky, eds. (Waltham: Academic Press), pp. 397–423.

Koca, K., Noss, C., Anlanger, C., Brand, A., and Lorke, A. (2017). Performance of the Vectrino Profiler at the sediment–water interface. Journal of Hydraulic Research *55*, 573–581. https://doi.org/10.1080/00221686.2016.1275049.

König, I., Drodt, M., Suess, E., and Trautwein, A.X. (1997). Iron reduction through the tangreen transition in deep-sea sediments. Geochimica et Cosmochimica Acta *61*, 1679–1683. https://doi.org/10.1016/S0016-7037(97)00007-0.

Koopmans, D.J., and Berg, P. (2015). Stream oxygen flux and metabolism determined with the open water and aquatic eddy covariance techniques. Limnology and Oceanography *60*, 1344–1355. https://doi.org/10.1002/lno.10103.

Kostka, J.E., Luther, G.W., and Nealson, K.H. (1995). Chemical and biological reduction of Mn (III)-pyrophosphate complexes: Potential importance of dissolved Mn (III) as an environmental oxidant. Geochimica et Cosmochimica Acta *59*, 885–894. https://doi.org/10.1016/0016-7037(95)00007-0.

Kouakou, C.R.C., and Poder, T.G. (2019). Economic impact of harmful algal blooms on human health: a systematic review. J Water Health *17*, 499–516. https://doi.org/10.2166/wh.2019.064.

Kristensen, E., Penha-Lopes, G., Delefosse, M., Valdemarsen, T., Organo Quintana, C., and Banta, G. (2012). What is bioturbation? Need for a precise definition for fauna in aquatic science. Marine Ecology Progress Series *446*, 285–302. https://doi.org/10.3354/meps09506.

Krom, M.D., Davison, P., Zhang, H., and Davison, W. (1994). High-resolution pore-water sampling with a gel sampler. Limnology and Oceanography *39*, 1967–1972. https://doi.org/10.4319/lo.1994.39.8.1967.

Lemaire, B.J., Noss, C., and Lorke, A. (2017). Toward relaxed eddy accumulation measurements of sediment-water exchange in aquatic ecosystems: Aquatic Relaxed Eddy Accumulation. Geophysical Research Letters *44*, 8901–8909. https://doi.org/10.1002/2017GL074625.

Lewerentz, A., Hoffmann, M., and Sarmento Cabral, J. (2021). Depth diversity gradients of macrophytes: Shape, drivers, and recent shifts. Ecology and Evolution *11*, 13830–13845. https://doi.org/10.1002/ece3.8089.

Li, M., Yu, R., Cao, Z., Jin, Y., Sun, H., and Qi, Z. (2021). Analysis of optimal environmental conditions for Microcystis blooms in large, shallow, eutrophic lakes. All Life *14*, 340–354. https://doi.org/10.1080/26895293.2021.1919569.

Li, Y., Huang, D., Sun, W., Sun, X., Yan, G., Gao, W., and Lin, H. (2022). Characterizing sediment bacterial community and identifying the biological indicators in a seawater-freshwater transition zone during the wet and dry seasons. Environ Sci Pollut Res https://doi.org/10.1007/s11356-021-18053-6.

Long, M.H., Charette, M.A., Martin, W.R., and McCorkle, D.C. (2015). Oxygen metabolism and pH in coastal ecosystems: Eddy Covariance Hydrogen ion and Oxygen Exchange System (ECHOES). Limnology and Oceanography: Methods *13*, 438–450. https://doi.org/10.1002/lom3.10038.

Lorke, A., and Macintyre, S. (2009). The Benthic Boundary Layer (in Rivers, Lakes, and Reservoirs). In Encyclopedia of Inland Waters, pp. 505–514.

Lorke, A., and Peeters, F. (2006). Toward a Unified Scaling Relation for Interfacial Fluxes. J. Phys. Oceanogr. *36*, 955–961. https://doi.org/10.1175/JPO2903.1.

Lorke, A., McGinnis, D.F., and Maeck, A. (2013). Eddy-correlation measurements of benthic fluxes under complex flow conditions: Effects of coordinate transformations and averaging time scales. Limnology and Oceanography: Methods *11*, 425–437. https://doi.org/10.4319/lom.2013.11.425.

Lorke, A., Bodmer, P., Koca, K., and Noss, C. (2019). Hydrodynamic control of gas-exchange velocity in small streams.

Lorrai, C., McGinnis, D.F., Berg, P., Brand, A., and Wüest, A. (2010). Application of Oxygen Eddy Correlation in Aquatic Systems. J. Atmos. Oceanic Technol. *27*, 1533–1546. https://doi.org/10.1175/2010JTECHO723.1.

Lyons, W.B., Loder, T.C., and Murray, S.M. (1982). Nutrient Pore Water Chemistry, Great Bay, New Hampshire: Benthic Fluxes. Estuaries *5*, 230–233. https://doi.org/10.2307/1351840.

Martinsen, K.T., Andersen, M.R., and Sand-Jensen, K. (2019). Water temperature dynamics and the prevalence of daytime stratification in small temperate shallow lakes. Hydrobiologia *826*, 247–262. https://doi.org/10.1007/s10750-018-3737-2.

Mateo-Sagasta, J., Marjani, S., and Turral, H. (2017). Water pollution from Agriculture: a global review. Executive summary.

Mayer, M., Schaffner, L., and Kemp, W. (1995). Nitrification potentials of benthic macrofaunal tubes and burrow walls: Effects of sediment NH4+ and animal irrigation behavior. Marine Ecology Progress Series *121*, 157–169. https://doi.org/10.3354/meps121157.

McGinnis, D.F., Berg, P., Brand, A., Lorrai, C., Edmonds, T.J., and Wüest, A. (2008). Measurements of eddy correlation oxygen fluxes in shallow freshwaters: Towards routine applications and analysis. Geophysical Research Letters *35*. https://doi.org/10.1029/2007GL032747.

McManus, J., Heinen, E.A., and Baehr, M.M. (2003). Hypolimnetic oxidation rates in Lake Superior: Role of dissolved organic material on the lake's carbon budget. Limnology and Oceanography *48*, 1624–1632. https://doi.org/10.4319/lo.2003.48.4.1624.

Mendonça, R., Müller, R.A., Clow, D., Verpoorter, C., Raymond, P., Tranvik, L.J., and Sobek, S. (2017). Organic carbon burial in global lakes and reservoirs. Nat Commun *8*, 1694. https://doi.org/10.1038/s41467-017-01789-6.

Meyers, P.A., and Teranes, J.L. (2001). Sediment Organic Matter. In Tracking Environmental Change Using Lake Sediments: Physical and Geochemical Methods, W.M. Last, and J.P. Smol, eds. (Dordrecht: Springer Netherlands), pp. 239–269.

Murniati, E., Geissler, S., and Lorke, A. (2015). Short-term and seasonal variability of oxygen fluxes at the sediment–water interface in a riverine lake. Aquatic Sciences *77*, 183–196. https://doi.org/10.1007/s00027-014-0362-7.

Nealson, K.H., and Saffarini, D. (1994). Iron and manganese in anaerobic respiration: environmental significance, physiology, and regulation. Annu Rev Microbiol *48*, 311–343. https://doi.org/10.1146/annurev.mi.48.100194.001523.

Ni, Z., Wang, S., Chu, Z., and Jin, X. (2015). Historical accumulation of N and P and sources of organic matter and N in sediment in an agricultural reservoir in Northern China. Environmental Science and Pollution Research International *22*. https://doi.org/10.1007/s11356-015-4169-4.

Nõges, P., Tuvikene, L., Nõges, T., and Kisand, A. (1999). Primary production, sedimentation and resuspension in large shallow Lake Võrtsjärv. Aquat. Sci. *61*, 168–182. https://doi.org/10.1007/PL00001323.

Nøhr Glud, R., Gundersen, J.K., Barker Jørgensen, B., Revsbech, N.P., and Schulz, H.D. (1994). Diffusive and total oxygen uptake of deep-sea sediments in the eastern South Atlantic Ocean:in situ and laboratory measurements. Deep Sea Research Part I: Oceanographic Research Papers *41*, 1767–1788. https://doi.org/10.1016/0967-0637(94)90072-8.

Norling, P., and Kautsky, N. (2007). Structural and functional effects of Mytilus edulis on diversity of associated species and ecosystem functioning. Marine Ecology Progress Series *351*, 163–175. https://doi.org/10.3354/meps07033.

Noss, C., Salzmann, T., and Storchenegger, I. (2010). Turbulent and advective momentum fluxes in streams. Water Resources Research - WATER RESOUR RES *46*. https://doi.org/10.1029/2010WR009297.

Odum, H.T. (1957). Trophic Structure and Productivity of Silver Springs, Florida. Ecological Monographs *27*, 55–112. .

Oncley, S.P., Delany, A.C., Horst, T.W., and Tans, P.P. (1993). Verification of flux measurement using relaxed eddy accumulation. Atmospheric Environment. Part A. General Topics *27*, 2417–2426. https://doi.org/10.1016/0960-1686(93)90409-R.

Pattey, E., Desjardins, R.L., and Rochette, P. (1993). Accuracy of the relaxed eddy-accumulation technique, evaluated using CO2 flux measurements. Boundary-Layer Meteorol *66*, 341–355. https://doi.org/10.1007/BF00712728.

Pauer, J.J., and Auer, M.T. (2000). Nitrification in the water column and sediment of a hypereutrophic lake and adjoining river system. Water Research *34*, 1247–1254. https://doi.org/10.1016/S0043-1354(99)00258-4.

Peleg, M. (1996). A model of microbial growth and decay in a closed habitat based on combined Fermi's and the logistic equations. Journal of the Science of Food and Agriculture *71*, 225–230. https://doi.org/10.1002/(sici)1097-0010(199606)71:2<225::aid-jsfa572>3.0.co;2-#.

Pepper, I.L., Gerba, C.P., Gentry, T.J., and Maier, R.M. (2011). Environmental Microbiology (Academic Press).

Phillips, G.L. (2004). Eutrophication of Shallow Temperate Lakes. In The Lakes Handbook, (John Wiley & Sons, Ltd), pp. 261–278.

Piccioni, F., Casenave, C., Lemaire, B.J., Le Moigne, P., Dubois, P., and Vinçon-Leite, B. (2021). The thermal response of small and shallow lakes to climate change: new insights from 3D hindcast modelling. Earth System Dynamics *12*, 439–456. https://doi.org/10.5194/esd-12-439-2021.

Polsenaere, P., Deflandre, B., Thouzeau, G., Rigaud, S., Cox, T., Amice, E., Bec, T.L., Bihannic, I., and Maire, O. (2021). Comparison of benthic oxygen exchange measured by aquatic Eddy Covariance and Benthic Chambers in two contrasting coastal biotopes (Bay of Brest, France). Regional Studies in Marine Science *43*, 101668. https://doi.org/10.1016/j.rsma.2021.101668.

Price, J.I., and Heberling, M.T. (2018). The Effects of Source Water Quality on Drinking Water Treatment Costs: A Review and Synthesis of Empirical Literature. Ecol Econ *151*, 195–209. https://doi.org/10.1016/j.ecolecon.2018.04.014.

Prieto, D., Devesa-Rey, R., Rubinos, D., Díaz-Fierros, F., and Barral, M.T. (2016). Biofilm Formation on River Sediments Under Different Light Intensities and Nutrient Inputs: A Flume Mesocosm Study. Environmental Engineering Science *33*. https://doi.org/10.1089/ees.2015.0427.

Quintana, C.O., Tang, M., and Kristensen, E. (2007). Simultaneous study of particle reworking, irrigation transport and reaction rates in sediment bioturbated by the polychaetes Heteromastus and Marenzelleria. Journal of Experimental Marine Biology and Ecology *352*, 392–406. https://doi.org/10.1016/j.jembe.2007.08.015.

Rajwa-Kuligiewicz, A., Bialik, R.J., and Rowiński, P.M. (2015). Dissolved oxygen and water temperature dynamics in lowland rivers over various timescales. Journal of Hydrology and Hydromechanics *63*, 353–363. https://doi.org/10.1515/johh-2015-0041.

Rast, W., and Thornton, J. (2007). The Phosphorus Loading Concept and the Oecd Eutrophication Programme: Origin, Application and Capabilities. In The Lakes Handbook, pp. 354–385.

Reitzel, K., Ahlgren, J., Rydin, E., Egemose, S., Turner, B., and Hupfer, M. (2012). Diagenesis of settling seston: Identity and transformations of organic phosphorus. Journal of Environmental Monitoring : JEM *14*, 1098–1106. https://doi.org/10.1039/c2em10883f.

Rheuban, J.E., and Berg, P. (2013). The effects of spatial and temporal variability at the sediment surface on aquatic eddy correlation flux measurements: Areal/time variance on eddy correlation. Limnology and Oceanography: Methods *11*, 351–359. https://doi.org/10.4319/lom.2013.11.351.

Rhoads, D. (1974). Organism-sediment relations on the muddy sea floor. Undefined.

Richards, K.S. (2004). Rivers: Form and Process in Alluvial Channels (Blackburn Press).

Robson, B.J. (2014). State of the art in modelling of phosphorus in aquatic systems: Review, criticisms and commentary. Environmental Modelling & Software *61*, 339–359. https://doi.org/10.1016/j.envsoft.2014.01.012.

Rodil, I., Attard, K., Norkko, J., Glud, R., and Norkko, A. (2019). Towards a sampling design for characterizing habitat-specific benthic biodiversity related to oxygen flux dynamics using Aquatic Eddy Covariance. PLOS ONE *14*, e0211673. https://doi.org/10.1371/journal.pone.0211673.

Romero, E., Le Gendre, R., Garnier, J., Billen, G., Fisson, C., Silvestre, M., and Riou, P. (2016). Long-term water quality in the lower Seine: Lessons learned over 4 decades of monitoring. Environmental Science & Policy *58*, 141–154. https://doi.org/10.1016/j.envsci.2016.01.016.

Roth, F., Wild, C., Carvalho, S., Rädecker, N., Voolstra, C.R., Kürten, B., Anlauf, H., El-Khaled, Y.C., Carolan, R., and Jones, B.H. (2019). An in situ approach for measuring biogeochemical fluxes in

structurally complex benthic communities. Methods in Ecology and Evolution *10*, 712–725. https://doi.org/10.1111/2041-210X.13151.

Ruiz-Fernández, A.C., Hillaire-Marcel, C., Ghaleb, B., Soto-Jiménez, M., and Páez-Osuna, F. (2002). Recent sedimentary history of anthropogenic impacts on the Culiacan River Estuary, northwestern Mexico: geochemical evidence from organic matter and nutrients. Environ Pollut *118*, 365–377. https://doi.org/10.1016/s0269-7491(01)00287-1.

Sander, R. (2015). Compilation of Henry's law constants (version 4.0) for water as solvent. Atmospheric Chemistry and Physics *15*, 4399–4981. https://doi.org/10.5194/acp-15-4399-2015.

Sarkar, C., Turnipseed, A., Shertz, S., Karl, T., Potosnak, M., Bai, J., Serça, D., Bonal, D., Burban, B., Lopes, P.R.C., et al. (2020). A portable, low-cost relaxed eddy accumulation (REA) system for quantifying ecosystem-level fluxes of volatile organics. Atmospheric Environment *242*, 117764. https://doi.org/10.1016/j.atmosenv.2020.117764.

Sas, H. (1990). Lake restoration by reduction of nutrient loading: Expectations, experiences, extrapolations. SIL Proceedings, 1922-2010 *24*, 247–251. https://doi.org/10.1080/03680770.1989.11898731.

Schieber, J. (2011). Iron Sulfide Formation. In Encyclopedia of Geobiology, J. Reitner, and V. Thiel, eds. (Dordrecht: Springer Netherlands), pp. 486–502.

Seitaj, D., Sulu-Gambari, F., Burdorf, L.D.W., Romero-Ramirez, A., Maire, O., Malkin, S.Y., Slomp, C.P., and Meysman, F.J.R. (2017). Sedimentary oxygen dynamics in a seasonally hypoxic basin. Limnology and Oceanography *62*, 452–473. https://doi.org/10.1002/lno.10434.

Seitzinger, S., Harrison, J.A., Böhlke, J.K., Bouwman, A.F., Lowrance, R., Peterson, B., Tobias, C., and Drecht, G.V. (2006). Denitrification Across Landscapes and Waterscapes: A Synthesis. Ecological Applications *16*, 2064–2090. https://doi.org/10.1890/1051-0761(2006)016[2064:DALAWA]2.0.CO;2.

Serra, T., Oldham, C., and Colomer, J. (2018). Local hydrodynamics at edges of marine canopies under oscillatory flows. PLOS ONE *13*, e0201737. https://doi.org/10.1371/journal.pone.0201737.

Shaw, D.A., and Hanratty, T.J. (1977). Turbulent mass transfer rates to a wall for large Schmidt numbers. AIChE Journal *23*, 28–37. https://doi.org/10.1002/aic.690230106.

Shields, A. (1936). Application of similarity principles and turbulence research to bed-load movement (Pasadena, CA: California Institute of Technology).

Smith, S.A., and Bella, D.A. (1973). Dissolved Oxygen and Temperature in a Stratified Lake. Journal (Water Pollution Control Federation) *45*, 119–133. .

Smith, K.L., White, G.A., and Laver, M.B. (1979). Oxygen uptake and nutrient exchange of sediments measured in situ using a free vehicle grab respirometer. Deep Sea Research Part A. Oceanographic Research Papers *26*, 337–346. https://doi.org/10.1016/0198-0149(79)90030-X.

Søndergaard, M. (2007). Nutrient dynamics in lakes - with emphasis on phosphorus, sediment and lake restoration - Research - Aarhus University.

Søndergaard, M., Jensen, J.P., and Jeppesen, E. (2003). Role of sediment and internal loading of phosphorus in shallow lakes. Hydrobiologia *506*, 135–145. https://doi.org/10.1023/B:HYDR.0000008611.12704.dd.

Stone, M., and Droppo, I.G. (1994). In-channel surficial fine-grained sediment laminae. Part II: Chemical characteristics and implications for contaminant transport in fluvial systems. Hydrological Processes *8*, 113–124. https://doi.org/10.1002/hyp.3360080203.

Stoodley, P., Sauer, K., Davies, D.G., and Costerton, J.W. (2002). Biofilms as complex differentiated communities. Annu Rev Microbiol *56*, 187–209. https://doi.org/10.1146/annurev.micro.56.012302.160705.

Straub, K.L., Benz, M., Schink, B., and Widdel, F. (1996). Anaerobic, nitrate-dependent microbial oxidation of ferrous iron. Applied and Environmental Microbiology https://doi.org/10.1128/aem.62.4.1458-1460.1996.

Stull, R.B. (1988). Turbulence Kinetic Energy, Stability and Scaling. In An Introduction to Boundary Layer Meteorology, R.B. Stull, ed. (Dordrecht: Springer Netherlands), pp. 151–195.

Stumm, W., and Lee, G. (1960). The chemistry of aqueous iron. Aquatic Sciences *22*, 295–319. https://doi.org/10.1007/BF02503278.

Stumm, W., and Morgan, J.J. (1981). AQUATIC CHEMISTRY - AN INTRODUCTION EMPHASIZING CHEMICAL EQUILIBRIA IN NATURAL WATERS (WILEY-INTERSCIENCE. NEW-YORK - ETATS-UNIS).

Stutter, M., Richards, S., Ibiyemi, A., and Watson, H. (2021). Spatial representation of in-stream sediment phosphorus release combining channel network approaches and in-situ experiments. Science of The Total Environment *795*, 148790. https://doi.org/10.1016/j.scitotenv.2021.148790.

Sukhodolov, A.N., and Sukhodolova, T.A. (2010). Case Study: Effect of Submerged Aquatic Plants on Turbulence Structure in a Lowland River. Journal of Hydraulic Engineering *136*, 434–446. https://doi.org/10.1061/(ASCE)HY.1943-7900.0000195.

Sukhodolov, A.N., Kozerski, H.-P., and Rhoads, B.L. (2009). Currents in Rivers. In Encyclopedia of Inland Waters, G.E. Likens, ed. (Oxford: Academic Press), pp. 522–529.

Syers, J.K., Harris, R.F., and Armstrong, D.E. (1973). Phosphate Chemistry in Lake Sediments. Journal of Environmental Quality *2*, 1–14. https://doi.org/10.2134/jeq1973.00472425000200010001x.

Tang, X., Xie, G., Shao, K., Sai·Bayartu, Chen, Y., and Gao, G. (2012). Influence of Salinity on the Bacterial Community Composition in Lake Bosten, a Large Oligosaline Lake in Arid Northwestern China. Applied and Environmental Microbiology https://doi.org/10.1128/AEM.07806-11.

Tengberg, A., Stahl, H., Gust, G., Müller, V., Arning, U., Andersson, H., and Hall, P.O.J. (2004). Intercalibration of benthic flux chambers I. Accuracy of flux measurements and influence of chamber hydrodynamics. Progress in Oceanography *60*, 1–28. https://doi.org/10.1016/j.pocean.2003.12.001.

Tengberg, A., Hall, P.O.J., Andersson, U., Lindén, B., Styrenius, O., Boland, G., de Bovee, F., Carlsson, B., Ceradini, S., Devol, A., et al. (2005). Intercalibration of benthic flux chambers: II. Hydrodynamic characterization and flux comparisons of 14 different designs. Marine Chemistry *94*, 147–173. https://doi.org/10.1016/j.marchem.2004.07.014.

Thamdrup, B. (2000). Bacterial Manganese and Iron Reduction in Aquatic Sediments. In Advances in Microbial Ecology, B. Schink, ed. (Boston, MA: Springer US), pp. 41–84.

Thomann, R.V., and Mueller, J.A. (1987). Principles of surface water quality modeling and control (New York: Harper & Row).

Thoms, M. (1987). Channel sedimentation within the urbanized River Tame, U.K. Regulated Rivers: Research & Management *1*, 229–246. https://doi.org/10.1002/rrr.3450010304.

Thomsen, U., Thamdrup, B., Stahl, D.A., and Canfield, D.E. (2004). Pathways of organic carbon oxidation in a deep lacustrine sediment, Lake Michigan. Limnology and Oceanography *49*, 2046–2057. https://doi.org/10.4319/lo.2004.49.6.2046.

Thorbergsdóttir, I., Gislason, S., Ingvason, H., and Einarsson, Á. (2004). Benthic oxygen flux in the highly productive subarctic Lake Myvatn, Iceland: In situ benthic flux chamber study. Aquatic Ecology *38*, 177–189. https://doi.org/10.1023/B:AECO.0000032057.95464.ad.

Tran Khac, V., Hong, Y., Plec, D., Lemaire, B.J., Dubois, P., Saad, M., and Vinçon-Leite, B. (2018). An Automatic Monitoring System for High-Frequency Measuring and Real-Time Management of Cyanobacterial Blooms in Urban Water Bodies. Processes *6*, 11. https://doi.org/10.3390/pr6020011.

Tšertova, N., Kisand, A., Tammert, H., and Kisand, V. (2011). Low seasonal variability in community composition of sediment bacteria in large and shallow lake. Environmental Microbiology Reports *3*, 270–277. https://doi.org/10.1111/j.1758-2229.2010.00221.x.

Ullman, W.J., and Aller, R.C. (1982). Diffusion coefficients in nearshore marine sediments1. Limnology and Oceanography *27*, 552–556. https://doi.org/10.4319/lo.1982.27.3.0552.

Vanderborght, J., Wollats, R., and Billen, G. (1977). Kinetic models of diagenesis in disturbed sediments. Part 2. Nitrogen diagenesis. Limnology and Oceanography *22*. .

Verpoorter, C., Kutser, T., Seekell, D.A., and Tranvik, L.J. (2014). A global inventory of lakes based on high-resolution satellite imagery. Geophysical Research Letters *41*, 6396–6402. https://doi.org/10.1002/2014GL060641.

Viana, P., Yin, K., and Rockne, K. (2018). Comparison of direct benthic flux to ebullition-facilitated flux of polycyclic aromatic hydrocarbons and heavy metals measured in the field. J Soils Sediments *18*, 1729–1742. https://doi.org/10.1007/s11368-017-1893-z.

Vinçon-Leite, B., and Tassin, B. (1990). Deep lakes water quality modelling: Thermal and biogeochemical model of Lake Bourget (France). La Houille Blanche *76*, 231–236. https://doi.org/10.1051/lhb/1990016.

Viollier, E., Rabouille, C., Apitz, S.E., Breuer, E., Chaillou, G., Dedieu, K., Furukawa, Y., Grenz, C., Hall, P., Janssen, F., et al. (2003). Benthic biogeochemistry: state of the art technologies and guidelines for the future of in situ survey. Journal of Experimental Marine Biology and Ecology *285–286*, 5–31. https://doi.org/10.1016/S0022-0981(02)00517-8.

Vitre, R.R.D., and Davison, W. (1993). Manganese Particles in Freshwaters. In Environmental Particles, (CRC Press), p.

Wahl, T.L. (2000). Analyzing ADV Data Using WinADV. Hotchkiss RH, Glade M (Eds) Building Partnerships. American Society of Civil Engineers 1–10. https://doi.org/10.1061/40517(2000)300.

Wang, W. (1981). Kinetics of sediment oxygen demand. Water Research *15*, 475–482. https://doi.org/10.1016/0043-1354(81)90058-0.

Wang, S., Liu, X., Liu, Y., and Wang, H. (2020). Benthic-pelagic coupling in lake energetic food webs. Ecological Modelling *417*, 108928. https://doi.org/10.1016/j.ecolmodel.2019.108928.

Wang, Y., Song, J., Duan, L., Yuan, H., Li, X., Li, N., Zhang, Q., and Liu, J. (2021). Historical reconstructions of sedimentary organic matter sources and phytoplankton evolution in the Jiaozhou Bay

based on sterols and carbon isotope. Marine Pollution Bulletin *165*, 112109. https://doi.org/10.1016/j.marpolbul.2021.112109.

Welch, E.B., and Cooke, G.D. (1995). Internal Phosphorus Loading in Shallow Lakes: Importance and Control. Lake and Reservoir Management *11*, 273–281. https://doi.org/10.1080/07438149509354208.

Wengrove, M.E., and Foster, D.L. (2014). Field evidence of the viscous sublayer in a tidally forced developing boundary layer. Geophysical Research Letters *41*, 5084–5090. https://doi.org/10.1002/2014GL060709.

Westrin, B.A., Axelsson, A., and Zacchi, G. (1994). Diffusion measurement in gels. Journal of Controlled Release *30*, 189–199. https://doi.org/10.1016/0168-3659(94)90025-6.

Wetzel, R.G. (2001). Limnology: Lake and River Ecosystems (Gulf Professional Publishing).

Wilczak, J.M., Oncley, S.P., and Stage, S.A. (2001). Sonic Anemometer Tilt Correction Algorithms. Boundary-Layer Meteorology *99*, 127–150. https://doi.org/10.1023/A:1018966204465.

Wong-Chong, G.M., and Loehr, R.C. (1975). The kinetics of microbial nitrification. Water Research *9*, 1099–1106. https://doi.org/10.1016/0043-1354(75)90108-6.

Wood, P.J., and Armitage, P.D. (1997). Biological Effects of Fine Sediment in the Lotic Environment. Environmental Management *21*, 203–217. https://doi.org/10.1007/s002679900019.

Woodruff, S.L., House, W.A., Callow, M.E., and Leadbeater, B.S.C. (1999). The effects of biofilms on chemical processes in surficial sediments. Freshwater Biology *41*, 73–89. https://doi.org/10.1046/j.1365-2427.1999.00387.x.

Wuest, A., and Lorke, A. (2003). Small-scale hydrodynamics in lakes. Annual Review of Fluid Mechanics *35*, 373–412. .

Yang, Y., Dai, Y., Li, N., Li, B., Xie, S., and Liu, Y. (2017). Temporal and Spatial Dynamics of Sediment Anaerobic Ammonium Oxidation (Anammox) Bacteria in Freshwater Lakes. Microbial Ecology *73*. https://doi.org/10.1007/s00248-016-0872-z.

Zhang, H., and Davison, W. (1999). Diffusional characteristics of hydrogels used in DGT and DET techniques. Analytica Chimica Acta *398*, 329–340. https://doi.org/10.1016/S0003-2670(99)00458-4.

Zhang, L., Liao, Q., He, W., Shang, J., and Fan, C. (2013). The effects of temperature on oxygen uptake and nutrient flux in sediment inhabited by molluscs. 1 *72*, e2–e2. https://doi.org/10.4081/jlimnol.2013.e2.

Zhang, L., Zhao, T., Shen, T., and Gao, G. (2019). Seasonal and spatial variation in the sediment bacterial community and diversity of Lake Bosten, China. Journal of Basic Microbiology *59*, 224–233. https://doi.org/10.1002/jobm.201800452.